論文 / 著書情報
Article / Book Information

題目(和文)	感熱記録紙用新規桂皮酸アミド誘導体の固相光反応挙動
Title(English)	Solid-State Photoreaction of Novel Cinnamic Amide Derivatives for Thermosensitive Papers
著者(和文)	兒玉智史
Author(English)	Satoshi Kodama
出典(和文)	学位:博士(理学), 学位授与機関:東京工業大学, 報告番号:甲第9237号, 授与年月日:2013年6月30日, 学位の種別:課程博士, 審査員:植草 秀裕,藤本 善徳,小松 隆之,尾関 智二,淺井 茂雄
Citation(English)	Degree:Doctor (Science), Conferring organization: Tokyo Institute of Technology, Report number:甲第9237号, Conferred date:2013/6/30, Degree Type:Course doctor, Examiner:,,,,
学位種別(和文)	博士論文
Type(English)	Doctoral Thesis

2012 Doctoral Dissertation

Solid-State Photoreaction of Novel Cinnamic Amide Derivatives for Thermosensitive Papers

Satoshi Kodama

Department of Chemistry and Materials Science, Tokyo Institute of Technology

Acknowledgement

I would like to express my deep gratitude to Associate Professor Hidehiro Uekusa for his valuable guidance, helpful suggestion and continual discussion throughout the course of this study. I would also like to thank Associate Professor Tomoji Ozeki, Dr. Akiko Sekine, Dr. Kotaro Fujii and Dr. Kohei Johmoto for appropriate advises and suggestive discussions. I am also indebted to Mr. Takashi Miyamoto and Ms. Aya Sakon for giving great support on *ab initio* crystal structure determination. I am indebted to my many colleagues of Uekusa Laboratory who has supported me. I would like to acknowledge the help of Mr. Hiroshi Fujii, Mr. Isamu Kasahara, and Mr. Toshio Aihara for their support on synthesis of compounds and on collecting needed data for this study. I am also indebted to Mr. Shinichi Sato for his great support in preparing and evaluation of thermosensitive papers. I of course cannot forget to thank Mr. Kazuo Ono, Dr. Natsuki Amanokura, Dr. Mitsuhiro Yanagita, Mr. Toshiaki Sato, Mr. Hideaki Oomura, Mr. Susumu Mizuuchi and Mr. Kazuya Matsunaga for giving me the opportunity and the needed understanding to accomplish my study. My thanks and appreciations also go to my colleague in Nippon Soda Co., Ltd. for developing the study and people who have willingly helped me out their abilities.

Finally, I am forever indebted to my parents and my brother for their understanding and encouragement when it was most required.

September 2012
Satoshi KODAMA

2012 DOCTORAL DISSERTATION

SOLID-STATE PHOTOREACTION OF NOVEL CINNAMIC AMIDE DERIVATIVES FOR THERMOSENSITIVE PAPERS

Chapter 1

General Introduction

1.1. Lightfast Thermosensitive Paper

1.1.1. Thermosensitive Paper

Thermal recording systems have been widely used in facsimiles, cash-register slips, word processor printers, point of sale receipts, etc.[1–3] In the direct thermal printing process, which is one of the major printing process in the thermal recording system, a printed image is produced by selectively heating a specific area of coated paper as it passes over a thermal print head.

The thermosensitive paper used in this recording system typically consists at least of two layers, the base paper and the thermal sensitive layer. The base paper is typically a standard paper and the thermal sensitive layer typically consists of three components: thermochromic dye, developer, and a dispersant. The dispersant is generally a long chain aliphatic compound with a melting point in the range of 45-65°C. The other components are dispersed within the dispersant retaining the crystal form. And upon heating, regions of the coating with a printer stylus, the dispersant acts as a medium in which the developer and dye are able to interact, resulting in the coloration of the thermochromic dye.

The thermochromic dye used in the thermosensitive paper on the market, is mostly the fluoran dye. The fluoran dye used, is colorless at ground state in ambient temperature. When the basic fluoran dye react with the acidic developer by heat above the melting point, results in an acid-induced cleavage of the phthalide bond (Scheme 1-1). By opening the lactone ring, the electronic state of spiro-carbon changes from sp^3 hybridization to sp^2, and π-electron conjugation in the xanthene ring extends over to give rise to a color-formation.[4–11] And for an

example, one of the major fluoran dye used in the thermosensitive paper, the black color is due to the strong absorption maxima in the visible region at around 450 nm (yellow) and 600 nm (purple), which are in a relation of complementary colors .[4,12] In addition, structural information on colored fluoran dye with a phenolic developer has recently been clarified.[13–15]

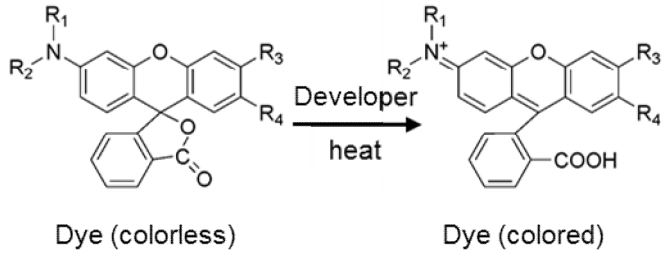

Scheme 1-1 : Acid-Induced cleavage by thermal reaction of fluoran dye under existence of developer.

The area and use which the thermal recording system is used has been expanding in these few years, due to its small system size, quietness during image printing, and need of low maintenance. The recent examples are reversible thermochromic system,[16–24] thermoresponsive recording of fluorescent images (TRF),[25,26] time temperature indicator (TTI),[27] evidence in crime (finger print extraction) ,[28–33] etc. Naturally enough, the environment which thermosensitive paper exposed became severe, and a wide variety of new characteristics is now demanded.[34]

One of the major problems that thermosensitive paper possesses is that durability against light (which is so-called lightfastness) is low. When thermosensitive paper is exposed to UV light, yellowish coloration of the paper easily occurs. This is due to the photodecomposition of the fluoran dye in the thermal layer, and because the decomposed dye is yellow, the paper turns into a yellowish color. As long as the system consist the leuco dye as the major ingredient, the degradation against light irradiation is cognized as an immortal challenge.

1.1.2. Development of Lightfast Thermosensitive Papers

As the prevention of the leuco dye's decomposition is an immortal challenge, there have been many attempts to prevent the decomposition and the following coloration of the thermosensitive paper, accomplished mainly by additives.[35–40]

One of the most common methods for development of lightfast thermosensitive paper is the addition of UV absorbers. Oda have been studying on many approaches to accomplish photostabilization of color formers, and have also tried on using UV absorbers. [35,40] For an example, he has investigated the influence of benzotriazole type UV absorbers containing an amphoteric counter-ion moiety on the photofading behavior of color formers on cellulose. The hydroxyphenylbenztriazole protects the dye by absorbing the UV radiation and converting it into heat energy by means of rapid tautomerism (Scheme 1-2). From his study, series of UV absorbers bearing a built-in amphoteric counter-ions moiety afforded excellent degree of protection against photodegradation. The promoted stability in the paper is stated as may be a result of the contribution of bifunctional amphoteric counter-ions such as **15** and/or **16**, and UV absorbing ability by UV absorbers in Figure 1-1. And consequently, these results demonstrate that the benzotriazole type UV absorbers containing an amphoteric counter-ion moiety can be applied as effective stabilizers against the photodegradation of the dye, and particularly nicked complexes are effective. Oda concludes that the novel functional UV absorbers discovered in the study may be applied as effective stabilizers against photofading of dyes used in thermosensitive papers.

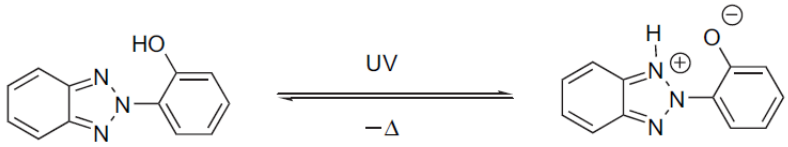

Scheme 1-2 : Rapid tautomerism of hydroxylphenylbenzotriazole compounds.

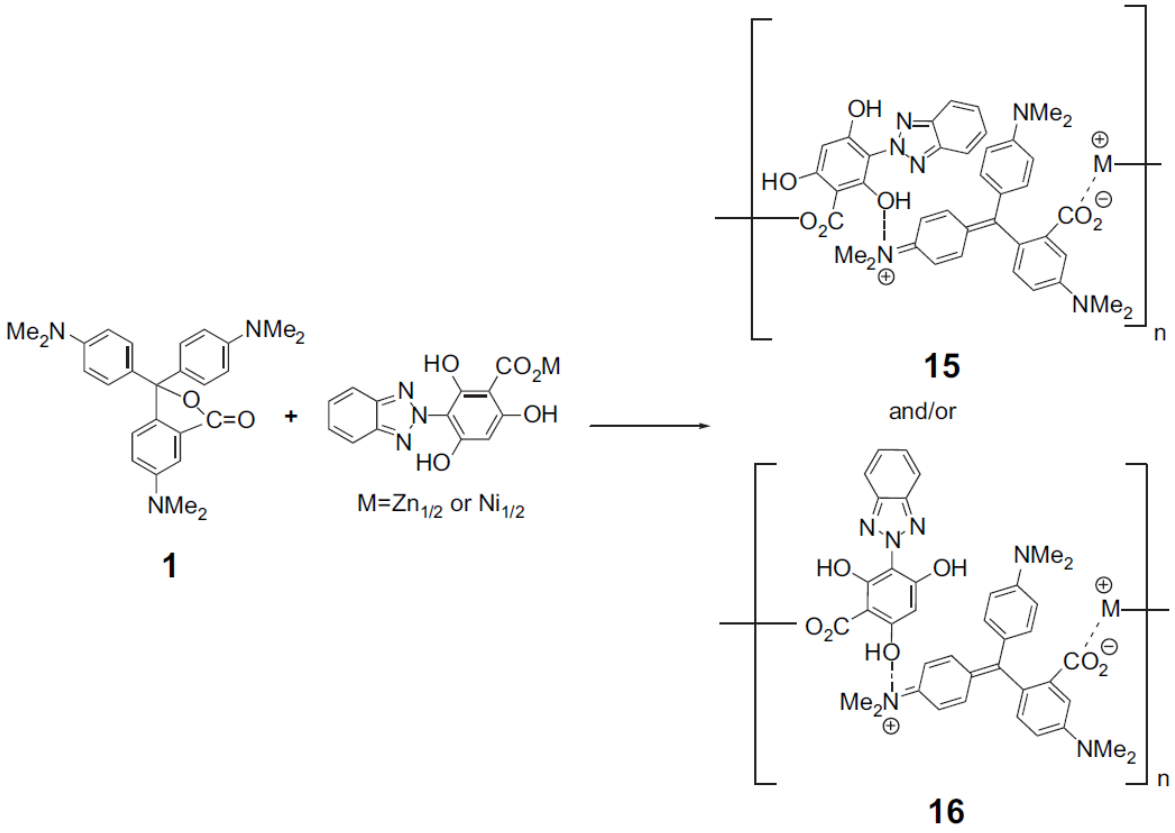

Figure 1-1 : The promoted stability caused by combined function of bifunctional amphoteric counter-ions effect and UV absorbing ability by UV absorbers.

A recent interesting example for measures of fading thermosensitive paper, is to progress a method to recover the faded text or image from the thermosensitive paper. Recent findings by Jasuja and Sigh have highlighted plausibility of using iodine vapor exposure method to enhance finger marks of thermal printer receipts.[29] And Kelly et al. have developed the method of fingerprint visualization to recovery of latent text.[41] Upon exposure to iodine vapor, the faded samples of thermal paper become stained with a pale brown coating that produces contrasting marks directly over areas that previously displayed thermally printed text. Figure 1-2 shows the physical appearance of a sample following each step of the treatment method, and illustrates the high resolution of latent thermal printing that is obtained following iodine fuming. More than just recovering the faded text, the treated samples were shown to be stable in air for many hours, with minimal fading occurring following several weeks of atmospheric storage. The exact mode of action is, at the present time, is still

little understood, it is clear that the enhancement of latent text from thermal paper using iodine is simple, quick, and highly efficient. But this example is dependent of precondition that thermosensitive paper fades, and does not afford a drastic conclusion to the prevention of the phenomenon.

Figure 1-2 : (A) A thermal paper receipt photographed as received, then (B) following removal of the leuco dye coating with acetone and finally (C) after latent text enhancement using iodine vapor. The lower image detail illustrates the clarity and resolution obtained following iodine treatment.

Along with the progress of the paper system, there have been many attempts to prevent the dye's decomposition from material point of view. Yanagita et al. have developed a novel fluoran dye which is photostable compared to dyes already known, and have succeeded in developing a lightfast thermosensitive paper.[42] Novel leuco dyes **2**-**5** were synthesized and the photobehavior was observed along with the commercially used dye **1** (Scheme 1-3). The acetonitrile solutions of dyes were irradiated by ultraviolet light (254 nm) to determine the progress of decompostion (Figure 1-3). The dyes **1** and **3** which have an *N*,*N*-dialkyl group at the 6-position on the xanthene ring showed a high speed of decompostion, and dyes **4** and **5** also showed decomposition in a lower speed. While other dyes tested decomposed by photoirradiation, dye **2** underwent substantially no photodecomposition during 36 hours of light irradiation, indicating that this dye was found to be significantly improved in lightfastness. The results of the study suggested that the photostability of fluoran compounds depends strongly on the kind of 6-substituted amino group on the xanthene ring. And it was also demonstrated that thermosensitive paper using dye **2** exhibited outstanding lightfastness even when using a conventional developer. But the study has been suspended because of the compound's safety problem became obvious and high cost compared to the commercially used dye was needed to produce.

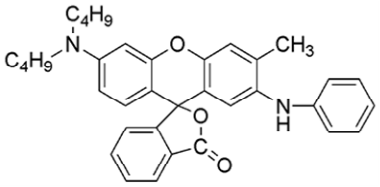

1

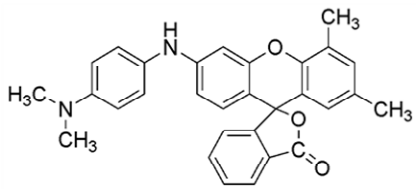

2

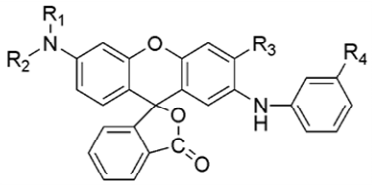

3: R_1=R_2=R_3=CH_3, R_4=H
4: R_1=n-C_4H_9, R_2=CH_3, R_3=H, R_4=CH_3
5: R_1=CH_3, R_2=H, R3=OCH_3, R_4=H

Scheme 1-3 : Molecular structure of leuco dyes **1**-**5**.

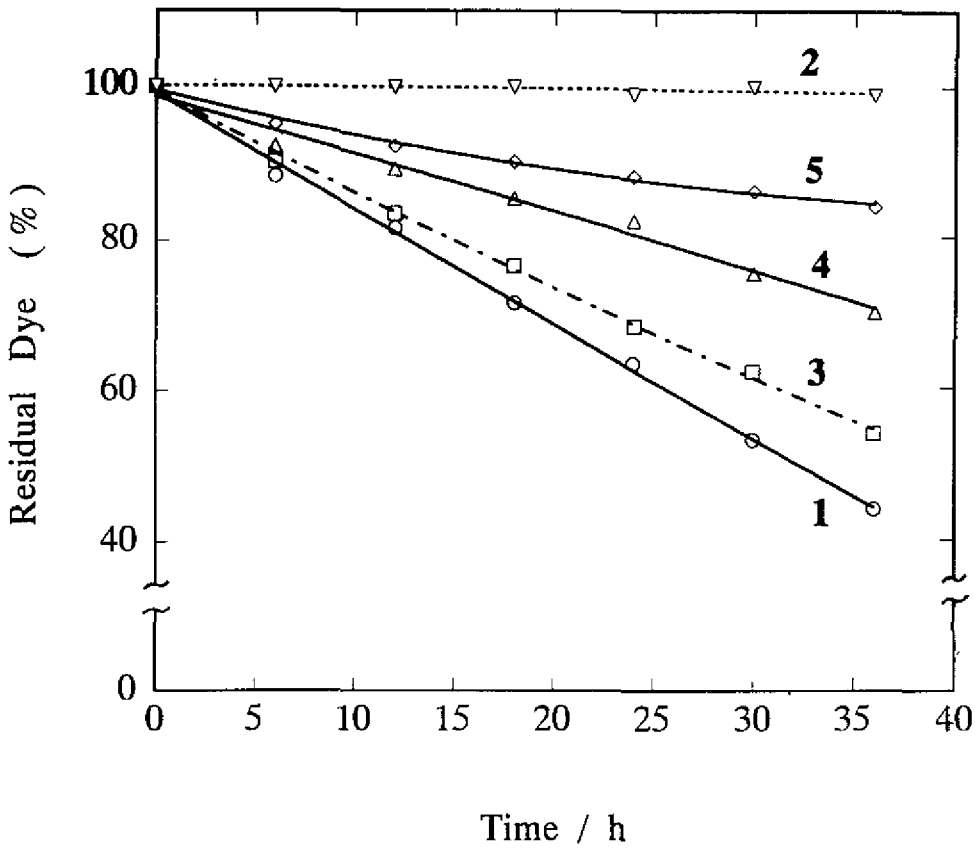

Figure 1-3: Percentage of residual dye after exposure to ultraviolet light (254nm) in acetonitrile.

Interestingly, despite the wide application of these materials in commercial products, there are only few examples on the study of high quality developer.[4344] And to our knowledge, there are no studies on development of photostable thermosensitive papers by using a novel developer. We have paid attention to this fact, and have started to study a development of photostable thermosensitive paper, by using novel developers.

1.1.3. Concept of the Novel Developer for Lightfast Thermosensitive Paper

A concept for the novel developer is to afford UV-absorbing property to the developer by introducing a moiety to the acidic moiety. For the selection of the UV-absorbent moiety, I have drawn upon the UV absorbers which achieved commercial significance and easy availability. And even though there are numbers of different types of UV absorbers, they can be classified into four fundamental groups by the containing absorbing moiety. These four are the derivatives of cinnamic acid,[45] phenyl ester,[46] hydroxyphenylbenzotriazole[47–52] and 2-hydroxybenzophenone.[52–55] Typical compounds from each fundamental groups are shown in Scheme 1-4.

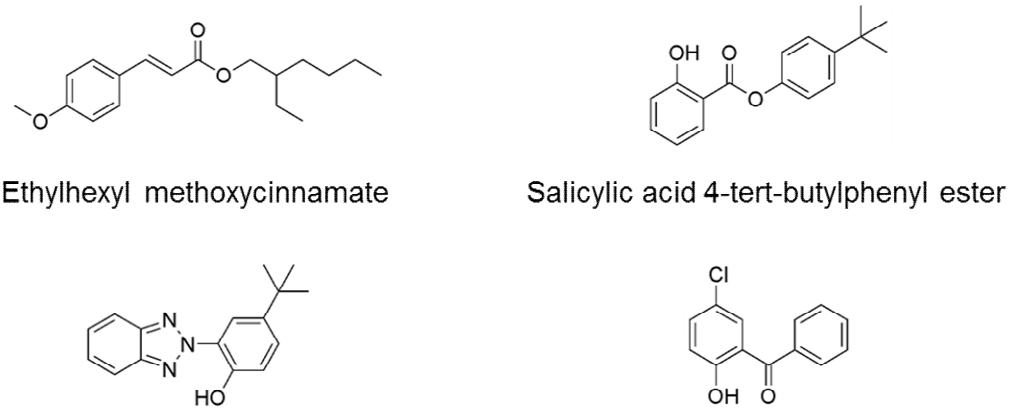

Scheme 1-4: Four classified fundamental groups of UV absorbers, cinnamic acid, phenyl ester, hydroxyphenylbenzotriazole, and 2-hydroxybenzophenone.

Among the four groups, a derivative of cinnamic acid was selected to be used in the study. This is based on the one of the most commonly used organic UV filter in sunscreens worldwide, ethylhexyl methoxycinnamate,[56–60] in which the cinnamoyl moiety is the cause of the UV-absorbent ability. And many studies have been expanded using the concept of inducing the cinnamoyl moiety into the molecule to afford UV-absorbent ability,[61–64] since the moiety can be introduced by simple synthesis methods.[65–71] In addition, UV-absorbers based on

cinnamoyl moiety, can afford solubility in oil and water resistance, which is an essential feature for developers since they need to be dispersed in water based dispersants before coating on paper. From these advantages, cinnamoyl moiety induced molecules were selected for the novel developer.

And there is also a need of introducing the acid moiety into the molecule, since the developer should be a solid acid. From the point of simple (and low cost) synthesis and the possibility for a variety of derivatives using the same method, reaction of cinnamic acid derivatives and amino phenol was selected. The acid moiety used for the thermal reaction with the leuco dye, will be originated from the phenolic hydroxyl group, which is the most universal acid moiety used in many developers for thermosensitive paper.[72,73] The simplified scheme from the reaction of cinnamic acid to novel cinnamic amide developer will be shown in Scheme 1-5. By this concept, novel cinnamic amide developers were selected as the material for lightfast thermosensitive paper.

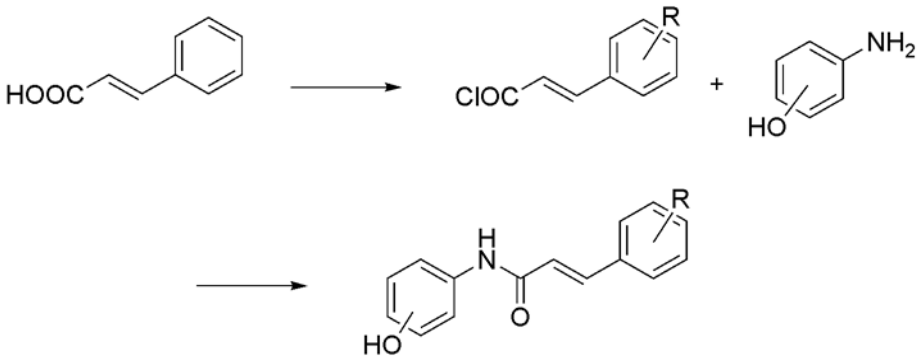

Scheme 1-5: Synthesis of novel cinnamic amide derivatives by the reaction of cinnamic acid and amino phenol.

1.2. Photoreaction in the Solid-state

1.2.1. Solid-state Organic Chemistry

The science of solid-state organic reaction and the area of lattice control over reaction pathways are not as widespread as studies the ones in solution, but are now seem to become the center of attention. With deeper understanding of intermolecular interactions and of topochemistry, solid-state organic reactions could become a significant method in synthetic organic chemistry.

Among the solid-state reactions, photochemical reactions in the crystalline state have been studied widely and are of particular interest since they tend to proceed with very high selectivity and specificity compared to as those in solution.[74,75] Some of the solid-state photoreactions are Norrish Type II,[76,77] oxygen transfer,[78] hydrogen abstraction,[79,80] and others[81,82] (Scheme 1-6).

Although the main factors required for the reaction to occur in the solid-state have been understood, there still is a lack of understanding the precise mechanism of solid-state reactions to proceed.

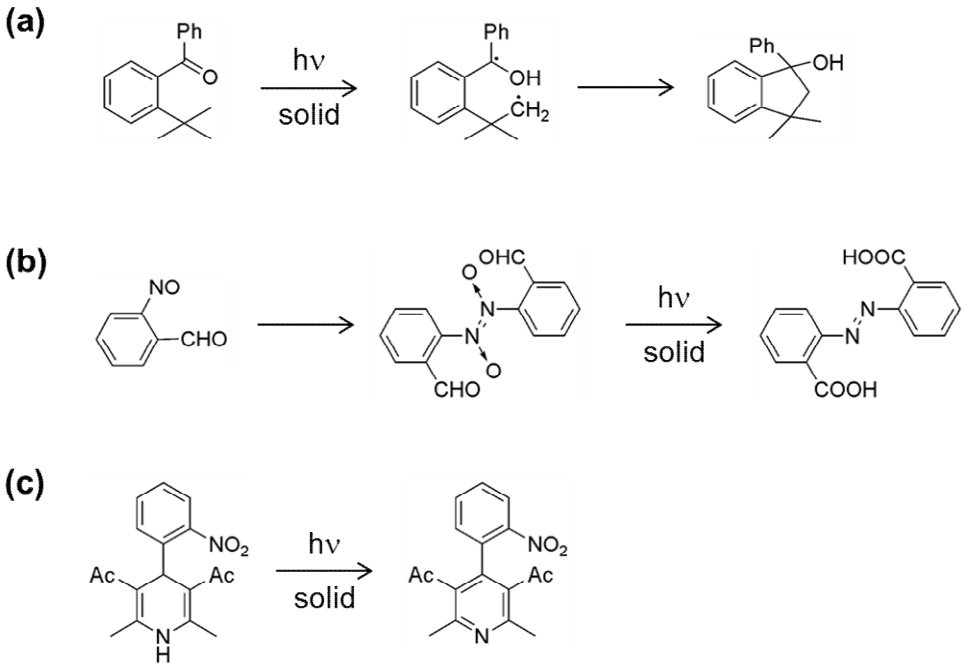

Scheme 1-6: Examples of photochemical reactions of organic compounds in the solid-state, (a) Norrish Type II and Yang cyclization, (b) oxygen transfer, and (c) hydrogen abstraction.

Among the photochemical reactions in the solid-state, [2+2] photodimerization is one of the most studied reaction and especially the reactions of cinnamic acid have been widely investigated extensively. And from application of newly developed techniques against the same phenomenon, much further study in detail are recently in progress.[83–87] Dramatic improvement through the recent studies implies that there are more conclusive research to be done, along with the possibility of betterment of the fore past studies.

1.2.2. Schmidt's Topochemical Postulate

Some of the derivatives of cinnamic acid give dimeric products selectively by photoirradiation in the solid-state. While in solution, trans-cis isomerization mainly occurs and photodimerization proceeds with less selectivity, producing co-products. Although there had been reports relating to solid-state photodimerization, the systematic and thorough studies by Schmidt and co-workers on cinnamic acids laid the foundation for the growth of this field,

[88–90] as summarized in Scheme 1-7.[91]

The cinnamic acids are observed to crystallize in three polymorphic forms, namely α-type, β-type, and γ-type. The behavior against photoirradiaton differs by the crystal structure, and the reason is originated from the adjacent stacked molecules.

In the α-type, the double bond of a molecule in one stacked overlaps with that of a centrosymmetrically related molecule in an adjacent stack. The distance between the overlapping double bond is less than 4.2Å. This type of crystal produces centrocymmetric dimers upon photoirradiation.

In the β-type structure, the molecules are separated in a distance of 3.8-4.2Å repeatedly. Therefore, the neighboring molecules are translationally equivalent and show considerable face-to-face overlap. The β-type packing arrangement reacts photochemically to give mirror symmetric dimers.

In the γ-type structure, the adjacent molecules are offset so that the reactive double bonds do not overlap. The distance between the centers of the adjacent double bonds becomes large compared to the other polymorphs (4.8-5.2Å). And the crystal of this type is intact against photoirradiation.

And Schmidt has drawn attention to the fact that not only the double bonds of the reacting monomers of cinnamic acid must be within 4.2Å, but also the double bonds need to be parallel to each other for photodimierization in the solid-state to proceed.[92] A reaction that behaves in this way is said to be topochemically controlled. Schmidt has formulated the geometrical criteria for dimerization only with the view of inferring how precisely the π-electron system of the reacting double bonds must be aligned in the crystal lattice for reaction to occur, which nowadays called the “Schmidt’s topochemical postulate”

The Schmidt's postulate for photodimerization to proceed are landmarks in organic solid-state photochemistry and are used as rules for an understanding of a large number of [2+2] photodimerization reactions of widely varying structures.

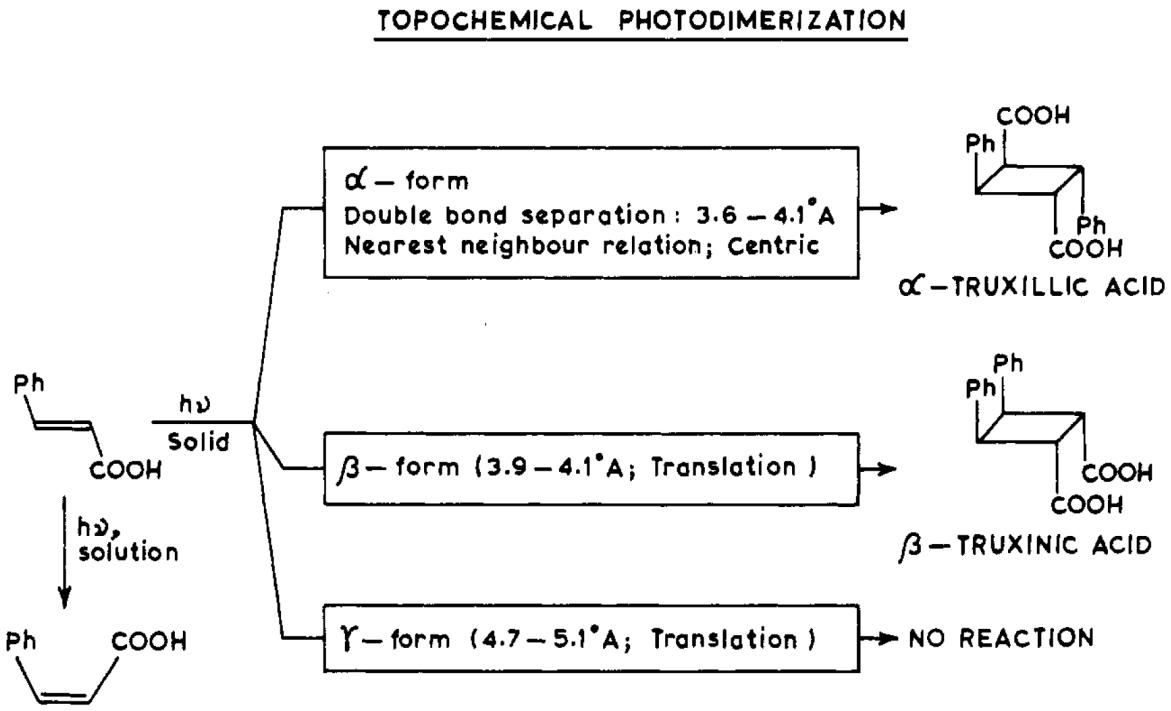

Scheme 1-7: Different behaviors against photoirradiation originated from crystal structure of cinnamic acids.

1.2.3. “Reaction Cavity” Concept

The Schmidt’s topochemical postulate also states that reaction in the solid-state is preferred and occurs with a minimum amount of atomic of molecular movement. This statement also implies that a certain amount of motion of atoms in the crystal state is tolerable. And for the formation of the cyclobutane ring by photoirradiation, the criterion of less than 4.2Å separation implicitly assumes that such a motion would be accommodated by the molecules surrounding the reactant pair in the crystal.

However, the postulate lacks important precisions that would be needed for the reaction to proceed. For instance, there is a possibility that neighboring molecules of the reacting partners play a certain role in the reaction. Another example is that when the change in molecular geometry upon excitation occurs. In order to take these phenomena into account, Cohen proposed the idea called the “reaction cavity”.[93]

The molecules going to participate directly in a solid-state reaction occupy a space of a certain size and shape in the initial crystal. The cavity or cage with a certain size and shape occupied by the reacting partners will be the reaction cavity. The concept of reaction control by the difference in reaction cavity is illustrated as Figure 1-4. Atomic movements during a reaction would exert pressures on the cavity wall, and becomes distorted. However, the close packing works against large-scale changes in shape, so that only minimal changes can occur. The minimal changes followed by small alteration in cavity size and shape are energetically favorable, and results in the possibility of reaction proceed. And the formation of cavity that extrude from the initial cavity, is supposed to be an energetically unfavorable reactions (Figure 1-4 (b)). The area or the space in which atomic movements tolerate can be regarded as the “dynamic environment” in the crystal lattice, and the representative example is the reaction cavity. This concept has been of help in qualitatively understanding the course of a variety of solid-state reactions.

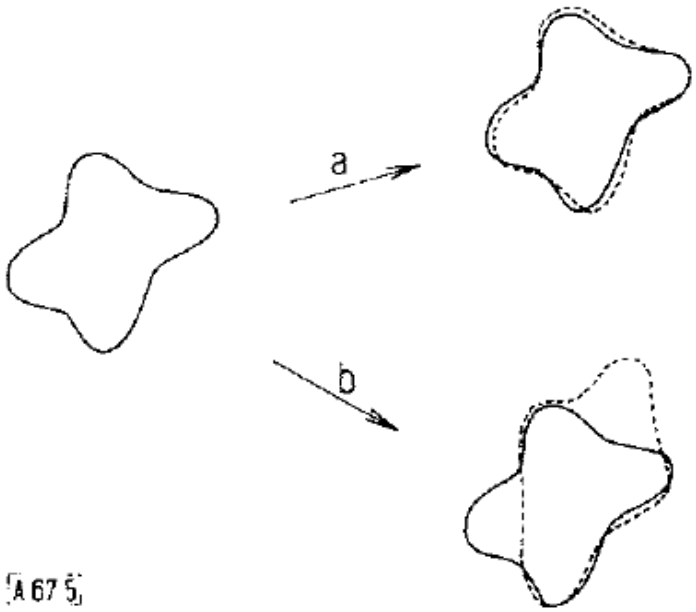

Figure 1-4: The reaction cavity before reaction (full line) and in the transition state (broken line) for energetically favorable (a) and unfavorable (b) reactions.

The usefulness of the reaction cavity concept is readily apparent when applied to photostable crystals that would be expected to be otherwise on the basis of topochemical postulate. There are some examples that the separation distances between the double bonds are less than 4.2Å, but they do not photodimerize.[94] A great example is summarized by V. Ramamurthy et al., as listed in compound (E) to (J) in Table 1-1.[95] And these exceptional cases are said to be able to understand qualitatively by invoking the “reaction cavity” concept.

Table 1-1: Examples of exceptions to original topochemical principles regarding distance. (V. Ramamurthy et al., *Tetrahedron*, **1987**, Vol. 43, 1225-1240).

Compound	Distance between reactive double bonds		Reactivity	Nature of Dimer
Methyl-p-iodo cinnamate (A)	ß-type	4.3 Å	Yes	minor symmetric
7-Chlorocoumarin (B)	ß-type	4.45 Å	Yes	Syn head-head
Eteretinate (C)		4.4 Å	Yes	-
p-Formyl cinnamic acid (D)	ß-type	4.825 Å	Yes	minor symmetric
Distyryl pyrazine (E)		4.19 Å	No	-
Enone (F)		3.79 Å	No	-
4-Hydroxy-3-nitrocinnamate (G)		3.78 Å	No	-
Benzylidene-dl-pipertone (H)		4.0 Å	No	-
(+) 2,5-Dibenzylidene-3-methyl cyclopentanone (I)		3.87 Å	No	-
2-Benzylidene cyclo-pentanone (J)		4.14 Å	No	-

There is a detailed study of polymorphs of distyryl pyrazine (Table 1-1 (E)), where the α-form photodimerizes by light irradiation,[96] but the γ-form is photostable. The crystal structure analysis of the photostable γ-form was undertaken to clarify the relation between photoreactivity and molecular arrangement, and potentially reactive double bonds are separated by 4.19Å (Figure 1-5).[97] The authors conclude that the photostability of the γ-form should be ascribed to the characteristic layered structure which suppresses the molecular deformation necessary for the cycloaddition reaction, since their studies of other photopolymerizable crystal possess the same feature, which they named a parallel plane-to-plane stack.[96,98,99] But by checking the results, the distance mentioned as 4.19Å does not indicate the distance of the centroid of the double bonds, and found to be the distance in between the nearest carbon atoms of the double bonds. The distance between the other carbon atoms of the double bond is 4.36Å, so the centroid distance is supposed to exceed maximum distance of the Schmidt's rule (>4.2Å). So, even though this example is shown as one of the example in controlling the reactivity in crystal, it is found that this compound (γ-form) does not fulfill the requirement for discussion.

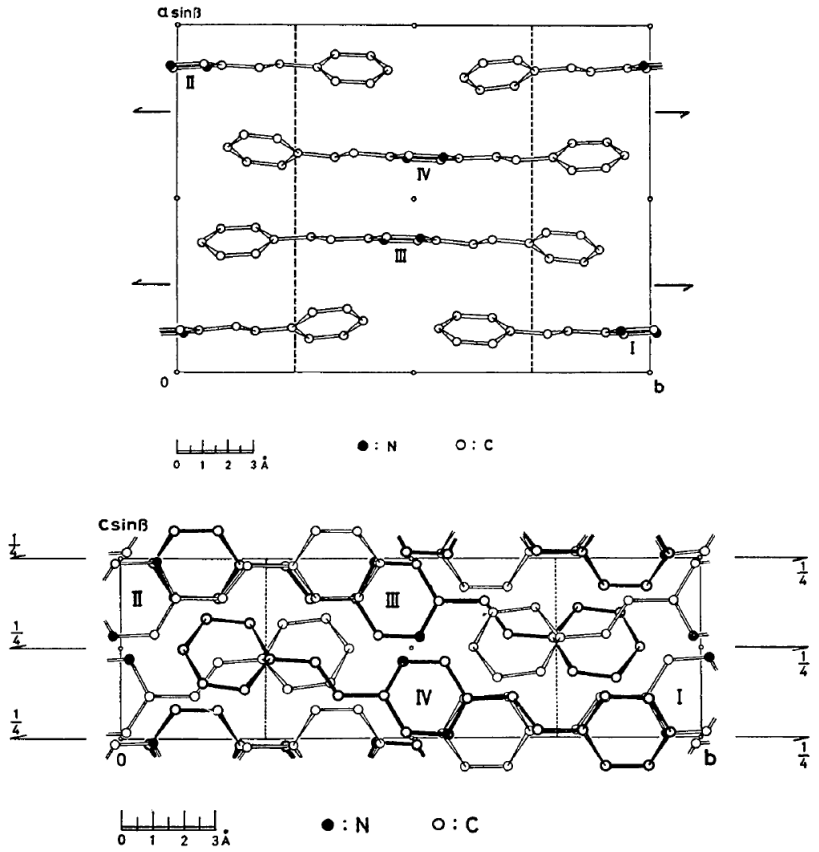

Figure 1-5: (a) The crystal structure viewed along c axis. (b) The crystal structure viewed along the *a* axis.

Trotter and his co-worker reported on a term “steric compression control”, for determining the change in reactivity caused by specific crystal lattice packing effects near the reaction site.[100,101] They have used this method to demonstrate the difference in solid-state photorearrangements of α,β-unsaturated ketones. For example, crystal structures and photochemical studies of a series of *cis*-4a,5,8,8a-tetrahydro-1,4-naphthoquinone derivatives (Scheme 1-8) have revealed that [2+2] photodimerization proceeds when the parallel C=C bonds of adjacent molecules are less than <4.1Å.[102,103] But even though the potentially reactive double bonds are parallel with a center-to-center distance of 3.79Å (Table 1-1 (F)), the molecule is photochemically inert when irradiated in the solid-state.[101] The attributed reason of the lack of solid-state reactivity, which they call the “steric compression control”, is the steric compression experienced by the reacting molecules at the initial stages of photodimerization. As the potentially reactive molecules *X* and $\overline{X}$ start to move toward one another in the

initial stages of [2+2] photocycloaddition, each experiences increasingly severe steric compression of two of its methyl group (dotted lines in Figure 1-6). Thus, molecules *Y* and $\bar{Y}$ act as stationary impediment to the dimerization, and the molecule becomes intact against photoirradiation. And the authors say that "steric compression control" can also be applied to bimolecular reactions (e.g., [2+2] photocycloadditions) in the solid-state.

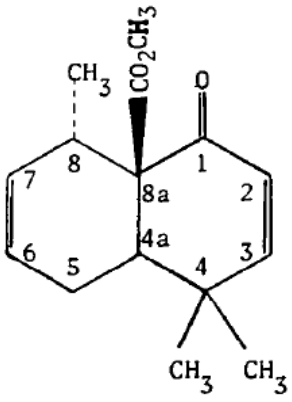

Scheme 1-8: Molecular structure of *cis*-4a,5,8,8a-tetrahydro-1,4-naphthoquinone.

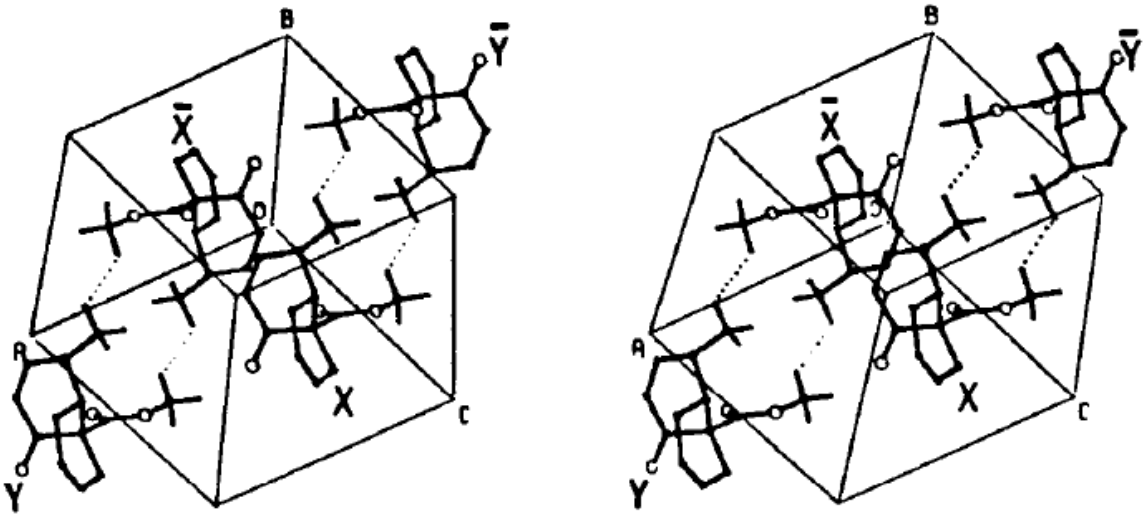

Figure 1-7: Stereo-packing diagram of *cis*-4a,5,8,8a-tetrahydro-1,4-naphthoquinone. Molecules X and X are related through a center of symmetry. Translation of X along a axis generates Y, and Translation of X along a axis generates Y. The dotted lines indicate the intermolecular H…H repulsion. For clarity of the picture, certain atoms are omitted.

In the crystal of 4-hydroxy-3-nitro methylcinnamate,[104] the center-to-center distance of potentially reactive double bonds of the neighboring molecules are related by a translation of 3.79Å (Table 1-1 (G)). But it has been observed that this compound is photostable in the solid-state. In the crystal structure, the molecules are linked by hydrogen bonds to form a sheet like structure close to the (102) plane. It is likely that the extensive intermolecular hydrogen-bond network and C-H···O type interactions involving the ethylenic carbon atom do not permit the easy spatial movement of the atoms of the double bond in the lattice for the reaction to proceed.

It has been reported that benzylidene-*dl*-pipertone (Table 1-1 (H)) is photostable in spite of the fact that there are two pairs of centrosymmetrically related double bonds that are parallel and at a distance of 3.92 and 3.98 Å, respectively (Figure 1-7).[105–107] It was proposed that for a possible explanation for the inertness of the compound is provided in terms of a large atomic displacement of the styrene group upon excitation in the crystal lattice. And the authors conclude that it seems most likely that the available cavity volume is insufficient as the molecular topology undergoes very large changes in the course of the reaction path from the reactant to the product. But there is no qualitative information that the cavity volume is insufficient for the solid-state reaction to advance, and the orientation of the potential reactive double bond are in the α packing mode.

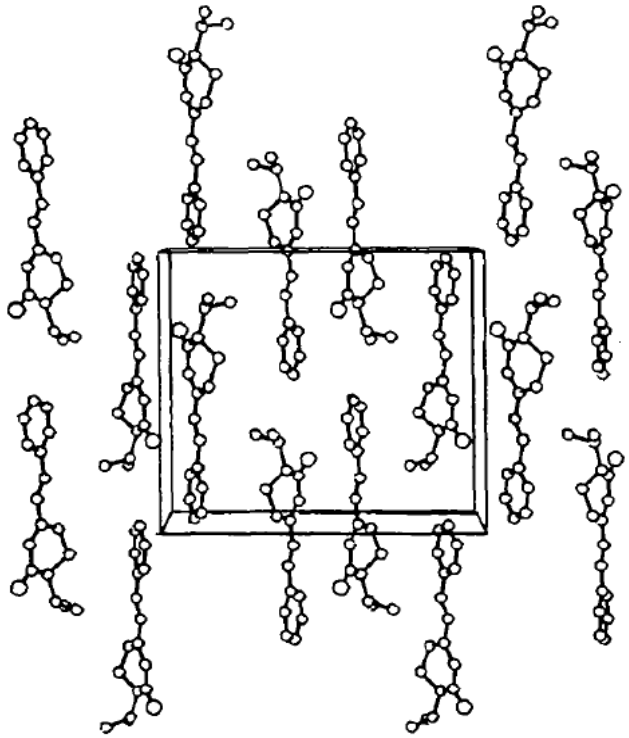

Figure 1-7: Packing of the molecules in the unit cell.

Crystalline (+)-2,5-dibenzylidene-3-methylcyclopentanone (Table 1-1 (I)) are photostable, while closely related molecules possessing similar packing arrangements undergo dimerization in a single crystal to single crystal manner.[108–111] The nearest-neighboring double bonds formed by C(5)=C(13) and C(2')=C(6') illustrated black in Figure, are related by a two-fold screw axis. The distance between the centers of the olefinic bonds is 3.87Å, suitable for [2+2] photodimerization to proceed, but stable against photoirradiation.[108] The authors argue that this situation arises because benzylidene groups which these two bonds belong are not parallel, and prevents the necessary overlap between potentially reactive C=C bonds (Figure 1-8). But actually, as the authors mention, the potential reactive double bonds are not parallel, so there is less possibility of photodimerization to precede the crystal structure from the beginning, and also there is no qualitative discussion using the reaction cavity concept.

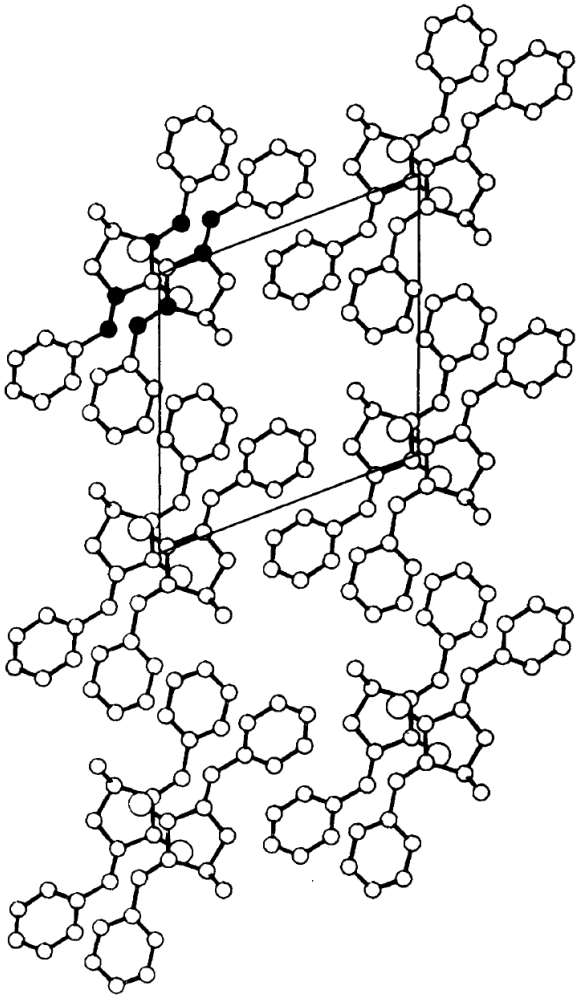

Figure 1-8: The DB(+)3MeCP crystal structure viewed along the b axis. The double bonds in one of the nearest neighboring pair is indicated.

And G. S. Murthy et al. discusses the photostability using the lattice energy calculations.[95] The packing arrangement of 7-chlorocoumarin shown in Figure 1-9 reveals that there are two potentially reactive pairs in the unit cell. One pair, being translationally related, has a center-to-center distance of 4.45Å. The other pair, being centrosymmetrically related, has a center-to-center distance of 4.12Å. Despite the favorable arrangement of the centrosymmetric pair, the dimer is obtained only from the translationally related pair, and is said to be the first example wherein photodimerization occurs between the double bond s separated more than 4.2Å.[112] To seek the difference in the reactivity of the two olefin pairs, the program WMIN developed by Busing[113] was used in the calculation of the lattice energy along with several photodimerizable olefins. It has been calculated

that the rise in the lattice energy to achieve the ideal geometry for the translated pair are 177 kcal mol^{-1}, whereas for the centrosymmetric pair, the energy is 18,083 kcal mol^{-1}. The authors mention that this shows that the reaction pathway leading to the experimentally observed dimer is energetically more favorable, and in other words, the free volume around the translationally related pair is much larger than that near the centrosymmetrically related pair whose double bonds are initially closer. And lack of free volume in the most topochemically favored pair leads to no reaction, while presence of sufficient free volume allows dimerization of the less favored pair. And they conclude that this example emphasizes the importance of void space around the reacting partners, the size of which may vary from system to system. But unfortunately, there is no obvious correlation between the lattice energy and the reaction cavity size, and the photoreactivity cannot be determined only from the values calculated. And also in the same paper, the authors have done the same calculation upon benzylidene-*dl*-pipertone and gave a lower lattice energy (0.8 kcal mol^{-1}) than photoreactive pair of 7-chlorocoumarin, even though it is a photostable compound. Authors mention that this is an unusual example, and probably brings to light the limitations of the method, and can be assumed easily that the method can be applied only to narrow areas.

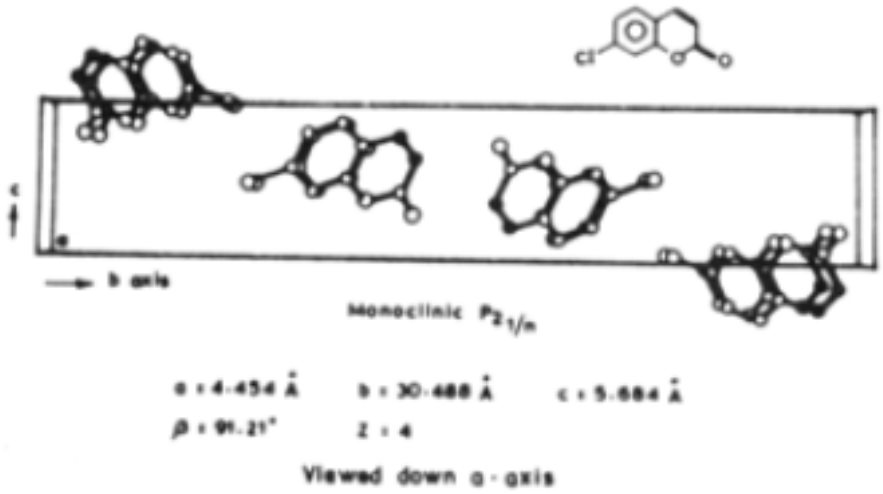

Figure 1-9: Packing arrangement of 7-chlorocoumarin. Darkened circle corresponds to reactive double bond.

From the concept, it is apparent that the reaction cavity concept can be a useful tool to determine reactivity of [2+2] photodimerization. But in the examples shown, the selected compound was not suited for the study or the method tested has no detailed qualitative study, so far as we know.

We have attracted attention to the program cavity and the cavity defined by Ohashi et al.[114] By calculation of the reaction cavity using this program, not only the volume can be calculated for the qualitative study, but also the shape of the cavity can be visualized. And the cavity can be calculated within the desired atoms, and enables intimate verification of the created cavity and the dynamic environment of the crystal structure. The reaction cavity can be calculated qualitatively by the following way; 1. Remove the reactive group from a molecule in a crystal, 2. Any space that is within van der Waals radius +1.2 Å from remaining atoms is omitted (Figure 1-10). The volume and the shape of the "Reaction Cavity" in crystal can be calculated using the program "cavity".[114]

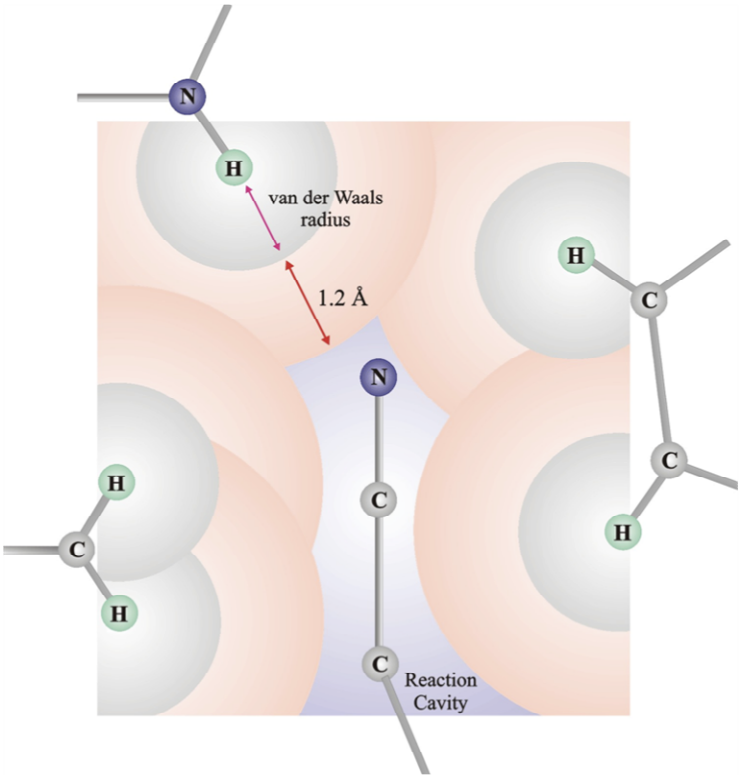

Figure 1-10: Calculation method for the "Reaction Cavity" around a molecule.

An example of the cavity created by this program is shown in Figure 1-11, the

cavity is created selectively on the cyanoethyl group of cobaloxime complexes.[114] Using the cavity created by this program, may afford us a new perspective to determine the reactivity of [2+2] photodimerization, which cannot be determined only by the static point of view.

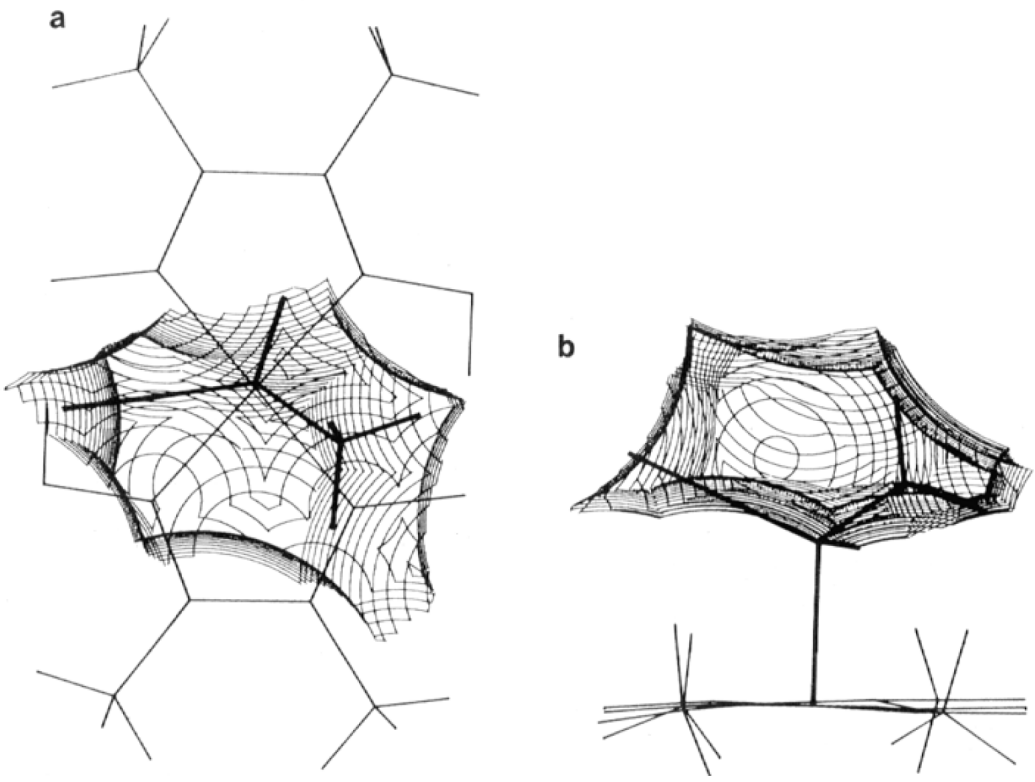

Figure 1-11: The cavity for the cyanoethyl group of cobaloxime viewed along the (a) the normal to the average plane of cobaloxime axis and (b) the long axis of cobaloxime. The contours drawn in the sections are separated by 0.10Å.

1.3. Photoreaction and Polymorphism

1.3.1. Polymorphism and Difference in Properties

Many organic crystals are known to have alternative crystalline phases in which the same compound has different crystal packing and molecular conformations, named polymorph and pseudopolymorph.[115,116] Polymorph is defined when the difference is only in the crystal packing.[117] And pseudopolymorph, or solvates, is due to the existence of solvent molecule in the crystal lattice.[118–122] The existence of many crystalline phases attract a lot of interest, since each phases exhibit different properties, such as electric conductivity, photoluminescence,[123,124] color,[125–128] dielectric property,[129] photoconductivity,[130] nonlinear optical activity,[131–133] photochromic property[134,135] and thermochromic property.

And the difference in photoreactivity between polymorphs is attracted many attention especially from the commercial view. This is because exposure to light can occur anywhere anytime, and controlling the photoreactivity by the use of different polymorphs can be a significant method for stabilizing or destabilizing the organic compound.

There are some examples where there are differences in reactivity and synthesized products between polymorphs. The most systematic work studied on [2+2] photodimerization and polymorphs are the work by Schmidt et al as described in Section 1.2.2, followed by other examples.[96,136,137] And in these cases, single crystal structure analysis followed by the measurement of satisfaction of the Schmidt's topochemical postulate, plays an important role in understanding the difference in photoreactivity between polymorphs.

1.3.2. Polymorphs and Phase Transition

Generally, crystalline phases which are alternative and results in polymorphism are often known to undergo transitions among the phases induced by the change of surrounding environment. Among the change in environment, thermal phase transition usually is accompanied by the changes of the molecular conformation or molecular packing arrangement or the change of both. This transition is interesting because it can be occurred occasionally in everyday life. And since the resulting crystalline phase after the transition usually possesses different solid-state properties, there are several reports which are attracted on the relationship between polymorphs obtained from thermal phase transition and the property during the transition itself.[138–144]

For example, affording thermal stability to the glutamic acid is important in the food and pharmaceutical industries because of its possible degradation, which may impact product safety and quality.[145] West et al. have studied the thermal behavior and the phase transition of glutamic acid.[138] α polymorph of glutamic acid were heated to various temperatures, cooled and analyzed by PXRD (Figure 1-12). On heating to 165°C, thermal transition proceeded and mixtures of α and β polymorph was obtained. By heating to higher temperature, both polymorphs eventually decreased, and pyroglutamic acid (P) and polyglutamic acid (PGA) was observed instead. And by following observation using thermogravimetry (TG), differential scanning calorimetry (DSC), gel permeation chromatography (GPC) and mass spectrometry (MS), a partial and irreversible transition of α to β polymorph at temperatures more than 140°C was determined for the first time, and the main transition sequence determined as α → β → P → PGA for temperatures in the range of 140-170°C.

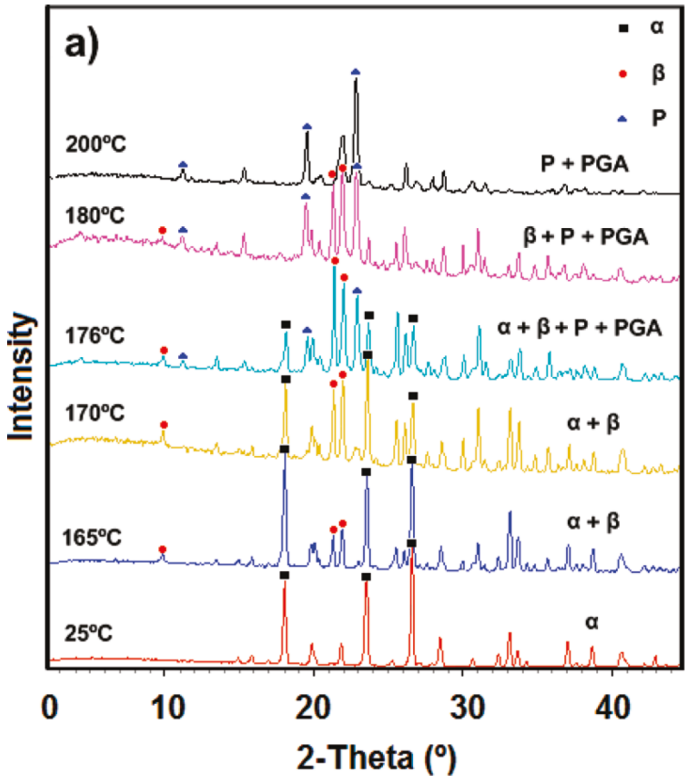

Figure 1-12: PXRD patterns of α glutamic acid heated to different temperatures and recorded at room temperature after cooling (α: α form, β: β form, P: pyroglutamic acid, PGA: polyglutamic acid).

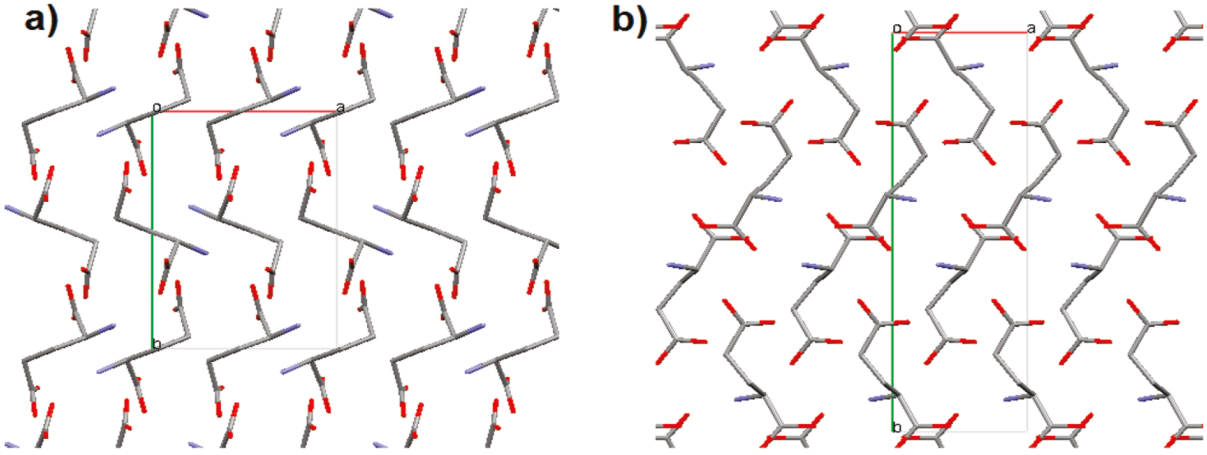

Figure 1-13: Molecular packing of glutamic acid in crystalline structure of (a) α form and (b) β form along c axis.

Another example of study on thermal transition of is shown by Bond et al.[142]

Pridopidine hydrochloride in this study is a new class of compounds that act dopaminergic stabilizer, and is now currently in development for the treatment of motor symptoms associated with Huntington's disease (Scheme 1-9). In the study, two polymorphic forms (form I and form II) are characterized. The existence of form II was discovered by examination of the DSC thermogram (Figure 1-14). After the endothermic peak resulting from the melting of form I is observed, an exothermic peak immediately followed by a second sharp endothermic peak due to form II was observed. The transition of form I to form II at elevated temperature was found to be able to occur either as a solid-state transition or from the melt of form I. The crystal structure of both polymorphs are similar in one dimension, with the molecules lying in directly comparable columns, along the *b* axis in form I and *c* axis in form II (Figure 1-15).

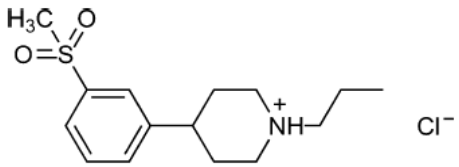

Scheme 1-9: Molecular structure of pidopidine hydrochloride.

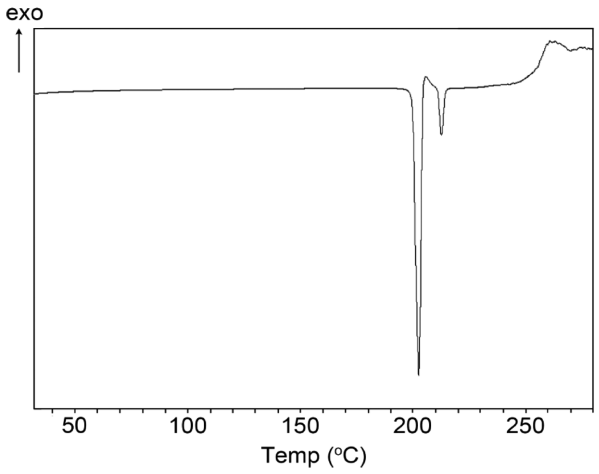

Figure 1-14: DSC thermogram of form I, showing melting of form I followed by crystallization and subsequent melting of form II.

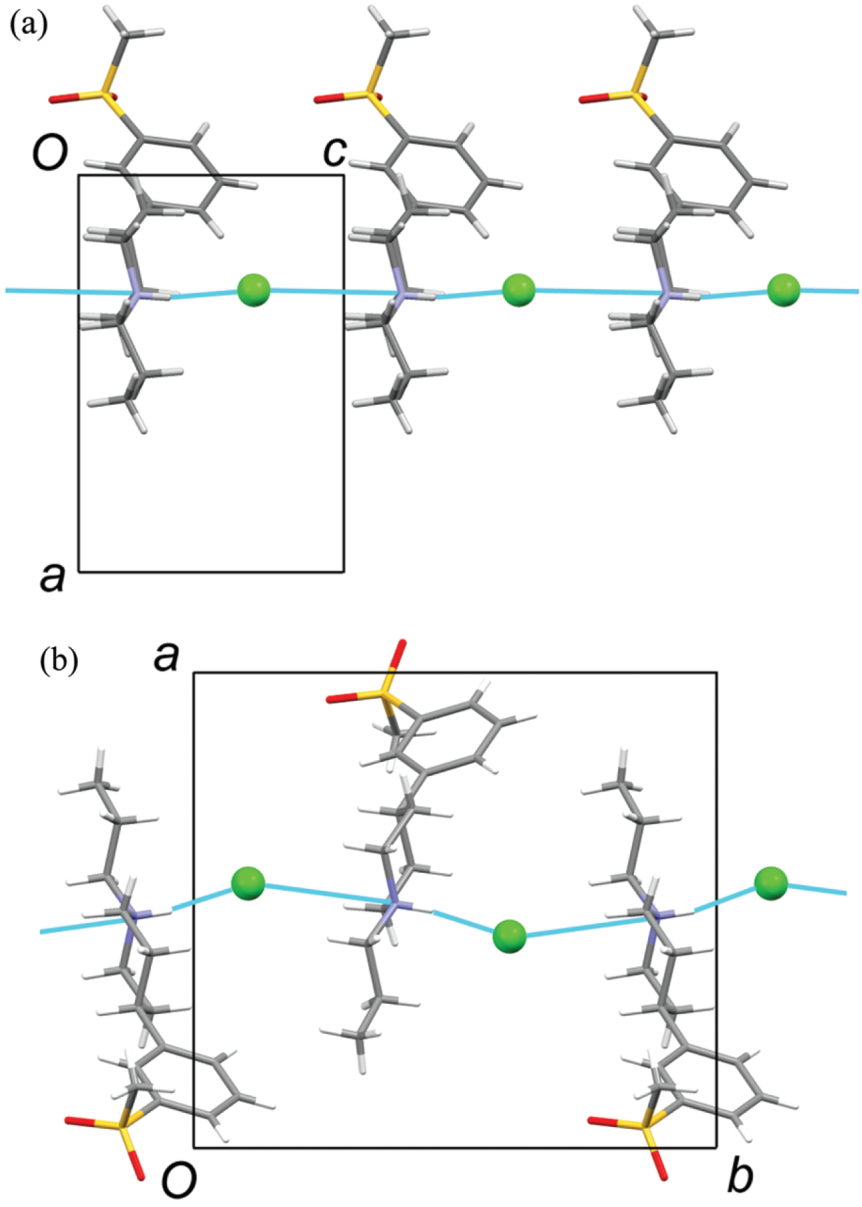

Figure 1-15: View of the crystal structure of form I (a) and form II (b). The molecular packing in the direction of the projection (along the *b* axis in form I and *c* axis in form II) is directly comparable. The blue line shows the $\cdots N^{+}\text{-}H\cdots Cl^{-}\cdots N^{+}\text{-}H\cdots$ interactions between the molecules.

However, many thermal phase transitions occur by melting and cooling, which are accompanied by disintegration of the single crystal. In most of these cases, solving the crystal structure of the compound using the single crystal analysis cannot be applied. And unfortunately, the crystals obtained by recrystallization of the product in these cases, usually results in the most stable form, or another different phase. So even though there is a difference in properties between polymorphs, detailed study of crystal structure different are rare, especially in the cases of thermal transition and [2+2] photodimerization.

Recently, the technique to determine the crystal structures from powder diffraction data has dramatically developed, and it became possible to analyze the crystal structure of organic materials from powder diffraction data, without the need of obtaining single crystals. This method, generally called the *ab initio* crystal structure determination, has been applied to clarify crystal structures of phases that can only be obtained by recrystallization, solid-state grinding, and polymorphic phase transition. These examples show that the crystal structure of unknown organic compounds can be determined by powder diffraction data, and implies that there is a possibility of clarifying the difference of properties in between polymorphs by using this method.

1.4. Purpose of This Dissertation

As described in section 1.1, there is a large demand for a lightfast thermosensitive paper in the industrial world. In order to fulfill this demand, improvement on the paper itself or the material included, will surely be the most direct and effective method. However, development in the paper structure, additive, or the dye itself is becoming crucial because of the safety of the using material and especially because of the cost of the novel material. Therefore, there is much interest in achieving lightfastness by development of other component in the thermosensitive paper. Especially, even though is a main component, there have not been an attempt for developing novel developers which can afford lightfastness, as author know so far, and is attracted much attention since its potential ability for affording lightfastness to thermosensitve paper.

On the other hand, to understand the difference in properties against photoirradiation between the derivatives, crystal structure analysis will be the most important information. Especially for compounds that have the possibility to dimerize by photoirradiation, fulfillment of the Schmidt's topochemical postulate will be an important data for determining the reactivity. However, as described in section 1.2, there are some exceptions which fulfill the Schmidt's postulate but are stable against photoirradiation. In these occasions, determining the crystal structure from a dynamic point of view has the possibility to give light to the reason for the exception.

And as described in section 1.3, there are occasions where photoreactivity differ in between the polymorphs of a single compound. Since structure determination of organic compounds from powder X-ray diffraction data have developed considerably in recent years, this technique enables us to analyze the crystal structures which cannot be obtained as a single crystal form. Therefore, *ab initio* powder crystal structure analysis would be a useful method to reveal the difference in properties of polymorphs.

In this context, the purpose of the dissertation is to develop a lightfast thermosensitive paper by using novel compounds, and to establish a method to

determine the photoreactivity qualitatively from the point of dynamic environment. The target compounds used throughout the dissertation are novel cinnamic amide derivatives, which possess UV-absorbent ability by the inducement of the cinnamoyl moiety to amino phenol. The property of cinnamic amide derivatives to afford lightfastness was investigated by preparing thermosensitive papers and implementation of lightfastness tests on both background regions and image regions. Differences and reasons of photostability or the photoreactivity in the solid-state between derivatives were determined through structures obtained by single crystal structure analysis, and clarified by determining the not only the static environment, but also from the dynamic environment in detail. And the difference in photoreactivity between polymorphs was determined through *ab initio* powder crystal structure analysis, and the result was refined by regarding the dynamic environment. Since traditional methods for determining the photoreactivity has many exceptional examples, this approach is important because it has the possibility to determine the reactivity of the solid-state reaction qualitatively.

Chapter 2

Realization of Lightfast Thermosensitive Papers Using Novel Cinnamic Amide Derivatives

2.1. Abstract

Thermosensitive paper is a functional paper, which can develop color images by thermal reaction of dye and developer. One major problem of the thermosentive paper is that when exposed to UV light, photodecomposition of leuco dye proceeds and yellowish coloration and image fading occurs. In order to improve its durability against light (lightfastness), novel cinnamic amide derivatives which possess' UV-absorbent ability was employed as a developer. By using the selected derivatives, we succeeded to realize a thermal paper that exhibit excellent lightfastness in both background and image. To afford lightfastness by using cinnamic amide derivatives, the developer's photostablility is also needed. And the derivative showing low photostability precede solid-state [2+2] photodimerization by UV irradiation, which decreases UV absorbing ability of the compound.

2.2. Introduction

Thermosensitive paper is now one of the products that is necessary in everyday life, and is used in various fields such as printer of cash registers and

ATM, label for food items and commodity distribution. In late years, the field of this system used is expanding, and many novel applications like tickets, lottery, cash voucher, boarding pass, etc.

Despite the fact that the scene, field, and environment that thermosensitive paper is used are expanding rapidly, there is one major challenge that is difficult to accomplish. The problem is the lowliness of the durability against light, which is called lightfastness. When irradiated to various lights including sunlight, the background (uncolored) region turns yellow, and image formed on the image (colored) region fades and eventually disappears. Even the commercially produced thermosensitive paper still possesses this problem (Figure 2-1), and still there is not a definite method for preventing this issue. The degradation by light is mainly having roots in the decomposition of leuco dye, so this degradation is known as a major problem of the thermosensitive paper.

For a solution for this problem, we have paid attention on preventing decomposition of dye and the following coloration or discoloration of the thermosensitive paper by using novel developers. If this method by using novel developer is possible, it might become the most direct method which does not exist in the market. And to our knowledge, this will be the first example to succeed in affording lightfastness to thermosensitive paper just simply by replacing an existing component. In this chapter, realization of lightfast thermosensitive paper using novel UV-absorbent ability appended cinnamic amide derivatives will be reported in detail.

Figure 2-1: Thermosensitive paper's degradation of the look by photoirradiation. The background region turns yellow, and the image region fades by irradiation.

2.3. Experimental

2.3.1. Synthesis of Novel Cinnamic Amide Derivatives

Materials and equipment

All chemical compounds used were available from commercial sources and used without further purification. Detail synthesis methods for typical four derivatives are shown in the following paragraphs. All other derivatives were synthesized by selecting the suited cinnamic acid and amino phenol.

^{1}H NMR and ^{13}C NMR spectra were recorded on a JEOL JNM-AL-400 FT NMR spectrometer. The ultraviolet-visible (UV-vis) spectra were measured with a JASCO V-560 spectrometer equipped for the diffuse relectance spectroscopy (ISV-469) with 0.2 nm resolution. The samples were prepared by mixing crystals in $MgSO_4$ powder. Melting points were recorded using Electrothermal IA 9300 digital melting point instrument.

*Synthesis of cinnamic amide derivative **1***

In a round bottom 500 mL flask equipped with a thermometer, 4-Methyl cinnamic acid (32.4 g, 0.2 mol) and dichloromethane (300 mL) were added.

Into the flask, oxalyl chloride (27.9 g, 0.22 mol) and dimethyl formamide (10 drops) were added, and the mixture was reacted at room temperature for 4 hours. Then the solution was evaporated to give 4-methyl cinnamoyl chloride. Next, 4-amino phenol (24.0 g, 0.22 mol) and sodium hydrogen carbonate (18.5 g, 0.22 mol) was added to a mixture of acetone (600 mL) and water (200 mL) in a round bottom 1L flask equipped with a thermometer. To the mixed solution, 4-methyl cinnamoyl chloride was added and the solution was stirred over night at room temperature. By evaporating the solvent and recrystallizing the residue from methanol, gave cinnamic amide derivative **1** (N-(4-hydroxyphenyl)-4-methylcinnamoyl amide) (28.4 g, yield 55%). mp 196-198°C; ^{1}H NMR (400MHz, DMSO-d_6, 297K, σ_{TMS}=0 ppm) σ=2.33 (s, 3H), 6.70-6.76 (m, 3H), 7.25 (d, 2H), 7.48 (m, 5H), 9.22 (brs, 1H), 9.97 (brs, 1H); ^{13}C NMR (100MHz, DMSO-d_6, 297K) σ= 21.0, 115.2, 120.9, 121.5, 127.6, 129.6, 131.0, 132.1, 139.3, 139.4, 153.4, 163.1; (Found C, 76.03; H, 5.94; N, 5.53. Calc. for $C_{16}H_{15}NO_2$: C, 75.87; H, 5.97; N, 5.53%).

*Synthesis of cinnamic amide derivative **2***

In a round bottom 500 mL flask equipped with a thermometer, 3-Methyl cinnamic acid (64.8 g, 0.4 mol) and dichloromethane (300 mL) were added. Into the flask, oxalyl chloride (55.8 g, 0.44 mol) and dimethyl formamide (2 drops) were added, and the mixture was reacted at room temperature for 4 hours. Then the solution was evaporated to give 3-methyl cinnamoyl chloride. Next, 4-amino phenol (48.0 g, 0.44 mol) and sodium hydrogen carbonate (37.0 g, 0.44 mol) was added to a mixture of acetone (600 mL) and water (200 mL) in a round bottom 1L flask equipped with a thermometer. To the mixed solution, 4-methyl cinnamoyl chloride was added and the solution was stirred over for two nights at room temperature. By evaporating the solvent and recrystallizing the residue from methanol, gave cinnamic amide derivative **2** (N-(4-hydroxyphenyl)-3-methylcinnamoyl amide) (59.1 g, yield 58%). mp 207-208°C; ^{1}H NMR (400MHz, DMSO-d_6, 297K, σ_{TMS}=0 ppm) σ=2.34 (s, 3H), 6.72 (d, 2H), 6.78 (d, 1H), 7.20 (d, 1H), 7.32 (t, 1H), 7.38-7.41 (m, 2H), 7.48 (m, 3H), 9.25 (brs, 1H), 9.94 (brs, 1H); ^{13}C NMR (100MHz, DMSO-d_6, 297K) σ= 20.1, 115.2, 120.9, 122.4, 124.8, 128.1, 128.9, 130.3, 131.0, 134.8, 138.1, 153.4, 162.9; (Found C, 76.08; H, 5.96; N, 5.47. Calc. for $C_{16}H_{15}NO_2$: C, 75.87; H, 5.96; N, 5.53%).

*Synthesis of cinnamic amide derivative **3***

In a round bottom 1 L flask equipped with a thermometer, 4-amino phenol (48.0 g, 0.44 mol) and sodium hydrogen carbonate (37.0 g, 0.44 mol) was added to a mixture of acetone (600 mL) and water (200 mL). To the mixed solution, cinnamoyl chloride (66.6 g, 0.4 mol) was added and the solution was stirred over for two nights at room temperature. By evaporating the solvent and recrystallizing the residue from methanol, gave cinnamic amide derivative **3** ((E)-N-(4-hydroxyphenyl)-3-*p*-tolylacrylamide) (50.1 g, yield 52 %). mp 208-212°C; ^{1}H NMR (400MHz, DMSO-d_6, 297K, σ_{TMS}=0 ppm) σ=6.72 (d, 2H), 6.79 (d, 1H), 7.38-7.55 (m, 6H), 7.60 (d, 2H), 9.24 (brs, 1H), 9.97 (brs, 1H); ^{13}C NMR (100MHz, DMSO-d_6, 297K) σ= 115.1, 120.8, 122.5, 127.6, 128.0, 129.6, 130.9, 134.8, 139.3, 153.4, 162.8; (Found C, 75.50; H, 5.40; N, 5.76. Calc. for $C_{16}H_{15}NO_2$: C, 75.30; H, 5.48; N, 5.85%).

*Synthesis of cinnamic amide derivative **4***

In a round bottom 200 mL flask equipped with a thermometer, 2-Methyl cinnamic acid (9.73 g, 0.06 mol) and dichloromethane (60 mL) were added. Into the flask, oxalyl chloride (9.15 g, 0.07 mol) and dimethyl formamide (10 drops) were added, and the mixture was reacted at room temperature for 2 hours. Then the solution was evaporated to give 2-methyl cinnamoyl chloride. Next, 4-amino phenol (7.19 g, 0.07 mmol) and sodium hydrogen carbonate (5.56 g, 66 mmol) was added to a mixture of acetone (120 mL) and water (30 mL) in a round bottom 300 mL flask equipped with a thermometer. To the mixed solution, 2-methyl cinnamoyl chloride was added and the solution was stirred over night at room temperature. By evaporating the solvent and recrystallizing the residue from methanol, gave cinnamic amide derivative **4** (N-(4-hydroxyphenyl)-2-methylcinnamoyl amide) (5.0 g, yield 33%). mp 192-194°C; ^{1}H NMR (400MHz, DMSO-d_6, 297K, σ_{TMS}=0 ppm) σ=2.34 (s, 3H), 6.67-6.76 (m, 3H), 7.23-7.32 (m, 3H), 7.48 (d, 2H), 7.56-7.59 (m, 1H), 7.75 (d, 1H), 9.25 (brs, 1H), 9.97 (brs, 1H); ^{13}C NMR (100MHz, DMSO-d_6, 297K) σ= 19.4, 115.2, 120.9, 123.7, 126.0, 126.4, 129.3, 130.7, 131.0, 133.7, 136.8, 153.5, 162.9; (Found C, 75.90; H, 5.83; N, 5.49. Calc. for $C_{16}H_{15}NO_2$: C, 75.87; H, 5.97; N, 5.53%).

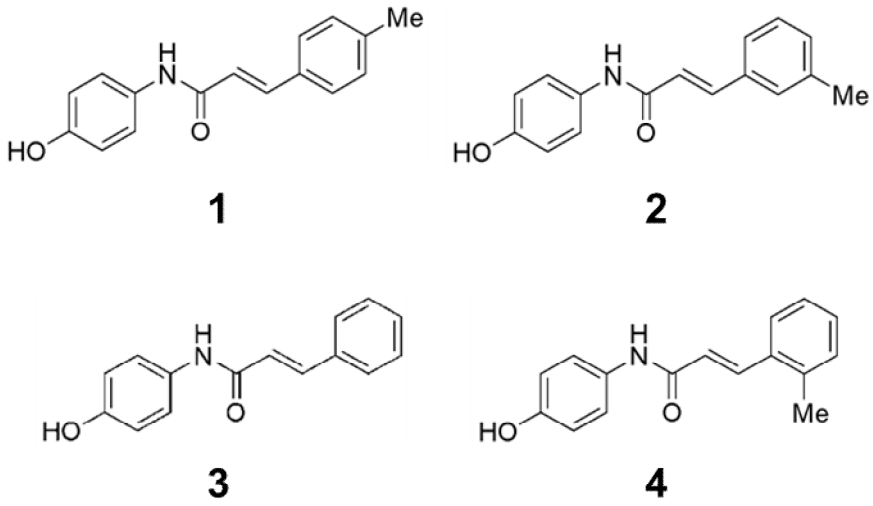

Scheme 2-1: Molecular structure of novel cinnamic amide derivatives **1**-**4**.

Structure and melting points of cinnamic amide derivatives

Structure and melting points of synthesized cinnamic amide derivatives are listed in Scheme 2-2 and 2-3.

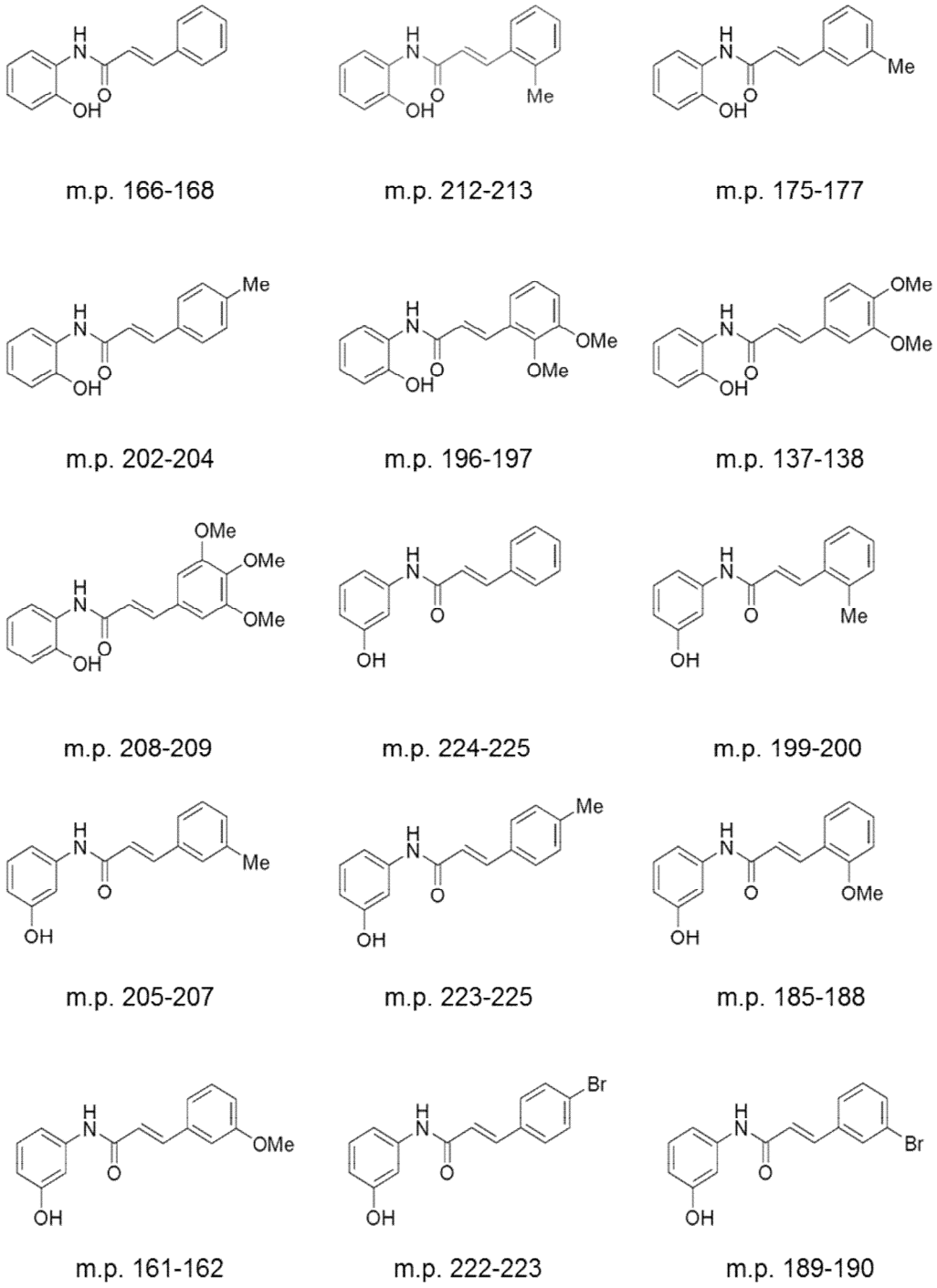

Scheme 2-2: Molecular structures and melting points of cinnamic amide derivatives.

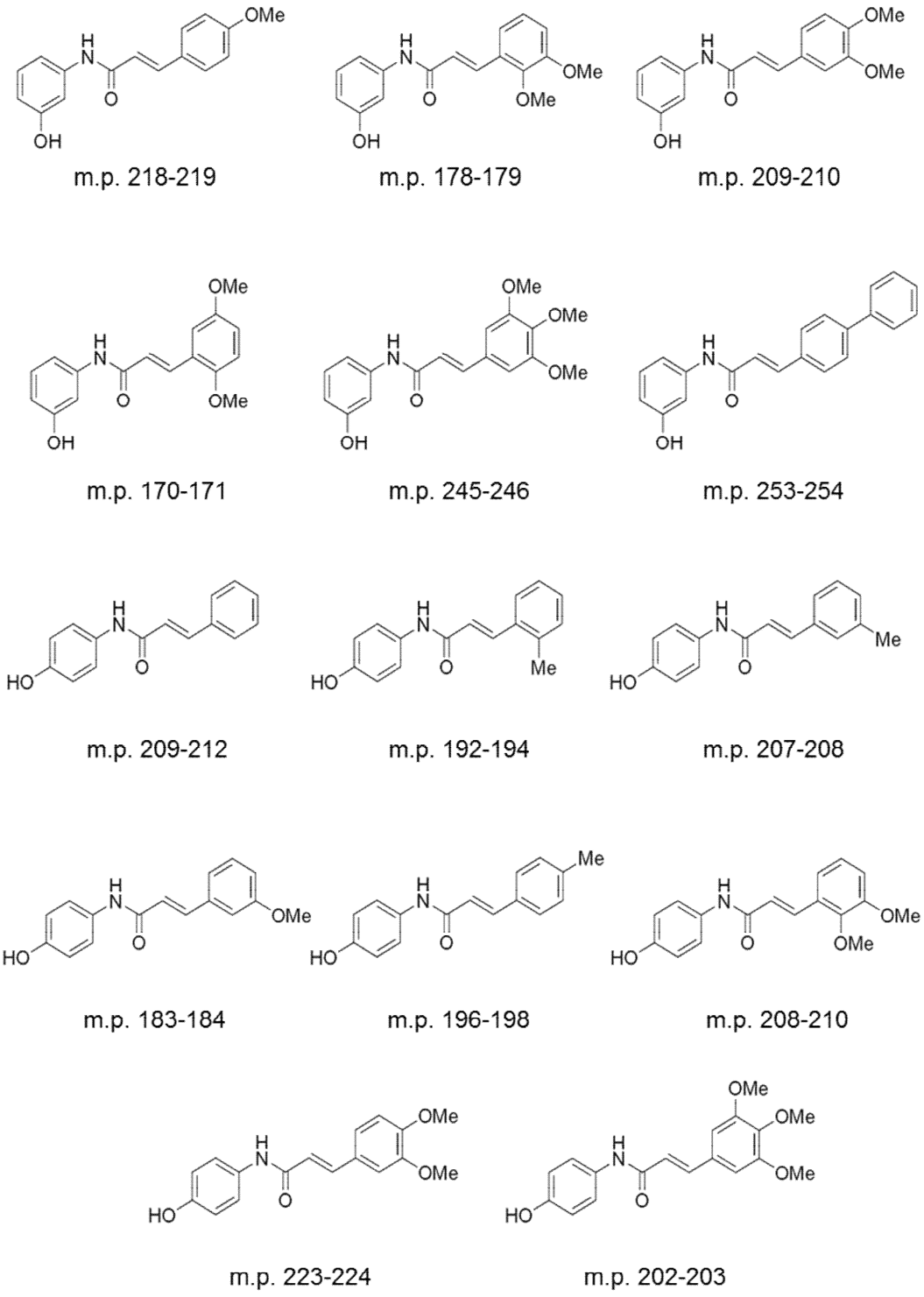

Scheme 2-3: Molecular structures and melting points of cinnamic amide derivatives.

2.3.2. Preparation of Thermosensitive Paper

For preparation of thermosensitive paper, cinnamic amide derivatives **1**-**4** or 4-isopropoxy-4'-hydroxydiphenyl sulfone **5** (Nippon Soda Co., Ltd.: D-8) used respectively for the developer, 2-anilino-6-dibutylamino-3-methylfluorane **6** (Nippon Soda Co., Ltd.: PSD-290) for the thermosensitive dye, polyvinylalcohol (Kuraray Co., Ltd.: PVA-105) for the binder, and calcium carbonate used for the filler. Each of the compounds were mixed with the ratio of 1.0 : 2.0 : 2.2 : 7.0 (dye : developer : binder : filler (weight %)) to give the coating liquid was prepared. The coating liquid was coated on the base paper, and the surface was calendar treated after drying to manufacture thremosensitive papers. The coating liquid is about 5.5 g/m^2 for dry amount, and all components are dispersed in the thermal layer retaining the crystal form. The thermal layer on top of the base paper of the thermosensitive paper prepared in this method was determined by SEM micrograph of the cut plane (Figure 2-2).

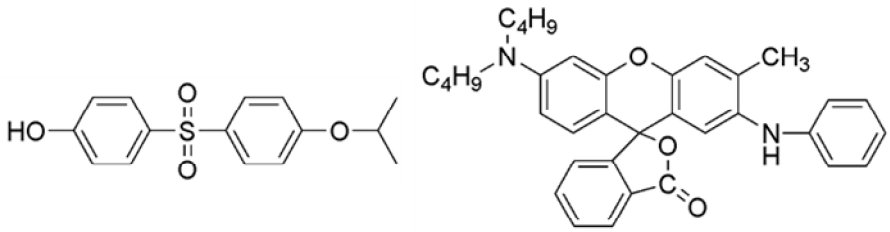

5 (D-8) **6** (PSD-290)

Scheme 2-4: Molecular structure of developer **5** (D-8) and leuco dye **6** (PSD-290).

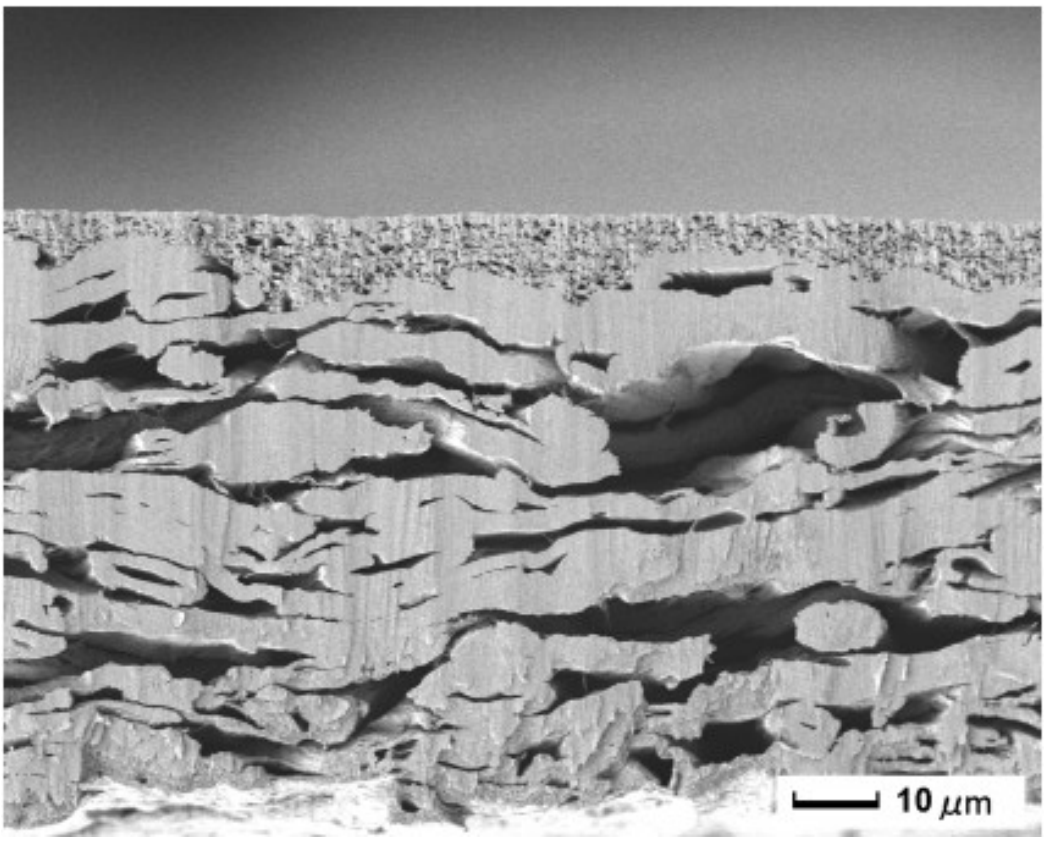

Figure 2-2: SEM micrograph of the cut plane of prepared thermosensitive paper.

2.3.3. Lightfastness test of Thermosensitive Paper (Background Region)

Lightfastness test of background region of thermosensitive paper prepared was done by using a lightfastness testing machine (Suga Test Instruments Co., Ltd.: UV Long-Life Fade Meter U48) using a piece of cut paper. The optical density (Y value) of the test paper was measured by Macbeth reflectance concentration meter (Macbeth Densitometer Model RD-918) through filter #47 (yellow) for paper after 0 hours, 6 hours, and 12 hours of testing period.

2.3.4. Lightfastness test of Thermosensitive Paper (Image Region)

Image was obtained using a thermosensitive paper image evaluation test machine (Ohkura Electric Co., Ltd.: TH-PMH, 17V; pulse width 1.8 msec) using a piece of paper cut. Lightfastness test of image region of thermosensitive paper prepared was taken place by using a lightfastness testing machine (Suga

Test Instruments Co., Ltd.: UV Long-Life Fade Meter U48) using a piece of cut paper. The optical density (B value) of the test paper was measured by Macbeth reflectance concentration meter (Macbeth , RD-918) through filter #106 (black) for paper after 6 hours, 12 hours, and 24 hours of testing period. Ratio of optical density of thermosensitive paper image before and after the test was calculated by using the next calculating formula.

Optical Density Ratio (%) =

Optical Density (After Test) / Optical Density (Before Test)

2.3.5. Photoirradiation test at Solid-state

50mg of cinnamic amide derivative was dissolved in 2.5g of acetone, dropped on a glass plate and dried to obtain test samples. Another glass plate placed on top of the test sample and clipped, the sample was installed inside a Xenone lightfastness test machine (Shimadzu Corporation: Suntester XF-180), and 300W/m^2 of light was irradiated. After the irradiation test, the cinnamic amide derivatives were extracted and diluted from the glass plate with DMSO-d_6, and the percentage of the residue developer was calculated using the ^{1}H NMR measurement results (400MHz).

2.4. Results and Discussion

2.4.1. Solid-state UV measurements of Cinnamic Amide Derivatives

The aim of this research is to prevent photodegredation of leuco dye by using novel cinnamic amide derivatives, so the UV-absorbent ability of the using compound becomes important. Especially, since photodegredation of the most common used leuco dye **6** easily proceeds by UV irradiation, the amplitude of the absorbance at the UV region is assumed to be important. To determine the UV-absorbent ability of the derivatives, solid-state UV measurement of the derivatives were done. The selected cinnamic amide derivatives **1**-**4** are ones which the hydroxyl group of the phenol moiety is located on the para position, and the position of the methyl substituent on the benzene ring of the cinnamic moiety differs from para, metha, ortho, or without a substituent. Results of the solid-state UV measurements are shown in Figure 2-3. Novel cinnamic amide derivatives **1** (light green line), **2** (blue line), **3** (dark blue line) and **4** (dashed blue line) are shown to possess wide absorbance in the UV region compared to common used developer **5** (dashed gray line). From these results, it was confirmed that the novel cinnamic amide derivatives possess UV-absorbent ability. By using them as developers, it is expected to afford lightfastness to the thermosensitive paper by inhibiting dye's photodecomposition.

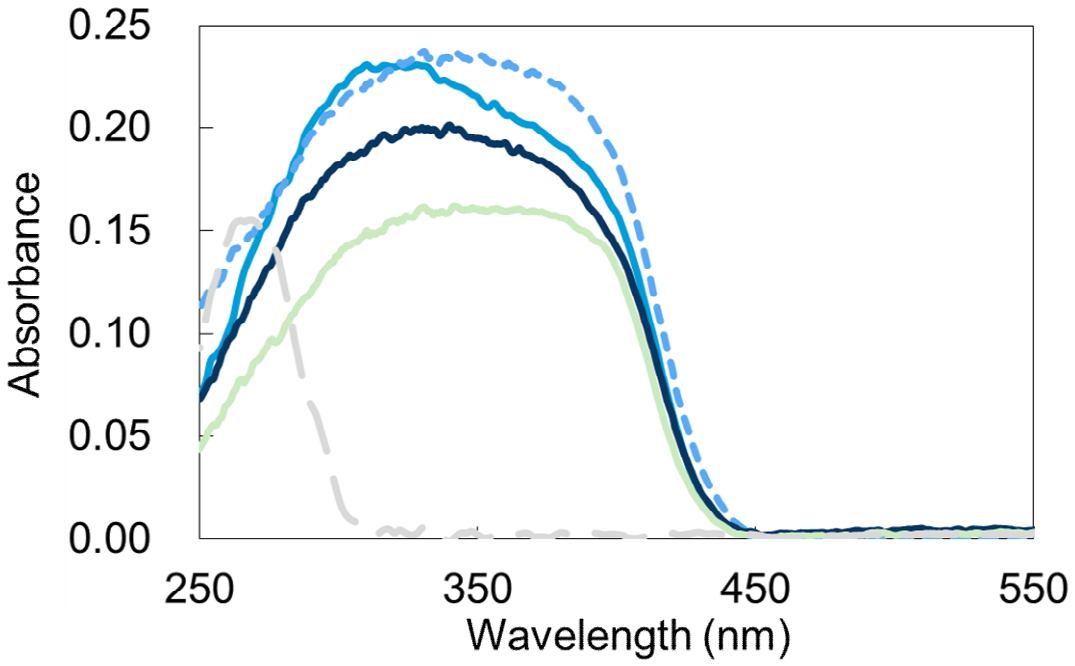

Figure 2-3: UV / vis spectra of developer **1** (light green line), **2** (blue line), **3** (dark blue line), **4** (dashed blue line) and **5** (dashed gray line) in the solid-state.

2.4.2. Lightfastness test of Thermosensitive Paper (Background Region)

To determine the ability of the novel derivatives, thermosensitive paper was prepared and lightfastness test of background region was implemented. Thermosensitive paper that is superior in lightfastness can be determined by observing the difference of yellowish coloration before and after the test, and the paper with less alteration means to have high lightfastness. Table 2-1 lists the optical densities (Y value) of thermosensitive paper background measured before (0 hr) and after (6 hr and 12 hr) light irradiation test, and Figure 2-4 shows the transition of the optical density during the background lightfastness test (**1** (light green line), **2** (blue line), **3** (dark blue line), **4** (dashed blue line), **5** (dashed gray line)). It should be noted that one of the guidepost for a thermosensitive paper that possess good lightfastness by this test, is the Y value being under 0.20 at 12 hour of test time. This Y value is due to the point where the yellowish coloration is apparent to everyone, and the ideal duration time for surpassing this value is said to be more than 12 hours.

From the test results, by using derivatives **2**-**4**, the Y value after 12 hours were less than 0.20 (**2** (0.14), **3** (0.19), **4** (0.16)) and the elevation of the Y value against time was able to be suppressed compared to **5**. So the yellowish coloration was able to be reduced as assumed, and was determined to be a thermosensitive paper with excellent lightfastness. And it should be noted that since the crystal of derivative **3** has a yellowish appearance and the thermosensitive paper prepared retained its color, the initial Y value of derivative **3** (dark blue line) became higher than other derivatives.

On the other hand, it became apparent that the resulting optical density of paper using **1** arises in a similar fashion as commonly used developer. Therefore, thermosensitive paper using derivative **1** was found to be not able to afford lightfastness of the background region.

Consequently, by using novel cinnamic amide derivatives **2**-**4**, the yellowish coloration of the thermosensitive paper due to the photodegradation of the dye was inhibited, and succeeded in the improvement of lightfastness of the background region by using a novel material.

Table 2-1: Optical densities of thermosensitive paper background measured before and after light irradiation test.

Developer	Optical density		
	0 hr	6 hr	12 hr
1	0.08	0.18	0.24
2	0.09	0.11	0.14
3	0.12	0.16	0.19
4	0.09	0.12	0.16
5	0.09	0.22	0.26

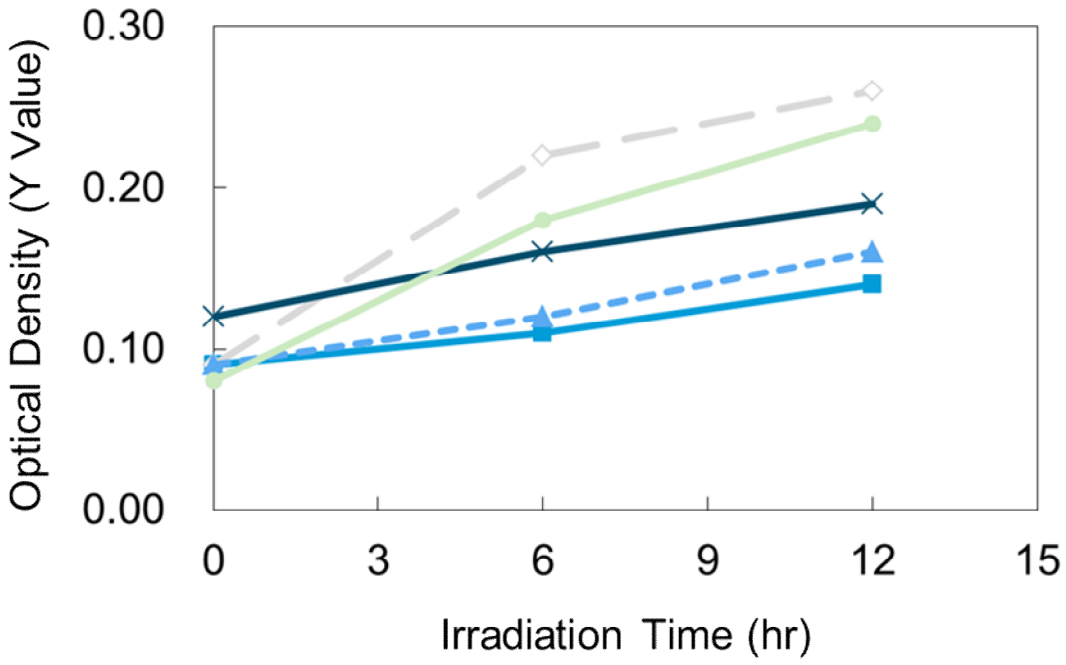

Figure 2-4: Optical density transition of thermosentive paper using cinnamic amide derivative **1** (●, light green line), **2** (■, blue line), **3** (×, dark blue line), **4** (▲, dashed blue line) and **5** (◇, dashed gray line) during the background lightfastness test.

2.4.3. Lightfastness test of Thermosensitive Paper (Image Region)

Thermosensitive papers possess not only the background region but also the image region resulting after the heat treatment, and both regions are in need of improvement in lightfastness. We now have tested the lightfastness test on the image region of the prepared thermosensitive paper. Table 2-2 shows the resulting ratio of the optical densities of thermosensitive paper image using each derivatives after 6, 12, 24 hours of light irradiation test, and Figure 2-5 shows the transition of percentage of the optical density during the image lightfastness test (**1** (light green line), **2** (blue line), **3** (dark blue line), **4** (dashed blue line), **5** (dashed gray line)). The percentage being high means that the fading by light irradiation is less, and is superior in lightfastness.

From the test results, it was determined that the decline of the image ratio can be reduced by using derivative **2-4**. The reason for affording lightfastness,

is that a part of the derivative which not used in image formation was isolated as a crystal, and its UV-absorbent ability realized the inhibition of the dye decomposition.

And for the occasion of derivative **1**, it became apparent that the resulting image ratio declines by light irradiation in a similar fashion as developer **5**, just as lightfastness in the background region. Thus, thermosensitive paper using derivative **1** cannot only afford lightfastness of the background region, but also in the image region.

The preparation of thermosensitive papers and lightfastness tests show that we have succeeded on affording lightfastness on both background region and image region just by replacing the commonly used developer into the selected cinnamic amide derivatives **2**-**4**. But we were not able to affirm efficacy when using derivative **1** compared to other derivatives.

Table 2-2: Ratio of optical densities of thermosensitive paper image measured before and after light irradiation test.

Developer	Ratio of image density		
	6 hr	12 hr	24 hr
1	87%	78%	53%
2	93%	89%	71%
3	93%	81%	63%
4	95%	93%	77%
5	90%	74%	33%

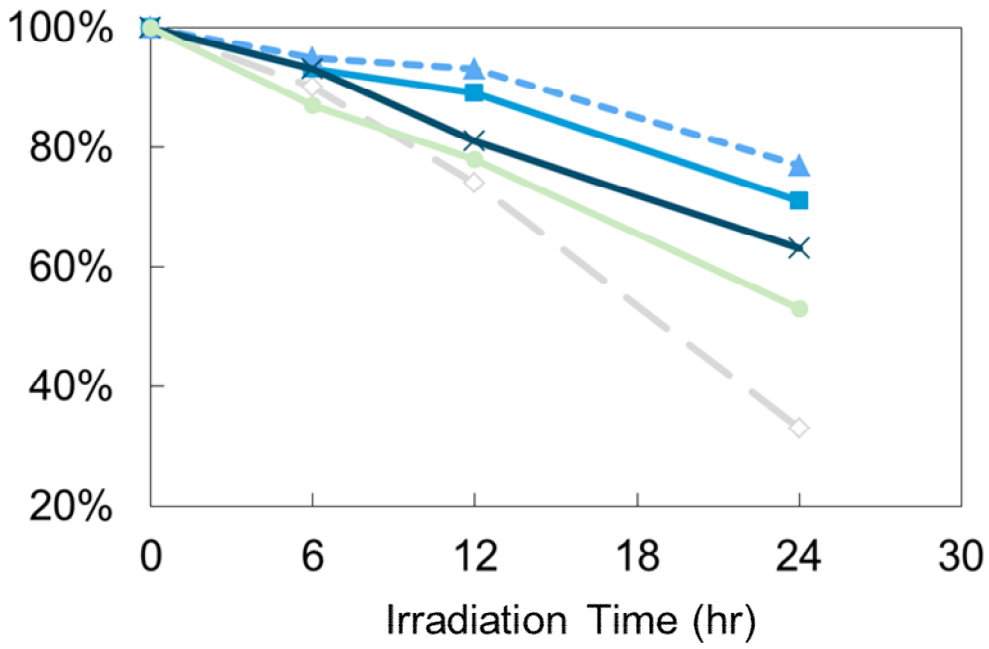

Figure 2-5: Percentage of optical density of thermosensitive paper using cinnamic amide derivative **1** (●, light green line), **2** (■, blue line), **3** (×, dark blue line), **4** (▲, dashed blue line) and **5** (◇, dashed gray line) after image lightfastness test.

2.4.4. Determination in the Fail of Lightfastness Achievement

Since cinnamic amide derivative **1** possessed wide absorbance in the UV-region along with other derivatives, it was assumed to be able to afford lightfastness. But despite the expectation, it was not possible to prevent the yellowish coloration on the background region and also the fading of the image region. To determine the reason of the ability between the derivatives, light irradiation experiment in the solid-state was implemented.

To observe the behavior of the derivative itself during light irradiation, cinnamic amide derivatives was exposed to light in the solid-state, and its behavior was observed. Figure 2-6 shows the change in percentage of residual cinnamic amide derivative against light irradiated time. From the test result, it became obvious that derivative **1** degrades by light irradiation and the residual percentage gradually declines, and reaches 0% after 4 hours of irradiation time. On the other hand, for derivatives **2-4** which can afford lightfastness to thermosensitive papers, no change in residual percentage was observed in the

range tested, and the percentage maintained 100% throughout the test time. Since there is no alteration in residue percentage, the plots of three derivatives are overlapped in Figure 2-6. Therefore, a derivative that was able to afford lightfastness was durable against light irradiation, and its degradation did not proceed.

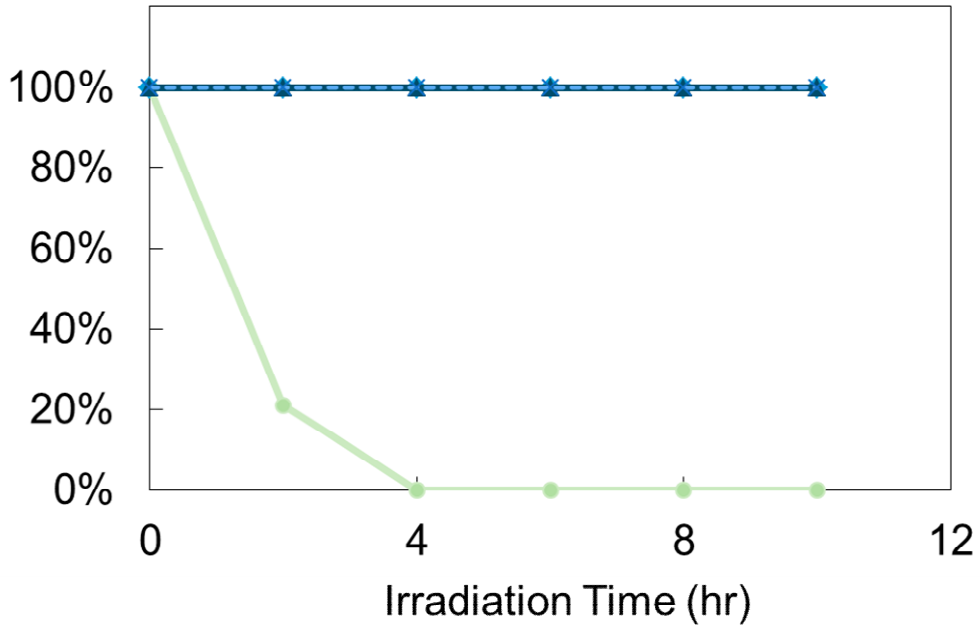

Figure 2-6: Percentage of residual derivative **1** (●, light green line), **2** (■, blue line), **3** (×, dark blue line), and **4** (▲, dashed blue line) after photoirradiation in the solid-state. The plots of derivatives **2**-**4** are overlapped in the figure.

Next, the change in solid-state UV/vis spectra before and after light irradiation of derivative **1** which residual percentage declined, and derivative **2** which the degradation did not precede was observed. Figure 2-7 and 2-8 shows the solid-state UV measurements before (line) and after 8 hours of light irradiation (dashed line). The result clarified that UV-absorbent ability of derivative **1** degrades by light irradiation. On the other hand, the UV-absorbent ability of derivative **2** does not change by light irradiation.

From these results, derivative **1** was determined to change into a compound with low UV-absorbent ability or decomposes by light irradiation, followed by the decline of the residual percentage declined. Because of the reaction

observed, it can be explained that derivative **1** cannot restrict the dye's degradation by light, and the following yellowish coloration of the thermosensitive paper. On the other hand, since derivative does not change by light irradiation and the UV-absorbent ability in the solid-state was retained, thermosensitive paper's yellowish coloration by light irradiation was prevented. Therefore, for affording lightfastness using novel cinnamic amide derivatives to thermosensitive paper, it was determined that not only possessing the UV-absorbent ability, but also it is important that the compound itself does not degrade by light irradiation.

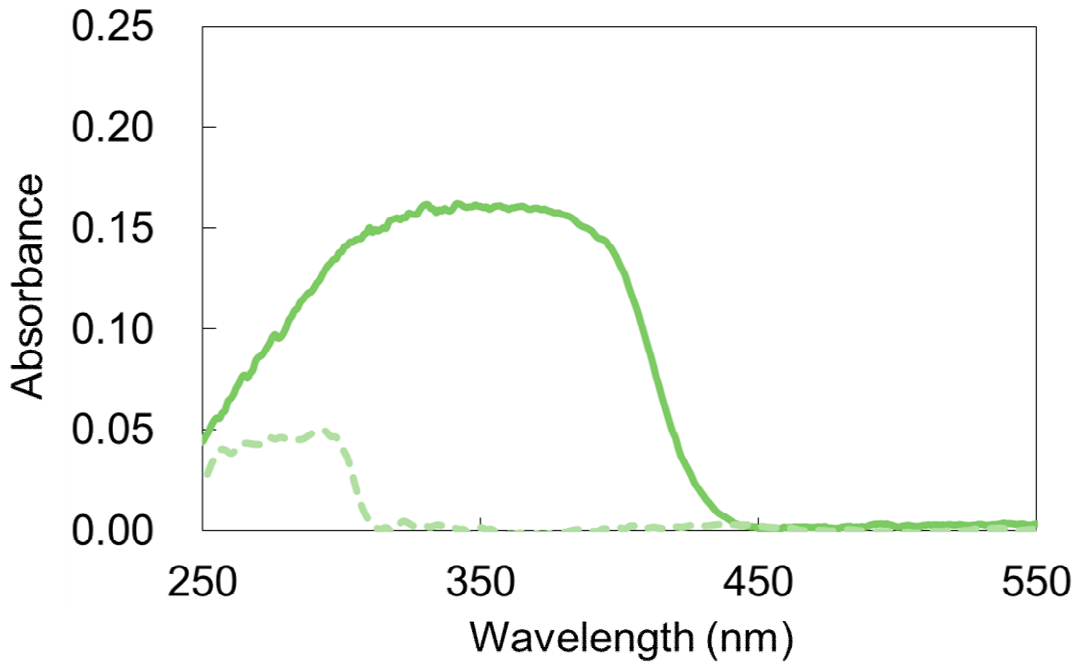

Figure 2-7: UV/vis spectra of derivative **1** before (line) and after (dashed line) photoirradiation.

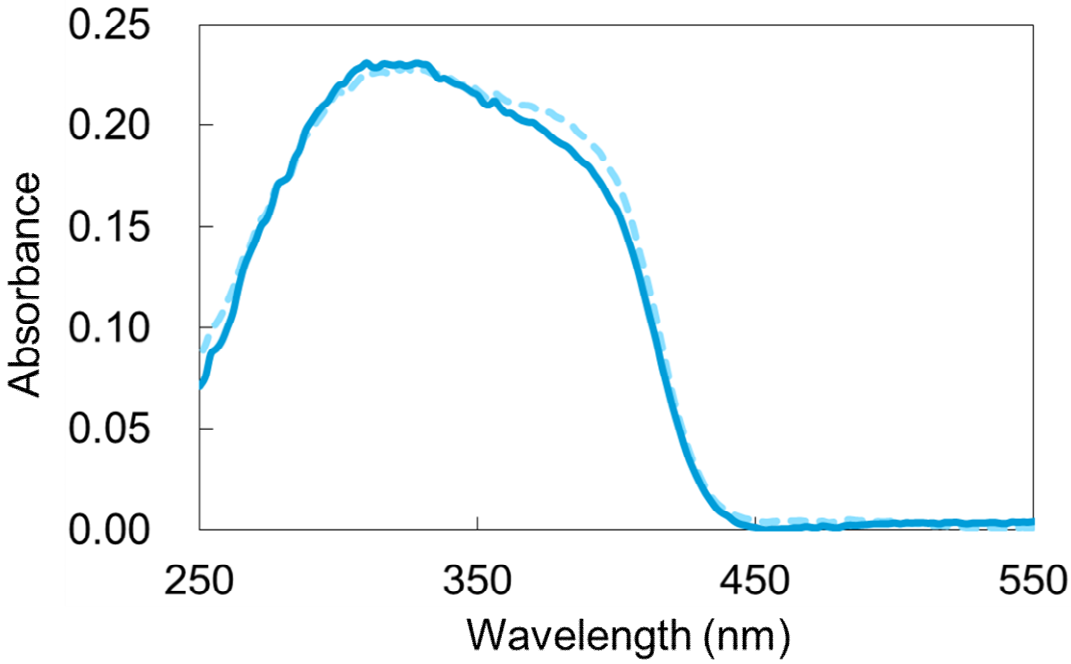

Figure 2-8: UV/vis spectra of derivative **2** before (line) and after (dashed line) photoirradiation.

2.4.5. Observation of the Degradation Behavior Against Light Irradiation

To observe the degradation of derivative **1** in detail, light irradiation in the solid-state followed by the NMR measurements were taken place. Powdered crystals of **1** were placed between two Pyrex plates and light irradiated using SUNTESTER for 0 to 6 hours. The progress was measured by recording ^{1}H NMR (solvent : DMSO-d_6) spectra at various stages of irradiation. Figure 2-9 shows the ^{1}H NMR spectra of derivative **1** (a) before photoirradiation, for photoirradiation for (b) 1 hour, (c) 2 hours, and (d) 5 hours. The figure shows that by photoirradiation, the signal originated from **1** disappears, and different signals appear. This change by photoirradiation can be assumed that intermolecular double bonds in the cinnamic moiety reacted, and the corresponding cyclodimer has formed.

The formation of the photodimer, was evidenced by the disappearance of the olefinic protons of **1** at 6.71 and 7.25 ppm and the emergence of two signals for the corresponding cyclobutane protons in the dimer at 3.92 and 4.33 ppm, as also shown in other related examples.[84,86,146–148] The photodimer formed has the possibility of four isomers (α-type, β-type, δ-type, ε-type) by the conformation of the reacting monomer.[149] From the shape of the ^{1}H NMR signals related to the cyclobutane protons as shown in Figure 2-10, the photodimer was determined as the α-type as the structure shown below according to other examples.[150] From the results shown, the degradation of derivative **1** by light irradiation was determined as the progress of [2+2] photodimerization in the solid-state.

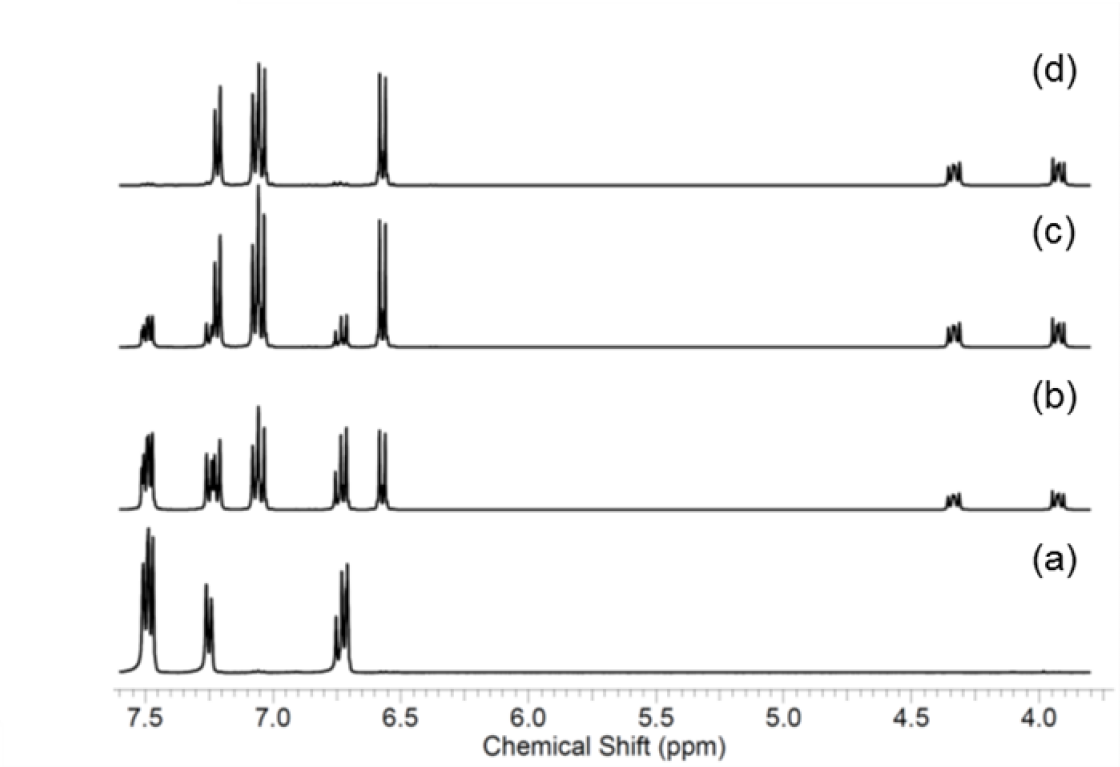

Figure 2-9: ^{1}H NMR spectra in DMSO-d_6: (a) **1** before irradiation, (b) **1** after irradiation for 1 hour, (c) **1** after irradiation for 2 hours, (d) **1** after irradiation for 5 hours.

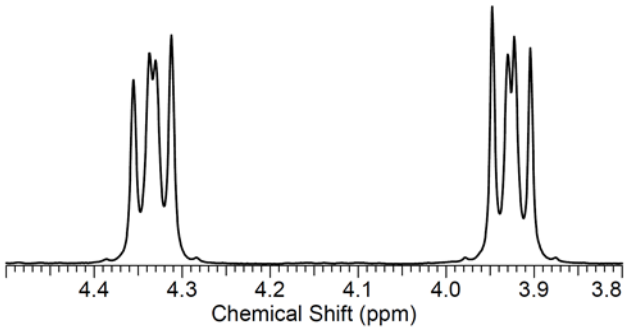

Figure 2-10: ^{1}H NMR spectra of **1** after irradiation for 5 hours in DMSO-d_6. The signals are originated from the cyclobutane protons.

2.5. Concluding Remarks

From the result of our study, we have succeeded in realization of thermosensitive paper possessing high lightfastness on both background region and the image region by using novel cinnamic amide derivatives. For the realization of lightfastness by using the derivatives, not only the UV-absorbent ability is needed but also durability of the compound itself against light in the crystal state is determined to be important. And from the detailed study of derivative that cannot afford lightfastness, we have determined that it degrades by light irradiation, and the progress of [2+2] photodimerization in the solid-state was the reason for the degradation.

Like the novel cinnamic amide derivatives shown in this chapter, there had been no existing method to improve lightfastness of both background region and image region of the thermosensitive paper only by using a single compound until now. By using these derivatives, establishment of a new method for affording lightfastness to thermosensitive paper is expected.

Chapter 3

Photoreactivity of Cinnamic Amide Derivatives and Correlation with its Crystal Structure

3.1. Abstract

The differences of photoreactivity between novel cinnamic amide derivatives were determined through its crystal structure. Single crystal structure analysis was taken place followed by the determination of both static environment (satisfaction of Schmidt's topochemical postulate, overlap parameters) and dynamic environment (area in which atomic movements tolerate). From the static environment, derivative **4** was found to not to fulfill the Schmidt's topochemical postulate, and the result showed good correlation with its photostability. On the other hand, derivatives **1-3** were found to fulfill the postulate, and the difference between the reactive **1** and the stable **2** and **3** was not clarified. To determine the difference from the dynamic environment, the cavity program was applied and the "Reaction Cavity" were calculated and visualized. The photoreactive derivative **1** found to possess the largest volume among the derivatives, and the cavity shape suited in the direction of the molecular movement during the photodimerization. This study allowed clarifying the difference in photoreactivity of derivatives including exceptions of the Schmidt's topochemical postulate, and determined that calculation and

visualization of the “Reaction Cavity” is an important tool for supplementing the postulate.

3.2. Introduction

Organic reactions in the solid-state are known to have advantage in yield and selectivity against reactions in solution, and now also attracts attention as a superb synthesis method since it practically does not exhaust waste and gives less influence against the environment.[74,151] Among the reactions in the solid-state, photocyclic reaction is energetically studied since this reaction has the possibility to occur in various types of molecules. And especially [2+2] photocycloaddition leading to formation of cyclobutanes, or [2+2] photodimerization for short, can be seen in derivatives of cinnamic acids,[152153] stilbene,[85154] anthracene,[155] chalcone,[156,157] coumarin,[158] pyridylethylene,[159–161] and others.[162163164] The reaction originates from the double bonds in the molecule, and the arrangement of the double bonds of the adjacent molecule in the solid-state will be an important parameter for the reaction to occur.

The reactivity of the photoreaction, can vary due to the position and the property of the substituent.[83] And in many of the cases, the difference between the derivatives can be attributed to the difference in the crystal structure, and moreover, the fulfillment of the Schmidt’s topochemical postulate. Therefore, determining the crystal structure is an important term for understanding the properties and the differences in photoreactivity.

For the occasion of novel cinnamic amide derivatives, the results shown in Chapter 2 clarified that the photoreaction of **1** was found to be due to [2+2] photodimerization in the solid-state. And from the result of the ^{1}H NMR measurements, the photodimer was estimated to be the α-type. Therefore, considering from other related examples, the crystal structure of derivative **1** is assumed to fulfill the Schmidt’s topochemical postulate for photodimerization proceed in the solid-state. Regarding from the same results, the derivatives **2**-**4** which dimerization did not proceed under same conditions, can also be assumed to possess the crystal structure that does not fulfill the postulate. Therefore, the difference in behavior against photoirradiation observed is expected to have some correlation with the crystal structure.

In this chapter, investigation of the difference in behaviors against

photoirradiation and correlation with its crystal structure observed from the static environment (satisfaction of Schmidt's topochemical postulate and overlap parameter) and dynamic environment (area in which atomic movements tolerate) will be reported. And the difference in photoreactivity between the derivatives was observed in detail using the "Reaction Cavity" concept.

3.3. Experimental

3.3.1. Photo-irradiation

Photo-irradiation was carried out in air with a 350W, ultra high-pressure Hg lamp (SEN-EI ELECTRIC UVF-352F), through a quartz fiber and a band pass filter (HOYA UV360) that passes the mercury emission line at 365 nm. In this study, photo-irradiation conditions were the same for all measurements.

3.3.2. X-ray measurements and refinements

The single crystal X-ray diffraction data were collected at ambient temperature in ω-scan mode with a R-AXIS RAPID imaging plate camera (Rigaku) using Mo Kα X-ray obtained from a rotating anode source with a graphite monochromator, or a R-AXIS RAPID II Imaging plate camera (Rigaku) using Cu Kα X-ray from a rotating anode source with a confocal multilayer X-ray mirror. The initial structures were solved by using direct methods with *SHELXS 97*[165] and refined on F_0^2 with *SHELXL 97*[165]. All the non-hydrogen atoms were refined anisotropically.

3.4. Results and Discussion

3.4.1. Crystal Structure of Cinnamic Amide Derivative 1 and its Photodimer 7

The results mentioned in Chapter 2 reveals that the cinnamic amide derivative **1** dimerizes by photoirradiation, and the cycloproduct was found to obtain. It is known that the cinnamic acid derivative and other compounds that possess double bonds, have the possibility for photodimerization to proceed in the solid-state if specific conditions in the crystal structure are satisfied. To determine whether **1** satisfies the condition or not, crystal structure analysis was taken place to measure the arrangement, and confirm if it actually possesses the structure that has the possibility of photodimerization in the solid-state.

1 was crystallized from slow evaporation of ethyl acetate (EtOAc) solution and confirmed the structure with single-crystal analysis (Table 1). Figure 3-1 shows the crystal structure of **1**. The phenyl ring is almost planar with respect to the attached double bond, with the torsion angel of C=C-C=C being 0.75°. The two benzene rings in the molecule are also coplanar having an angle of 5.35° to each other. Thus, the molecule of **1** in the crystal structure can be said that it is nearly flat.

From the crystal structure, the molecules of **1** laid parallel forms a sheet like structure, which are bridged by another molecule laid vertically by hydrogen bonds in between N-H···O and O-H···C=O, and results in a herring-bone network. There are two individual herring-bone networks in the crystal, colored red and pink in Figure 3-1, and the both are not connected to each other by hydrogen-bonds. The two herring-bone networks are densely packed, which results in placing two molecules from each network close and facing each other. As no hydrogen bond is observed in-between the two herring-bone networks or the adjacent two molecules facing each other, the π-π interactions between the phenyl groups of two molecules through the inversion center, with distance between the phenyl group centroids of 4.50Å, are speculated to play an important role in the formation of the packing network.

The two adjacent molecules of **1** are stacked facing opposite directions from

the point of cinnamic acid moiety. If the cinnamic acid moiety of the molecule is regarded as the “head”, and phenol group the “tail”, the adjacent two molecules are packed in head against tail (head-to-tail manner), which shall lead to a centrosymmetric product if photodimerization proceeds. This result is correlated with the ^{1}H NMR result shown in Chapter 2 (Figure 2-10), which the cycloproduct is estimated to be the centrosymmetric product.

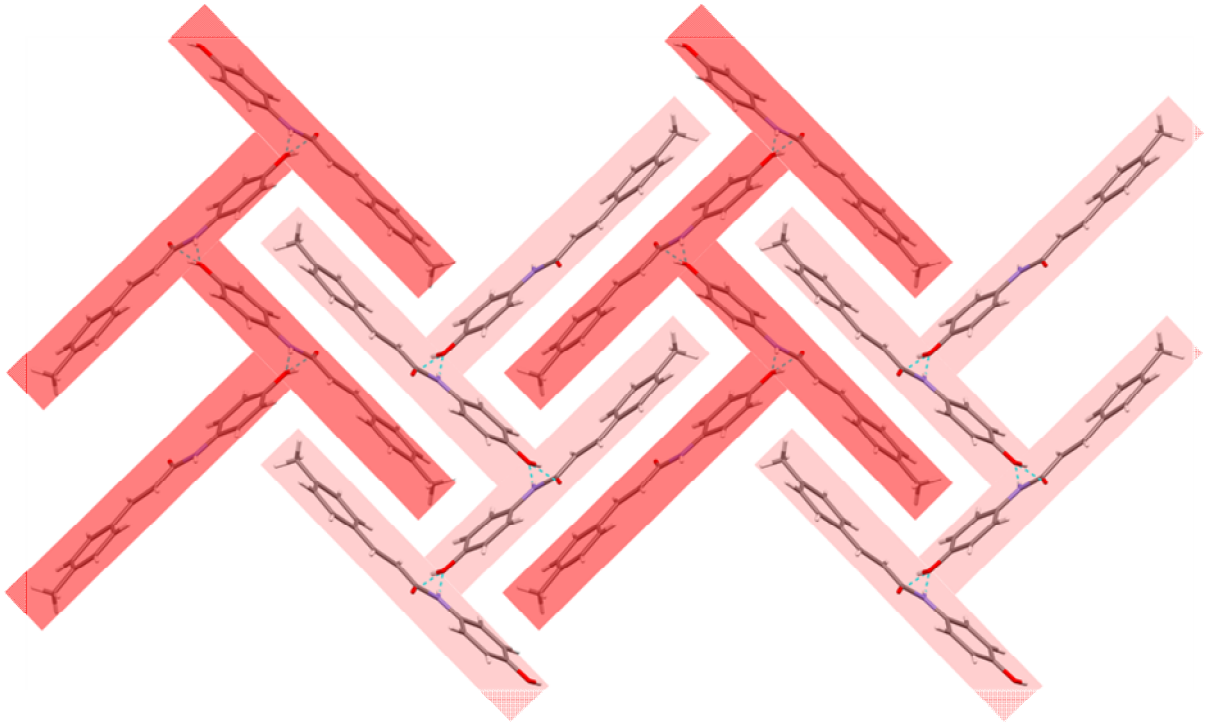

Figure 3-1 : Crystal structure of **1** viewed along the a-axis. The red and pink highlighted molecules are related to each individual herring-bone network via N-H···O and O-H···C=O hydrogen bonds. The blue dash lines indicate the hydrogen bonds.

Figure 3-2 shows the molecular packing of two adjacent molecules of **1**. The intermolecular carbon-carbon double bonds are aligned parallel, and the distance between centers of the double bonds is 3.72 Å. The intermolecular double bond distances are within 4.2 Å, so **1** is found to satisfy the Schmidt’s topochemical postulate for solid-state photochemical reaction to proceed.[92]

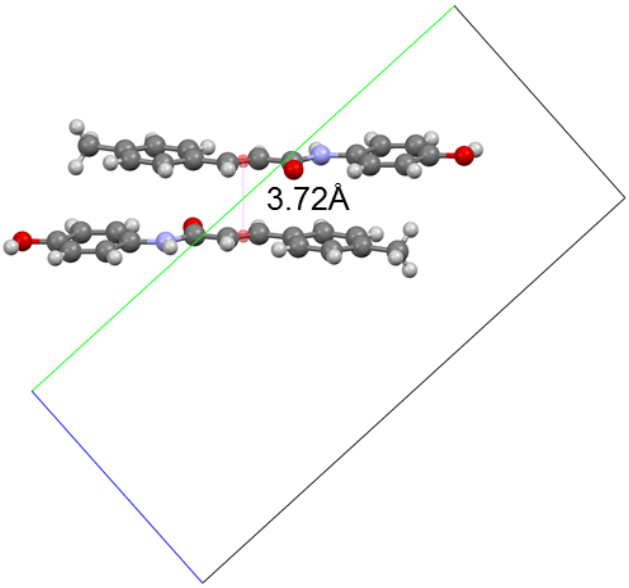

Figure 3-2 : Molecular packing of two adjacent molecules of **1**. The red sphere indicates the center of the double bond.

Also, the reaction in the solid-state occurs with a minimum amount to atomic or molecular movement, so not only the distance between the reactive bonds but also the geometry should play an important role in controlling the chemical transformations in molecular crystals.[88,90,91,94,112,152] Therefore, overlap parameters of the olefins of the two adjacent molecules, as Ramamurthy et al. has defined, are also said to be useful in determining the possibility of photodimerization to occur.[92,148,166] Each parameter θ_1, θ_2, θ_3 is defined a followed (Figure 3-3). θ_1 corresponds to the rotational angle of one double bond with respect to the other, indicating the parallel criteria. θ_2 corresponds to the obtuse angle of the parallelogram formed by double bond carbons. θ_3 measures the angel between the least square plane formed by the potentially reactive double bonds and that of a intramolecular plane formed by the double bond and the neighboring atoms. The best overlap between the reacting double bonds can be achieved when θ_1, θ_2, and θ_3 are 0°, 90°, and 90° respectively.

As listed in Table 3-1, each parameter for adjacent molecules of **1** are 0.0°, 101.1°, and 65.1° respectively. θ_1 is the same as the ideal degree, and θ_2 and θ_3 is close to the ideal degree. From these results it is apparent that **1** fulfills the distance and the overlap parameters for photodimerization to proceed.

Therefore, **1** satisfies the Schmidt's topochemical postulate for solid-state

photochemical reaction from both double bond distances and overlap parameter point of view, so the possibility for [2+2] photodimerization has been determined from the crystal structure analysis.

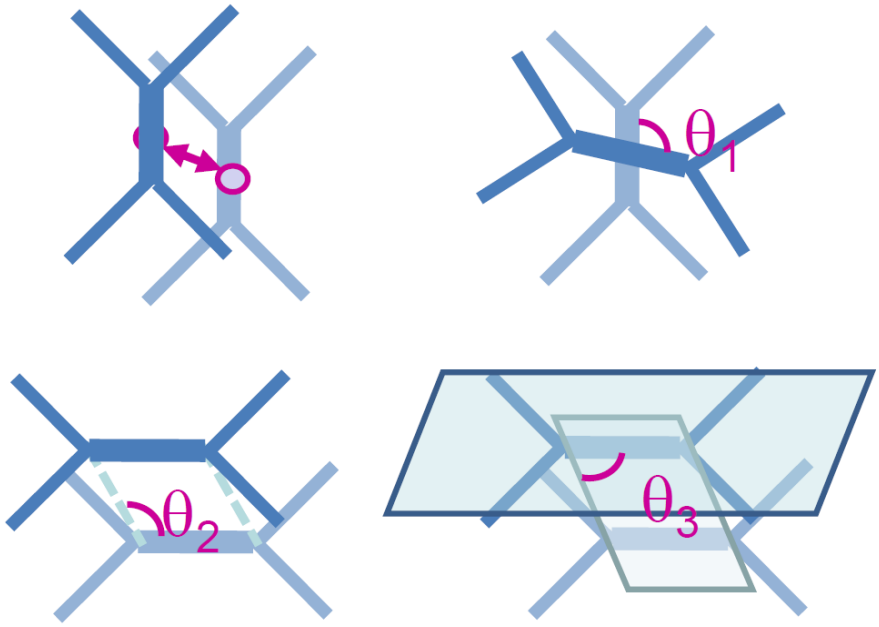

Figure 3-3 : Pictures of the distance and overlap parameters for adjacent molecules. The dark blue and light blue line indicates each molecule.

Table 3-1 : Overlap parameters for the alignment of adjacent molecules of cinnamic amide derivative **1**.

Compound	θ_1	θ_2	θ_3
1	0.0	101.1	65.1

Derivative **1** after photoirradiation was successfully isolated form the fully irradiated materials by column chromatography (SiO_2, EtOAc : hexane = 3 : 1). The isolated compound was crystallized from slow evaporation of EtOAc solution and confirmed the structure in the same way as **1**. Crystal structure analysis revealed that [2+2] photodimerization in the solid-state preceded by photo irradiation to **1**, and the deserved cyclic compound **7** was synthesized (Figure 3-5 (b)).

The photoreaction was monitored by the change of peaks in the powder X-ray diffraction (PXRD) pattern. Figure 3-4 shows the change in the PXRD patterns during the transformation from monomer **1** to the photodimer **7** by photo irradiation. The diffraction peak at 9.96°, 12.22°, 13.90°, 15.98° and 24.60° of **1** disappears and the corresponding new peaks grow at 9.56°, 11.98°, 14.66°, 16.22° and 24.14°. The new grown peak is consistent with the PXRD pattern calculated from the result of crystal structure analysis of **7** (Figure 3-4 (f)). And it was found that neither other peak than neither **1** nor **7** is observed throughout the reaction. Therefore, the degradation of **1** is confirmed to be due to [2+2] photodimerization in the solid-state retaining the crystal manner.

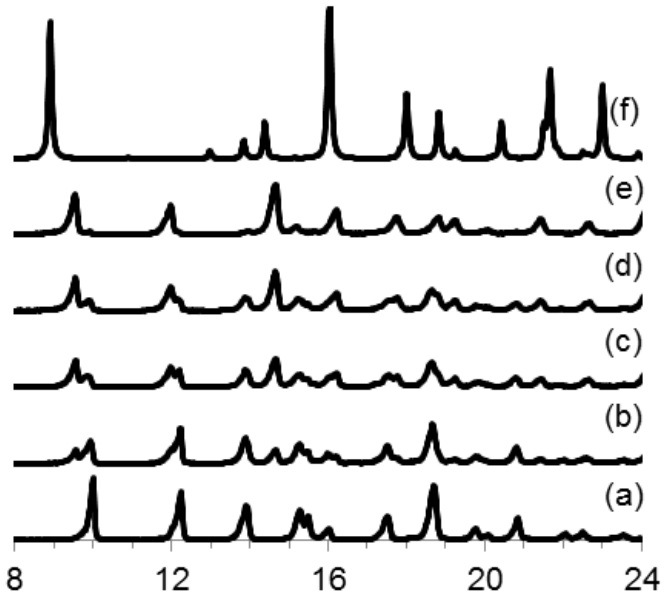

Figure 3-4 : PXRD patterns at various stages of the reaction: (a) before irradiation; the gradual changes as the reaction progresses showed in (b) to (e); (f) simulation from crystal structure analysis result.

Figure 3-5 shows the molecular packing of derivative **1** and photodimer **7**. By comparison of the two structures, the crystal packing is found to remain mostly intact. Especially, the intermolecular hydrogen bonds between the amide group and the phenol group, which stabilizes the herring bone structure of **1**, remains intact in **7**. So, the [2+2] photodimerization of **1** to **7** can be said to proceed by the smallest moves possible in the crystal. And this photoreaction of **1** to **7**, followed by the decrease of the absorbance in the UV region was confirmed as

the reason for lack of prevention of dye decomposition when used in the thermosensitive paper.

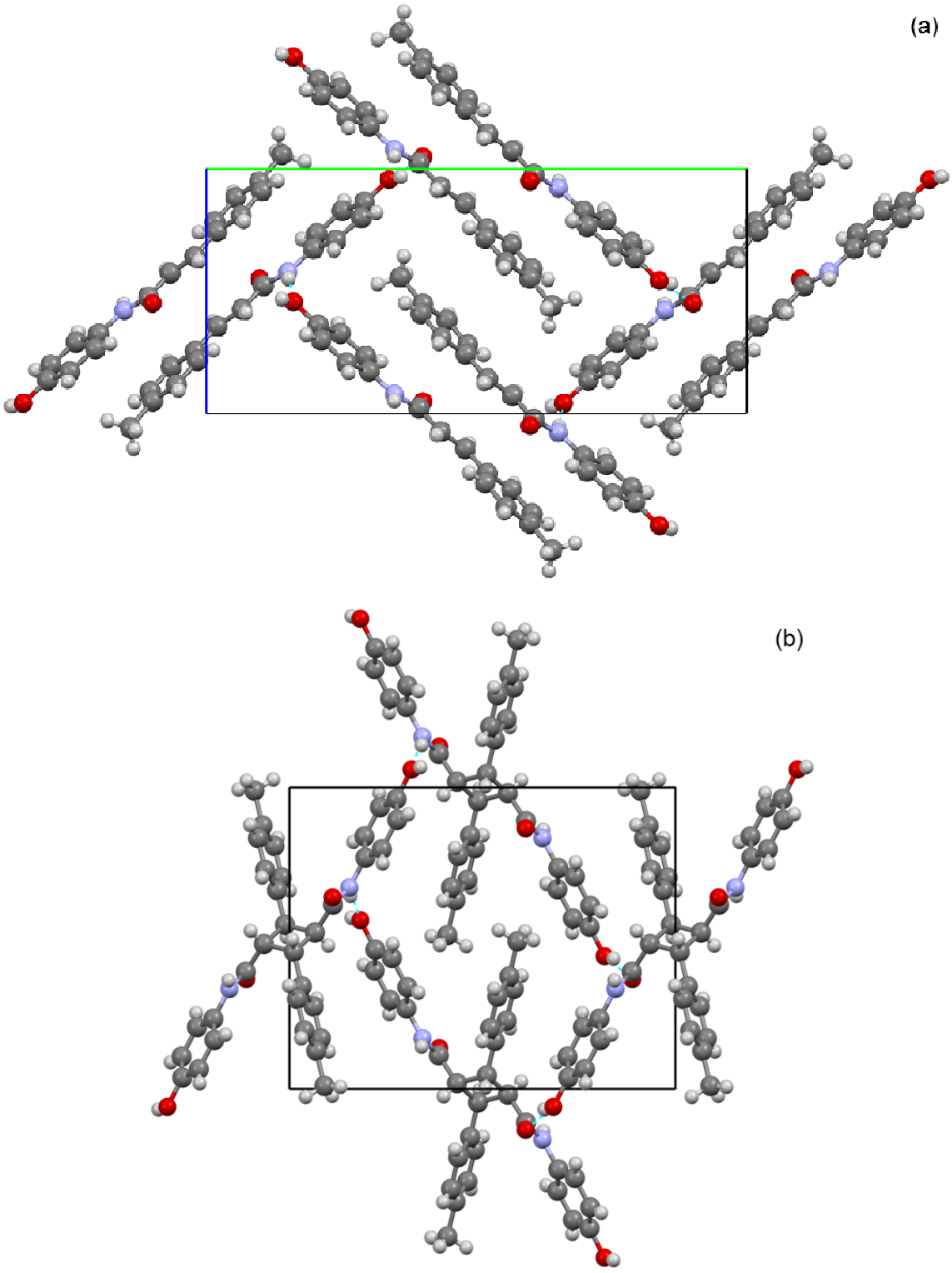

Figure 3-5 : Molecular packing of (a) monomer **1** and (b) photodimer **7**. The blue dashed lines indicate the hydrogen bonds.

3.4.2. Crystal structure of cinnamic amide derivative 2-4

Thermal recording systems have been widely used in facsimiles, cash-register slips, word processor printers, point of sale receipts, etc.[1–3] In the direct thermal printing process, which is one of the major printing process in the thermal recording system, a printed image is produced by selectively heating specific areas of coated thermal paper as it passes over a thermal print head.

Cinnamic amide derivative **1** resulted in the progress of photodimerization due to the satisfaction of the Schmidt's topochemical postulate in the crystal structure, as shown in Section 3.4.1. On the other hand, other derivative that was able to prevent the dye decomposition was intact against photo irradiation, as shown in Chapter 2. Therefore, the difference in photoreactivity can be assumed to have some relation with crystal structure, especially with the satisfaction of the Schmidt's topochemical postulate. To confirm this estimation, crystal structure analysis of each derivative was taken place, and the relation of the two adjacent molecules was determined in detail.

Crystal structure analysis revealed that as like the crystal structure of **1** that already discussed, all derivatives **2-4** possess two individual herring-bone networks, densely packed in the crystal as shown in Figure 3-6 to Figure 3-8. The packing manner is as same as **1**, and two adjacent molecules from each network facing each other in a head-to-tail manner. The distance between the centroids of the nearest facing aromatic ring from each network is 3.88 Å for **2**, 3.87 Å for **3**, and 3.98 Å for **4**.

For derivative **2** and **3**, the carbon-carbon double bond are almost coplanar to the attached benzene ring, the torsion angle of C=C-C=C being 3.72° and 3.89° respectively. The intermolecular carbon-carbon double bonds of the packed two molecules were aligned parallel for both crystal structures. The distance between the adjacent molecules' olefinic carbon centers are 4.19 Å and 4.08 Å, fulfilling the distance for Schmidt's topochemical criterion for solid-state photodimerization to proceed (Figure 3-9 (a), (b)).

For derivative **4**, the carbon-carbon double bond is twisted from the attached benzene ring, the torsion angle of C=C-C=C being 14.03°, larger than other three derivatives. The two benzene rings are also twisted having an angle of 16.98°, meaning the structure of **4** is the most twisted among the four derivatives. The intermolecular carbon-carbon double bonds were twisted, and the distance between the centers of the olefinic double bonds are 4.76 Å (Figure 3-9 (c)). The

distance in-between the double centers are beyond the Schmidt's topochemical postulate for solid-state dimerization, so the photodimerization is not supposed to proceed in **4**.

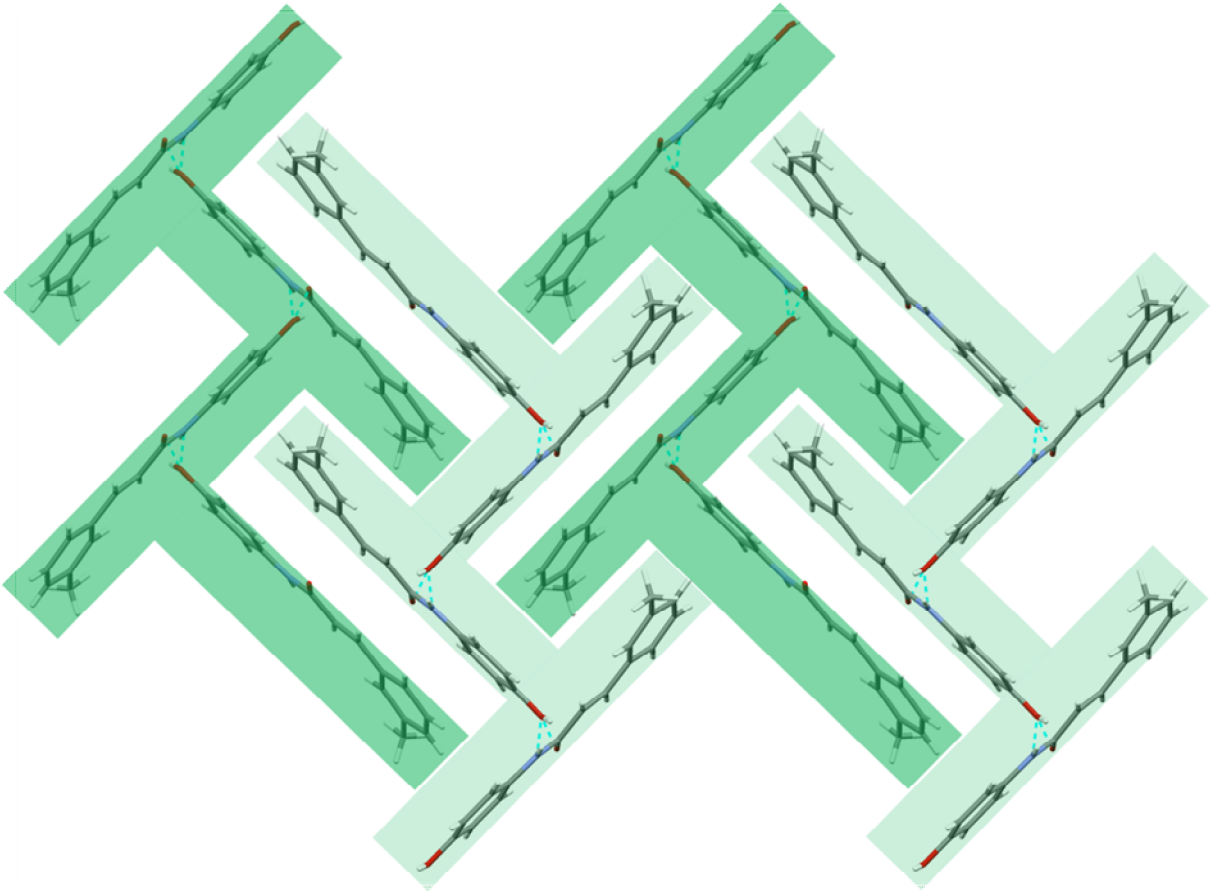

Figure 3-6 : Crystal structure of **2** viewed along the *a*-axis. The green and light green highlighted molecules for **2** are related to each individual herring-bone network via N-H···O and O-H···C=O hydrogen bonds. The blue dash lines indicate the hydrogen bonds.

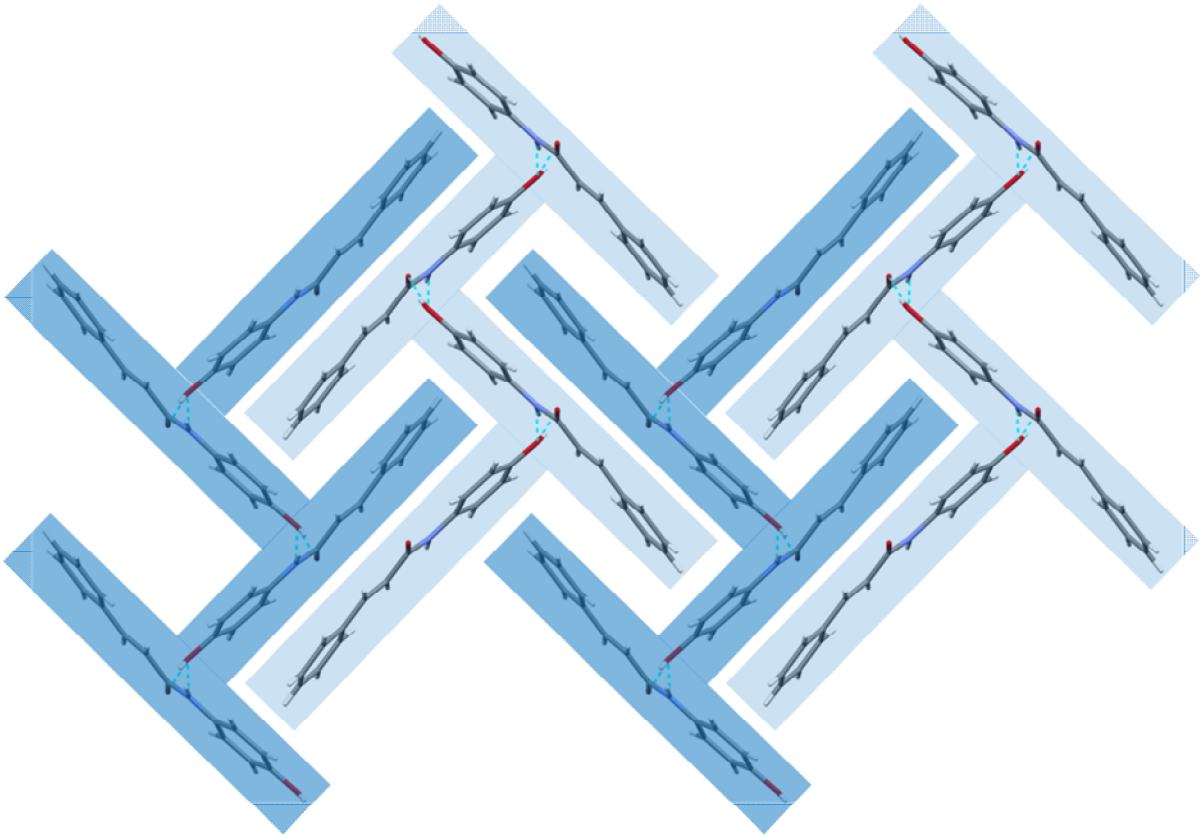

Figure 3-7 : Crystal structure of **3** viewed along the *a*-axis. The blue and light blue highlighted molecules for **3** are related to each individual herring-bone network via N-H···O and O-H···C=O hydrogen bonds. The blue dash lines indicate the hydrogen bonds.

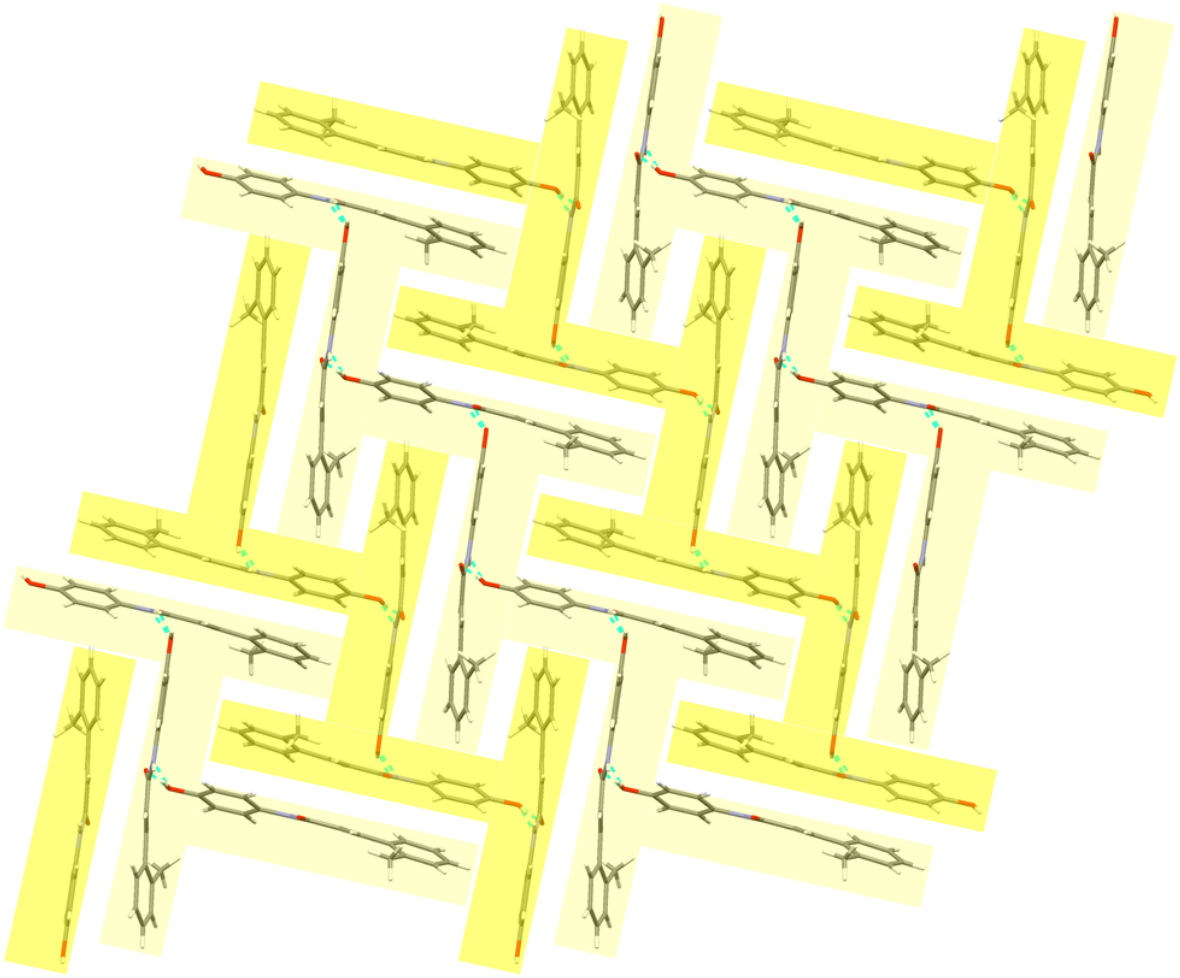

Figure 3-8 : Crystal structure of **4** viewed along the *b*-axis. The yellow and light yellow highlighted molecules for **4** are related to each individual herring-bone network via N-H···O and O-H···C=O hydrogen bonds. The blue dash lines indicate the hydrogen bonds.

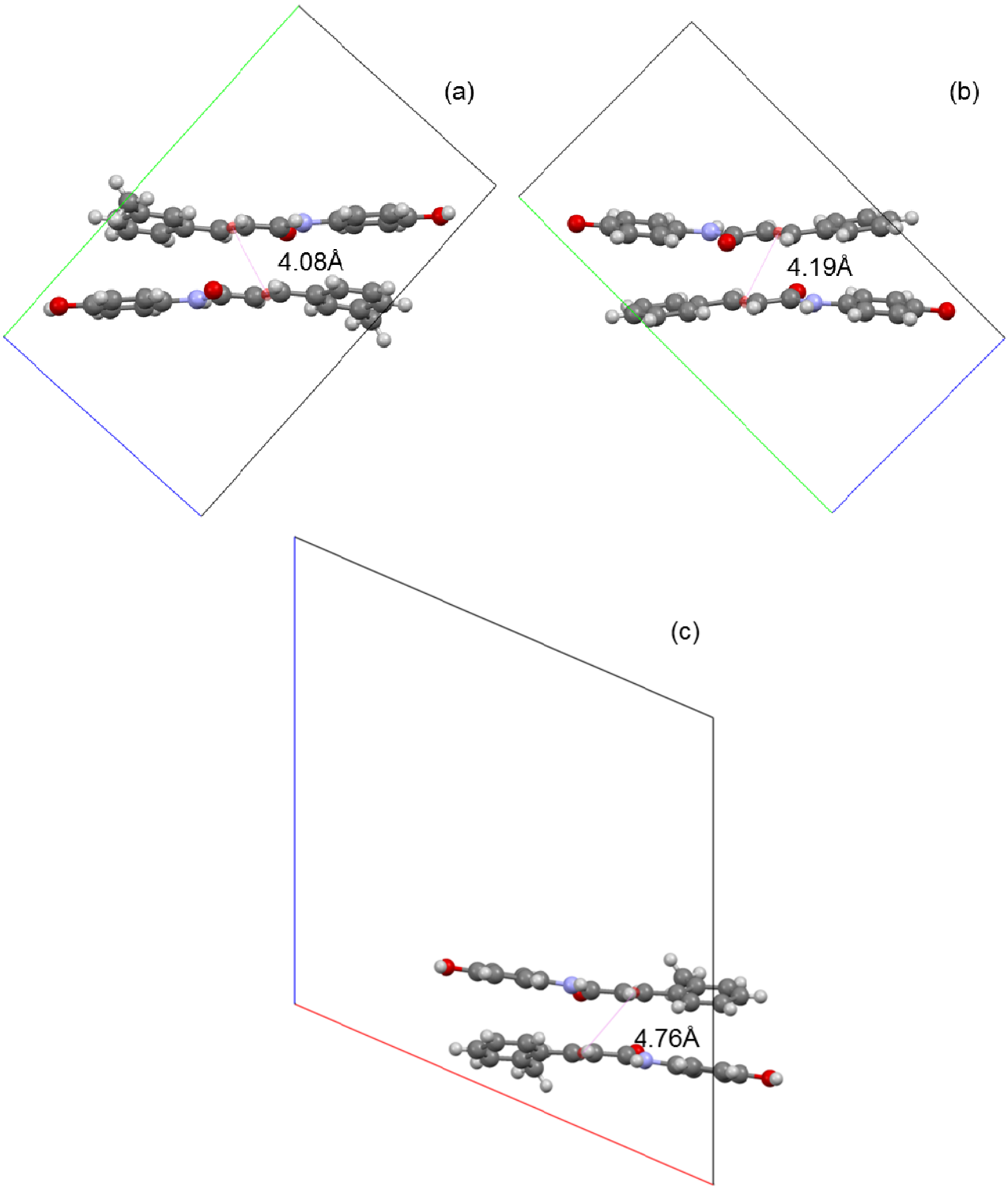

Figure 3-9 : Molecular packing of two adjacent molecules of (a) **2**, (b) **3**, and (c) **4**. The red sphere indicates the center of the double bond.

To determine the possibility for dimerization to proceed, overlap parameters for the alignment of adjacent molecules of **2-4** were also measured. Table 3-2 lists the overlap parameters for all derivatives. θ_1 for **2**, and **3** are 0.0°, and **4** as the angle of 80.1°. Compared with the ideal degree for θ_2, **1** mentioned in Section 3.4.1 possess the nearest amount which is 101.1°, followed by **2** (127.1°) and **3** (126.9°), and **4** shows the largest amount, which is 134.0°. For θ_3, **3** (81.0°) has the closet amount compared to the ideal degree, followed by **2** (72.6°), and **4** has the smallest amount, which is 38.4°. From these results of the overlap parameters of the olefins, it is apparent that **4** have the lowest possibility for photodimerization to proceed due to the lack of parallelism of the double bonds and the gap from the ideal degree of the parameter.

On the other hand, there is no major difference between the overlap parameters of **1** which photodimerize and **2** and **3** which do not photodimerize. Therefore, along with **1**, it can be said that **2** and **3** also satisfies the Schmidt's rule from both double bond distance and overlap parameter. Thus, these three derivatives have the possibility to photodimerize in the crystal state, but actually, only one derivative dimerized. Therefore, the difference in photostability cannot be explained only by the overlap parameters and the satisfaction of the Schmidt's topochemical postulate in this case.

Table 3-2 : Overlap parameters for the alignment of adjacent molecules.

Compound	θ_1	θ_2	θ_3
2	0.0	127.1	74.6
3	0.0	126.9	81.0
4	80.1	134.0	38.4

3.4.3. Determination of Reaction Cavity

The crystal structures of derivative **1**, **2** and **3** are similar and cannot provide an answer to the difference in photoreactivity by comparing them. Especially, **2** and **3** are found to be one of the rare examples where the potentially reactive double bonds satisfies the Schmidt's topochemical postulate but do not react by photo irradiation, as shown in other examples also.[94,167] Therefore, another parameter should be needed to compare the difference between the photostability from a different point of view, and we paid attention to the "Reaction Cavity".

The reaction cavity can be defined as the space around the reactive group in a crystal. Reactions with geometries that do not fit within the cavity built are assumed to be strongly disfavored. The influence of reaction cavity, also meaning the available cavity space in the crystal lattice with respect to the particular molecular volume for reaction to proceed, has been studied for some organic solid-state reactions.[91,151,168–172]

And for some compounds that possess potentially reactive double bonds which the separation distances in-between 4.2 Å in the crystal state and do not undergo dimerization upon photo irradiation, is said to be able to understand by invoking the reaction cavity concept. [97,100,104,105,108]

But in these examples, the reaction cavity is used only as a general idea for the assumption in the difference in photoreactivity, and there isn't a detailed discussion of size or the shape of the created cavity and correlation with photoreactivity. To figure out the differences in behaviors of cinnamic amide derivatives against photoirradiation and the following reaction, the size and the shape of reaction cavity was calculated and were determined qualitatively.

To determine the size and the shape of the reaction cavity, the molecule was divided into three sections (Figure 3-10). The first divided section is the phenyl group located on the end of the cinnamic acid moiety including the methyl group for **1**, **2**, and **4**. The second section is the phenol group, where the selected atoms are the phenyl ring and the hydroxide group. The third section will be the cavity around the moiety connecting the two sections, which is the amide group and the double bond. Each section's cavity size was calculated individually for derivative **1**-**4**. The volume of each cavity was calculated by the summation of

the volumes allotted to the grid points in the cavity.

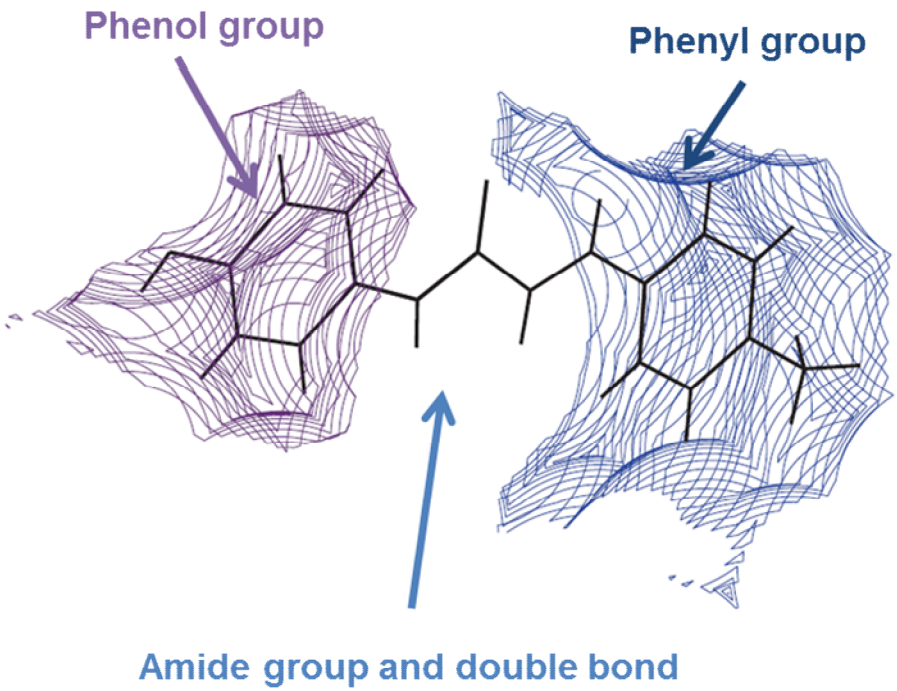

Figure 3-10 : A drawing of the cavity for the divided section of **1**, (a) the phenyl group (blue line), (b) phenol group (purple line), and (c) amide group and double bond.

The cavities of **1** had the volume of 46.4 $Å^3$, 30.1 $Å^3$ and 30.7 $Å^3$ for each section respectively, and the total size is 107.2 $Å^3$. For **2**, the volumes for each section are 35.9 $Å^3$, 29.6 $Å^3$ and 31.1 $Å^3$ and for **3** are 32.9 $Å^3$, 27.3 $Å^3$ and 29.5 $Å^3$ respectively. The total cavity size is 96.6 $Å^3$ for **2** and 89.7 $Å^3$ for **3**. For derivative **4** which the distance and the overlap parameters are beyond the Schmidt's criteria are 29.3 $Å^3$, 32.6 $Å^3$ and 11.1 $Å^3$ respectively, and the total size of 73.0 $Å^3$.

Figure 3-11 shows the total volume of reaction cavity for each derivative. Comparing the total volume, derivative **1** is found to possess the largest cavity among the four derivatives. More than that, the major difference in the cavity size is observed within the first section, which is the cavity around the phenyl group located at the end of the cinnamic acid moiety. Therefore, the reaction cavity volume and the cavity around the phenyl group must have some correlation with the difference in photoreactivity.

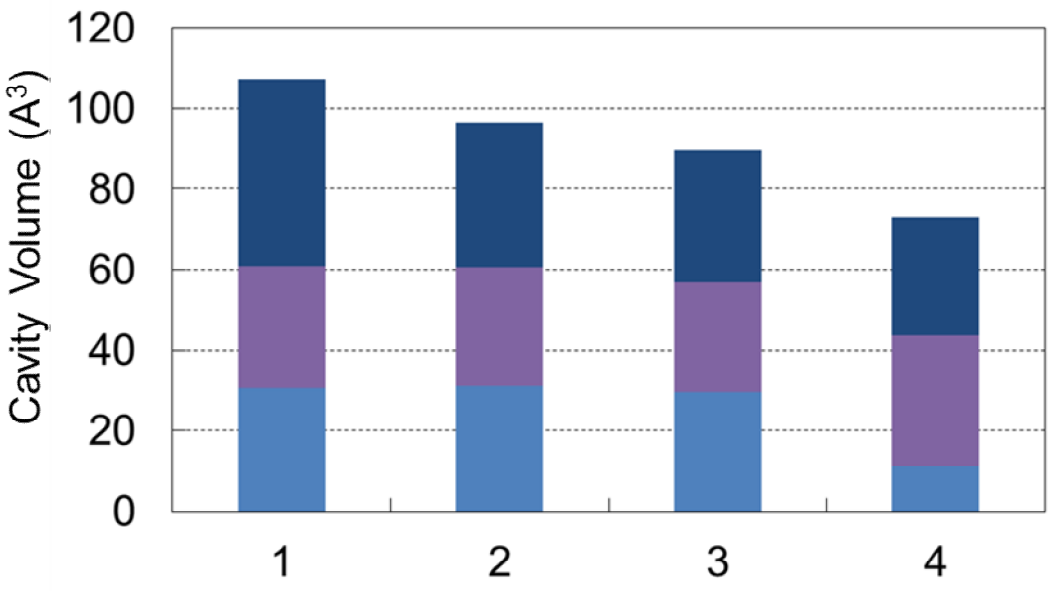

Figure 3-11 : Total volume of reaction cavity for cinnamic amide derivative **1**-**4**. The (a) volume of phenyl group colored in blue, the (b) phenol group colored in purple, and (c) amide group and double bond colored in light blue.

Figure 3-12 shows the superposition of packed molecule of **1** and its photodimer **7**. From the figure, the major difference in molecular shape of the largest move for photodimerization to proceed is found to be around the phenyl group. This is in good relation with the result of the section which possesses the largest difference among the derivatives. So next, the shape of “Reaction Cavity” around the phenyl group was compared in detail.

To determine the differences in cavity shape for each derivative, the cavity around the phenyl group viewed from two directions, A and B (Figure 3-13). The cavity around the phenyl group was drawn overlapped within each molecule with the pink line. And the partial structure of the phenyl group from the position of the photodimer also overlapped in the drawing in a light blue line. Since photodimerization did not proceed for **2** and **3**, the structure if the photodimerization proceeded is overlapped within the drawing in a light blue line. The position of the expected structure of **2** and **3** is estimated from the relation between **1** and **7**.

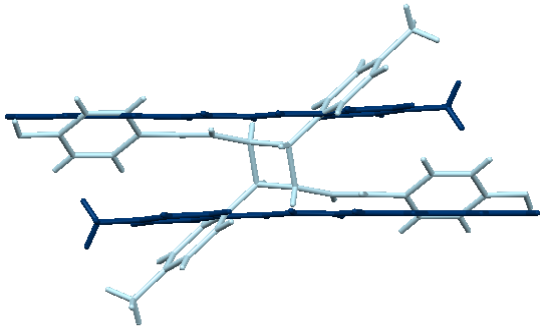

Figure 3-12 : Overlap of cinnamic amide derivative **1** (dark blue) and the corresponding photodimer **7** (light blue)

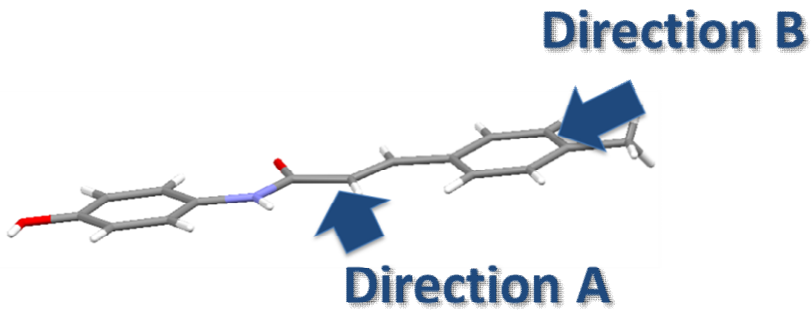

Figure 3-13 : The two directions (Direction A and Direction B) which the cavity shape was observed.

From comparing the cavity formed from **1** and the position of the overlapped structure of **7**, it can be seen that **7** mostly fits in the cavity made from **1** (Figure 3-14 (a), (b)). So it can be said that 1 possesses good cavity shape and volume to tolerate the molecular movement when photodimerization proceed.

The cavity shape for photostable derivatives **2** and **3** were also determined in the same way. The drawings show that a part of the phenyl group of expected photoproduct would be located out of the cavity (Figure 2-11 (c)-(f)). Therefore, it can be said that there is not enough cavity for **2** and **3** with suitable shape for the photodimerization to proceed. And for this case, the lack of cavity is the reason why **2** and **3** are photostable even they have good molecular overlap in the crystal and satisfying the Schmidt's topochemical postulate. Thus, the "Reaction Cavity" can be said to govern photostability in this case.

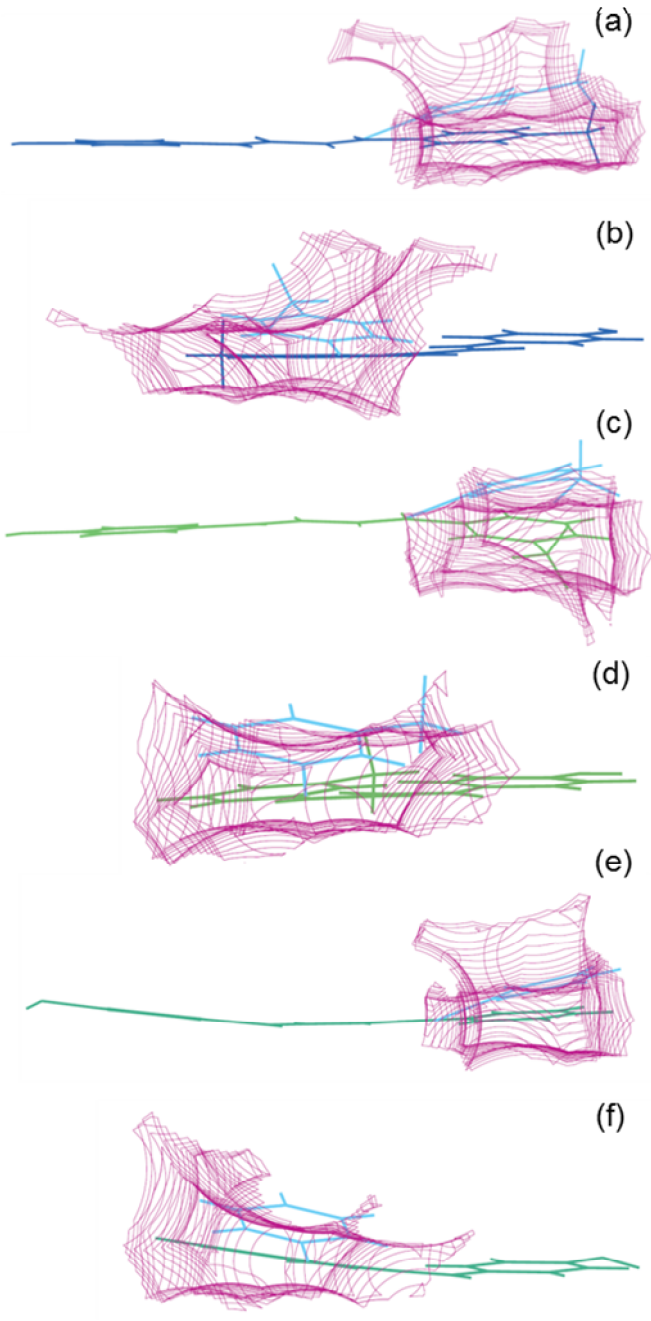

Figure 3-14 : A drawing of the overlap between monomer and the photodimer or an expected photodimer structure for (a) **1** from direction A, (b) **1** from direction B, (c) **2** from direction A, (d) **2** from direction B, (e) **3** from direction A, and (f) **3** from direction B.

3.5. Concluding Remarks

The differences of photostability between novel cinnamic amide derivatives and correlation with its crystal structure were determined. Derivative **1** which degrades by photoirradiation was observed to precede [2+2] photodimerization in the solid-state. On the other hand, derivatives **2-4** were intact against photoirradiation. The photostability was determined from both static environment and dynamic environment in the crystal structure. From static environment (satisfaction of Schmidt's rule and overlap parameters), we were not able to seek the difference between derivatives since **1**-**3** all resulted in the fulfillment of the Schmidt's topochemical postulate. From dynamic environment (area in which atomic movements tolerate), we were able to find the difference in the size and the shape of the space around the reactive group by calculating the "Reaction Cavity". This study clarifies the importance of not only fulfilling the static environment but also the suited dynamic environment for solid-state reaction to proceed. Calculation and visualization of "Reaction Cavity", should become a powerful and important tool for supplementing the Schmidt's topochemical postulate, and also has the possibility to expand for other solid-state photochemical reactions

Chapter 4

Polymorphic Transformation of Cinnamic Amide Derivative and Differences in Photoreactivity

4.1. Abstract

Polymorphic transformation of cinnamic amide derivative and difference in photoreactivity was determined from crystal structure analysis. Existence of two phases of cinnamic amide derivative **8** was determined from thermal analysis and in detail by simultaneous measuring of XRD and DSC. The original phase named phase **A**, was stable against photoirradiation and the crystal structure determined that the conformation does not fulfill the Schmidt's topochemical postulate. On the other hand, phase **B** which was obtained by thermal transformation, showed progress of [2+2] photodimerization in the solid-state. From *ab initio* crystal structure analysis of phase **B**, two possibilities of crystal structure (result I and result II) was observed. And from the crystal structure analysis of photodimer obtained, result I was determined as the structure of phase **B**. The difference between the two results obtained were analyzed from the viewpoint of dynamic environment, and found that the difference in photoreactivity can be accounted with toleration of the molecular movement during photodimerization. The result reveals that observation of dynamic environment was also found to be a helpful tool for determining and

scrutinizing the result of the *ab initio* crystal structure analysis.

4.2. Introduction

Crystal polymorphism of the organic compounds is an extremely attractive topic in material science and medical chemistry. The main reason for the topic being attractive is that because of the different arrangement of molecules in the crystal, polymorphs can exhibit different properties. The properties are both chemical and physical perspective, such as melting point, particle size, shelf life enhancement, bioavailability, dissolution rates, pharmacological activity, etc. And among the properties that polymorphs can differ, photoreactivity has attracted greater attention, due to the fact that exposure to light can occur anytime anywhere, which is a crucial point to control for commercial use.

The difference in photoreactivity between the polymorphs is mainly due to the difference whether a reaction proceeds in the solid state by photoirradiation or not. Among the diverse photoreactions in the solid state, [2+2] photodimerization is one that has been most extensively studied as described in other Chapters. According to the Schmidt's topochemical postulate, reaction in the crystal lattices occur with minimum atomic motions, and thus the arrangement of molecules in the crystal lattice can permit prediction to the progress of photochemical reactions and the out coming compound. Therefore, the satisfaction of Schmidt's topochemical postulate will also be one of the key factors in determining the possibility of difference in photoreactivity among the polymorphs.

In this work, we studied the polymorphic system of a novel cinnamic amide derivative. The selected derivative was also found to afford lightfastness when used as a developer in the thermosensitive paper. The phase transition between the polymorphs was observed by simultaneous measurement of Differential Scanning Calorimetry (DSC) and X-Ray Diffraction (XRD).[173174] The crystal structure of the polymorphs were obtained by single crystal structure analysis or by *ab initio* crystal structure analysis, and found the difference in fulfillment of the Schmidt's topochemical postulate, followed by the difference in photoreactivity.

4.3. Experimental

4.3.1. Synthesis of Novel Cinnamic Amide Derivatives

Materials and equipment

All chemical compounds used were available from common commercial sources and used without further purification. Detail synthesis method for typical four derivatives is shown in the following paragraphs.

^{1}H NMR and ^{13}C NMR spectra were recorded on a JEOL JNM-AL-400 FT NMR spectrometer. Melting points were recorded using Electrothermal IA 9300 digital melting point instrument.

*Synthesis of cinnamic amide derivative **8***

In a round bottom 1 L flask equipped with a thermometer, 2-amino phenol (48.0 g, 0.44 mol) and sodium hydrogen carbonate (37.0 g, 0.44 mol) was added to a mixture of acetone (600 mL) and water (200L). To the mixed solution, cinnamoyl chloride (66.6 g, 0.4 mol) was added and the solution was stirred over for two nights at room temperature. By evaporating the solvent and recrystallizing the residue from methanol, gave cinnamic amide derivative **8** ((E)-N-(2-hydroxyphenyl)-3-p-tolylacrylamide) (62.0 g, yield 65 %). mp 166-168°C; ^{1}H NMR (400MHz, acetone-d_6, 297K, σ_{TMS}=0 ppm) σ=6.72 (d, 1H), 6.94 (dd, 1H), 7.03-7.12 (m, 2H), 7.40-7.48 (m, 3H), 7.58 (d, 1H), 7.68 (dd, 2H), 7.75 (d, 1H); ^{13}C NMR (100MHz, DMSO-d_6, 297K) σ= 118.8, 120.6, 121.5, 122.9, 126.7, 127.7., 128.8, 129.8, 130.8, 135.8, 142.9, 149.4, 165.9; (Found C, 75.44; H, 5.45; N, 5.78. Calc. for $C_{16}H_{15}NO_2$: C, 75.30; H, 5.48; N, 5.85%).

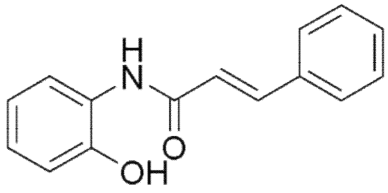

Scheme 4-1 : Molecular structure of novel cinnamic amide derivatives **8**.

4.3.2. Observation of Thermal Transformation

Thermal transformation was analyzed by Differential Scanning Calorimetry (DSC) using a TA Instruments Q2000 under dry N_2. The powder was weighed into an Al sample pan fitted with a clipped lid. The measurement was carried out from ambient temperature to 200°C at a heating rate of 10°C/min (1^{st} run), 200°C to 40°C for standing to cool, and 40°C to 200°C at a heating rate of 10 °C/min (2^{nd} run).

Thermogravimetry (TGA) was observed by using a Mettler Toledo TGA/DSC 1 under dry N_2. The measurement was carried out from ambient temperature to 500°C at a heating rate of 10 °C/min.

4.3.3. XRD-DSC Measurements

The simultaneous measuring apparatus for XRD-DSC consisted of a specific heat-flux type of Rigaku Thermo Plus DSC8320 (DSC) modified and combined with an Rigaku RINT-UltimaIV X-ray diffractometer (XRD). The XRD-DSC measurements were carried out from ambient temperature to 200°C at a heating rate of 10°C/min (1^{st} run), 200°C to 40°C for standing to cool, and 40°C to 200°C at a heating rate of 10 °C/min (2^{nd} run). The specimen (approximately 10 mg) was mounted on a square aluminum container (7 mm x 7 mm and 0.25 mm in depth). A line shape X-ray source was operated at 40 kV and 40 mA and the data were collected in the range of $5 < 2\theta < 40°$ with an interval of 0.02° and a scan speed of 1°/min. With a temperature scan rate of the DSC measurements, the change of sample temperature during each XRD scan corresponds to 30 °C upon temperature elevation, and 5-30 °C while temperature decrease. The θ and 2θ calibration was done using a silicon standard.

4.3.4. Photoirradiation test at Solid state

50mg of cinnamic amide derivative **8** was dissolved in 2.5g of acetone, dropped on a glass plate and dried to obtain test samples. Another glass plate placed on top of the test sample and clipped, the sample was installed inside a Xenon lightfastness test machine (Shimadzu Corporation: Suntester XF-180), and 300W/m^2 of light was irradiated. After the irradiation test, the cinnamic

amide derivatives were extracted and diluted from the glass plate with methanol, and the percentage of the residue derivative was calculated from the area% of HPLC measurement results.

4.3.5. X-ray measurement and refinements

The single crystal X-ray diffraction data were collected at ambient temperature in ω-scan mode with a R-AXIS RAPID imaging plate camera (Rigaku) using Mo Kα X-ray obtained from a rotating anode source with a graphite monochromator. The initial structures were solved by using direct methods with *SHELXS 97*[165] and refined on F_0^2 with *SHELXL 97*[165]. All the non-hydrogen atoms were refined anisotropically.

4.3.6. *Ab initio* Crystal Structure Analysis of x from Powder X-ray Diffraction Data

The powder X-ray diffraction pattern of **8-B** was indexed using the program X-Cell[175] (M20 = 21.9[176]), giving the following unit cell with monoclinic symmetry: a = 6.078 Å, b = 3.9653 Å, c = 25.4535, β = 91.628. From the systematic absences and consideration of the unit cell volume (corresponding to Z = 2), the space group was assigned $P2_1/c$. The profile was fitted using the Pawley method[177] in the program DASH. The simulated annealing structure solution calculation was carried out using the program DASH, and the molecular model was taken from the crystal structure of **8-A**. Subsequent Rietveld refinement[178] was carried out using the GSAS[179] program. In the Rietveld refinement, standard restraints were applied to bond lengths and bond angles, planar restraints were applied to the aromatic rings, and a global isotropic displacement parameter was also refined. The final Rietveld refinement gave the following parameters: a = 6.08291(13) Å, b = 3.96797(6) Å, c = 25.4915(11) Å, β = 91.5402(17)°, V = 615.06(4) Å^3, R_{wp} = 2.77%, R_p = 1.96%, R_F^2 = 4.13% (2θ range, 5.0-69.99°; 6500 profile points; 126 refined variables).

4.4. Results and Discussion

4.4.1. Thermal Transformation of Cinnamic Amide Derivative 8

Since the novel cinnamic amide derivatives are an ordinary organic compound, there is a possibility to possess different polymorphs with different properties. Therefore, possibility of thermal transformation of novel cinnamic amide derivative was observed by DSC, TGA-DSC and XRD-DSC measurements.

DSC data obtained on heat-cool cycles starting is shown in Figure 4-1. On heating from room temperature to 200°C in a heating rate of 10°C/min, an exothermic peak is observed at 165.2°C. On cooling from temperatures above the exothermic peak, two endothermic peaks close to each other are observed. On heating the same sample for the second run, an exothermic peak at a different from the first run is observed at 160.1°C. From this result, the existence of a polymorph is apparent for cinnamic amide derivative **8**.

TGA data on heating **8** between room temperature and 500°C are shown in Figure 4-2. Sample mass is constant up to around 200°C then decrease at higher temperature with the onset temperature of 263.5°C. The TGA results show that the polymorphic transitions observed in the DSC measurement are at lower temperature and the sample melting do not involve any loss of weight.

Simultaneous measurements of DSC and X-ray powder diffraction (XRD-DSC) were performed on powder crystals to investigate the phase transition. Figure 4-3 shows the result of a XRD-DSC measurement for **8**; the XRD patterns correspond to each area on DSC curve with the same temperature and represented on the left side. By thermal elevation, the powder pattern (blue line) disappears around 180°C with melting (purple line), and by cooling, a new powder pattern (red line) gradually appears. The change in the XRD pattern before and after melting, which is the blue line and the red line, indicates that the original **8** has changed into another phase or a reaction proceeded by heat.

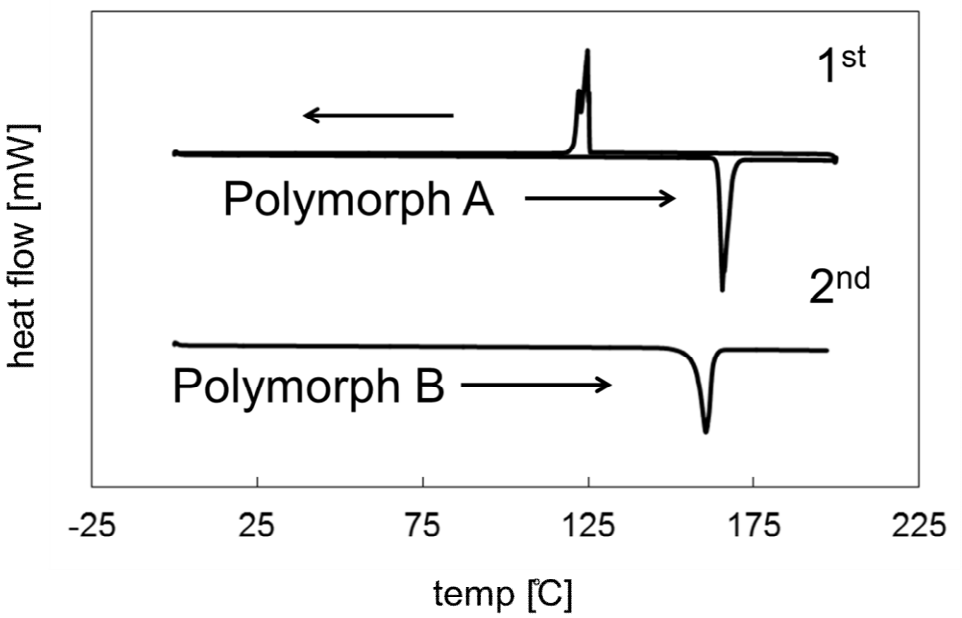

Figure 4-1: DSC curves on heating and cooling between room temperature and 200°C. The top curve shows the 1st run of heating and cooling, the bottom shows the 2nd run of heating.

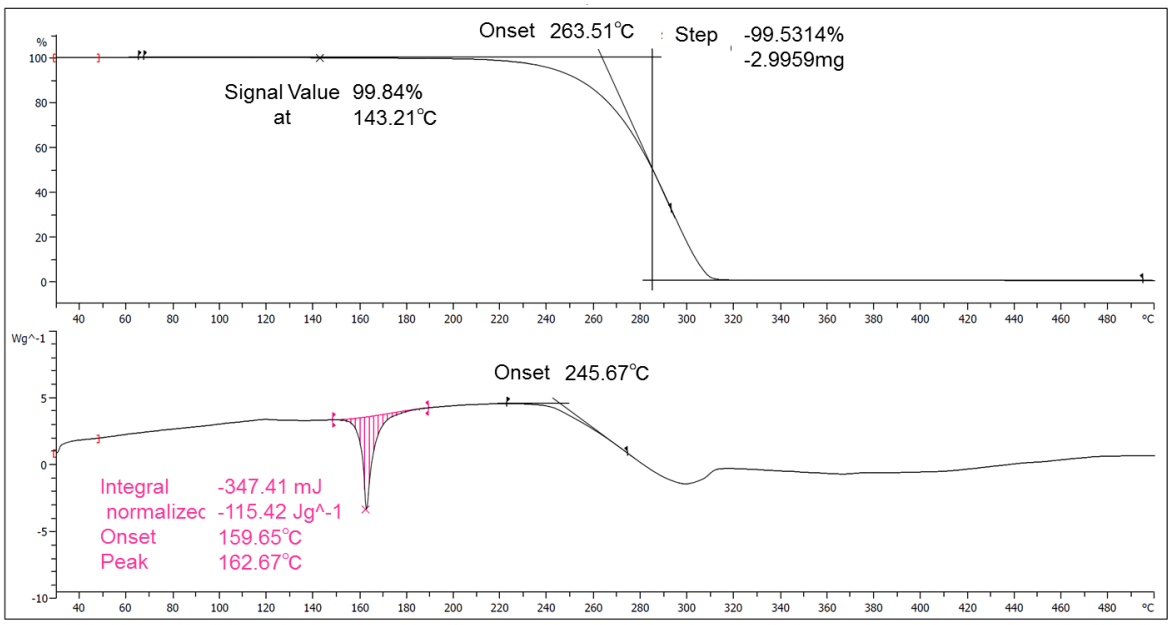

Figure 4-2: TGA/DSC plot of cinnamic amide derivative **8**. The top chart shows the TGA curves, and the bottom chart shows the corresponding DSC curves.

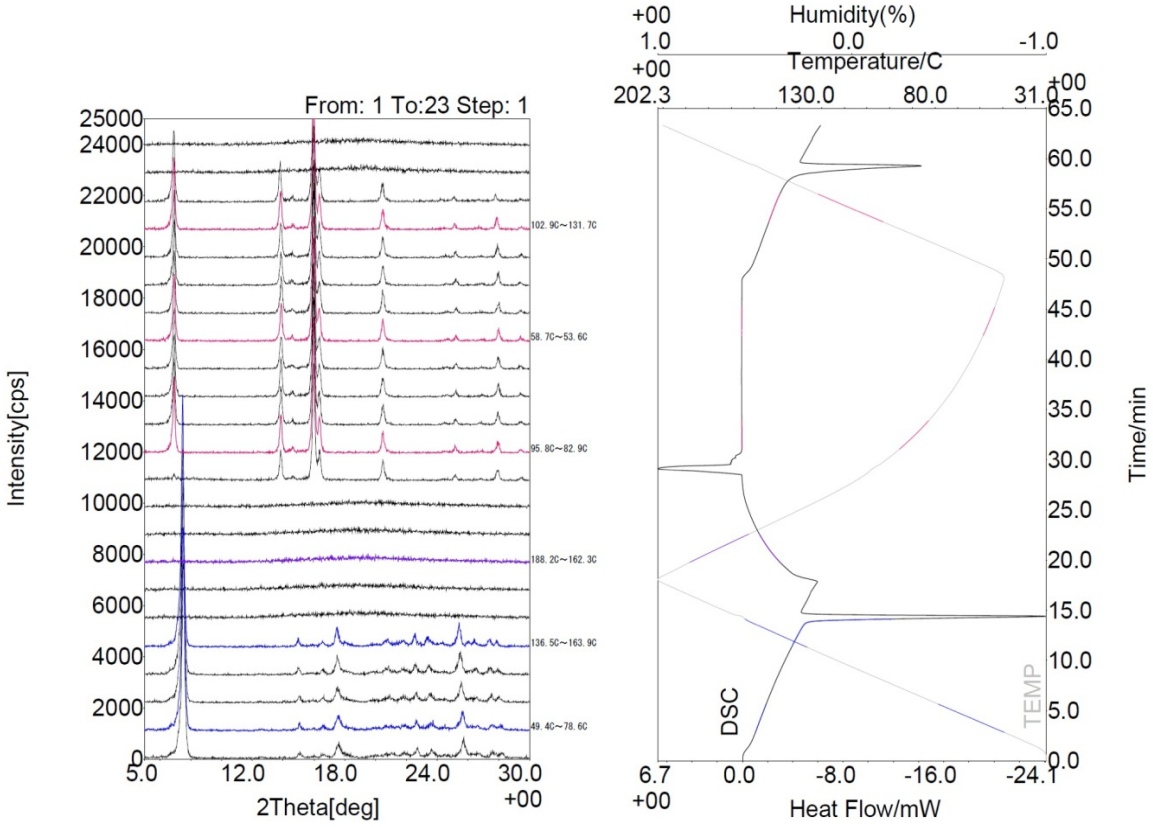

Figure 4-3: XRD-DSC analysis of **8**. The colored form of powder XRD patterns (left) correspond to the same colored areas of the DSC thermogram (right).

4.4.2. Preparation of Novel Phase of Derivative 8

If the sample which the powder pattern differed from the original phase is a polymorph of cinnamic amide derivative **8**, there is a possibility that it can be obtained by crystallization from different solvents. So, crystallization from various solvents such as acetone, methanol, ethanol, ethyl acetate was tested, and each crystal obtained was grinded and the XRD pattern determined. Unfortunately, all crystals obtained from the solvents tested resulted in the original pattern, as summarized in Table 4-1. Therefore, the only method the different XRD pattern of **8** observed was during the thermal analysis or the XRD-DSC measurement or in other words by thermal transformation so far.

To obtain the phase which possesses the different XRD pattern, **8** was melted in the same condition practiced in the XRD-DSC measurement. Powder crystals of **8** were placed in a sample tube, and heated in an oil bath for 170°C, and cooled gradually. The solid obtained after melting was grinded, and determined to possess the same XRD pattern with the **8** as shown in the XRD-DSC measurement.

Figure 4-4 shows the results of the ^{1}H NMR measurements before and after thermal transformation. The results determined that thermal reaction did not proceed, and the obtained powder had the same pattern with **8** before heating. From these results, the powder obtained by melting was determined as a different phase of **8**, and the thermal transformation was determined as a phase transformation.

Pictures of different phases of **8** are shown in Figure 4-5. **8-A** which is the original phase recrystallized from various solvents, looks white in color. On the other hand, **8-B** which is a phase obtained by thermal transition, looks pale in color, and shows difference in appearance.

Table 4-1: Solvents used for recrystallization of **8** and the obtained phase.

Solvent	Obtained Phase
Acetone	**8-A**
Chloroform	**8-A**
Ethyl Acetate	**8-A**
Ethyl Acetate / Hexane	**8-A**
Ethanol	**8-A**
Methanol	**8-A**
Toluene	**8-A**

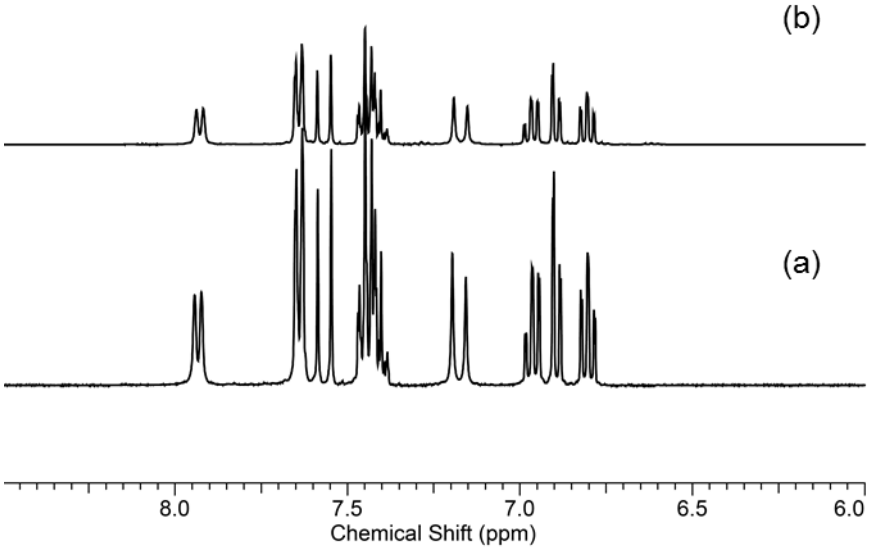

Figure 4-4: ^{1}H NMR results (a) before and (b) after thermal transformation.

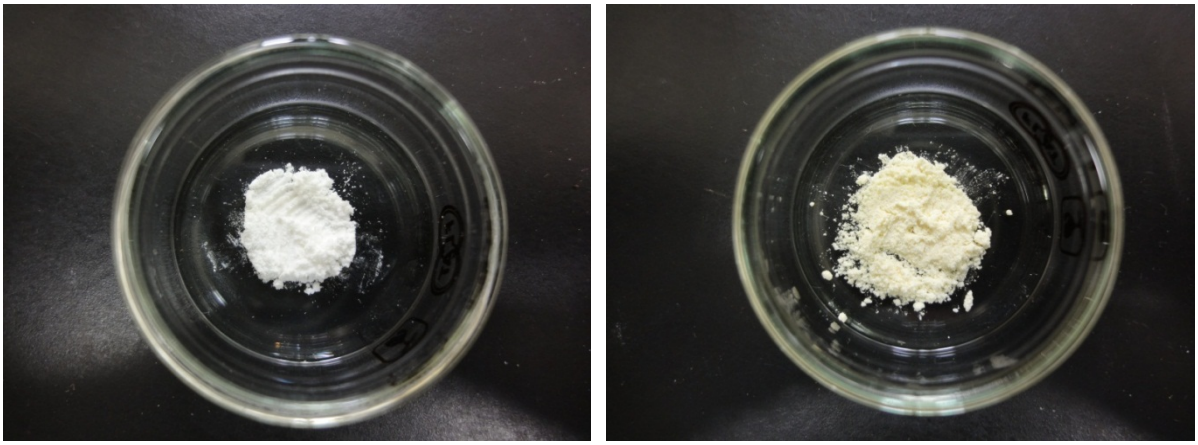

Figure 4-2 : Pictures of different phases of cinnamic amide derivative **8**. The left picture shows **8-A** and the right picture shows **8-B**.

4.4.3. Crystal Structure Analysis of 8-A

To determine the difference between the polymorphs, single crystal analysis was taken place. **8-A** was crystallized from slow evaporation of ethyl acetate solution, and confirmed the structure with single-crystal analysis. Figure 4-6 shows the crystal structure of **8-A**.

The carbon-carbon double bond is twisted from the attached benzene ring, the torsion angle of C=C-C=C being 13.03°. The two benzene rings are also twisted having an angel of 5.19°. The intermolecular carbon-carbon double bonds were twisted, and the distance between the centers of the olefinic double bonds are 4.81 Å (Figure 4-7). The distance in-between the double centers are beyond the Schmidt's criteria for solid state dimerization, so the photodimerization is not supposed to proceed in **8-A**.

The two adjacent molecules of **8** are stacked facing same directions from the point of cinnamic acid moiety. If the cinnamic acid moiety of the molecule is regarded as the "head", and phenol group the "tail", the adjacent two molecules are packed in head against head (head-to-head manner).

To determine the possibility for dimerization to proceed, overlap parameters for the alignment of adjacent molecules were also measured. The detailed explanation of overlap parameters are shown in Chapter 3. Table 4 lists the overlap parameters, and each value are 137.4° for θ_1, 121.7° for θ_2, and 46.6° for θ_3. From these results of the overlap parameters of the olefins, the progress of photodimerization is found to be rather hard due to the lack of parallelism of the double bonds and the gap from the ideal degree of the parameter.

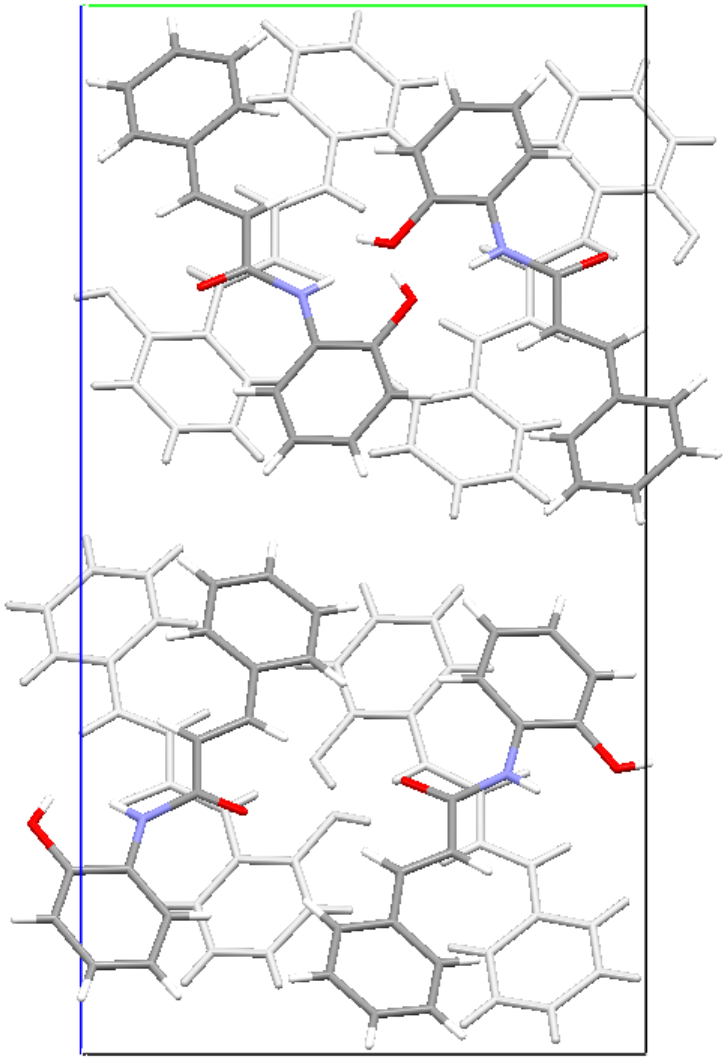

Figure 4-6: Crystal structure of **8-A** viewed along the *a*-axis. The colored molecules are on the front, and the light gray colored molecules are located on the back side of the cell.

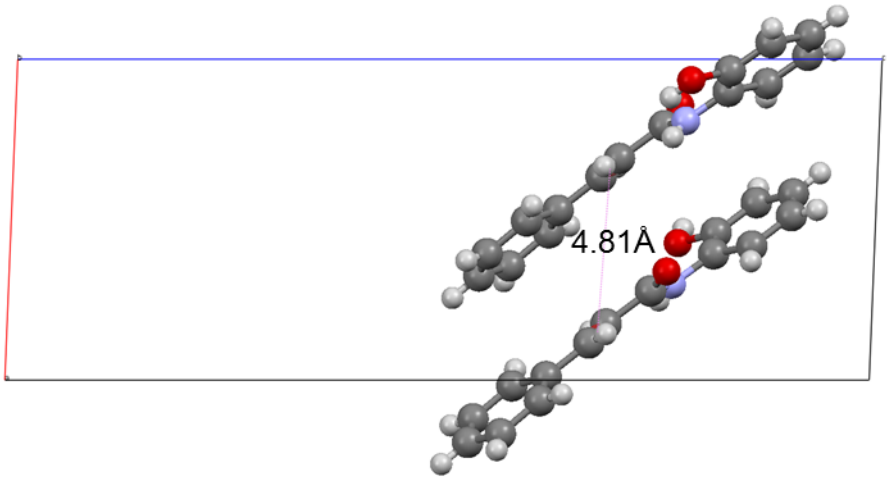

Figure 4-7: Molecular packing of two adjacent molecules of **8-A**. The red sphere indicates the center of the double bond.

4.4.4. Crystal Structure Analysis of 8-B

Unfortunately, single crystal of **8-B** was not able to obtain because it can only be obtained by thermal transition, and recrystallization from solvents all resulted in **8-A**. Therefore, *ab initio* crystal structure determination of **8-B** was taken place to determine the structure. To begin with the measurement of the powder X-ray diffraction, **8-B** was needed to grind conscientiously for more than 30 minutes since the powder was found to possess preferred orientation.

The powder X-ray diffraction pattern of **8-B** was indexed using the program X-Cell,[175] giving the following unit cell (M20 = 21.9[176]) with triclinic metric symmetry: a = 6.078 Å, b = 3.9653 Å, c = 25.4535 Å, β = 91.628°, V = 613.22 Å^3. Given the volume of this unit cell, and consideration of density, the number of formula units in the unit cell is assigned as Z = 2.

The structure determination first focused on space group *P*c. Profile fitting using the Le Bail method did not give a good fit (profile χ^2 = 35.60, intensity χ^2 = 288.40). Next, the structure determination on space group $P2_1$ but the profile fitting was worse than *P*c. The structure determination now focused on space group $P2_1/c$. The molecule is on the inversion center, and the head type arrangement and the tail type arrangement is mixed in 1 : 1 ratio. The profile fitting using the Le bail method was good resulting profile χ^2 = 13.90, intensity χ^2 = 37.49, showing that this space group has the highest possibility among the

other tested results.

As the molecule structure of **8** has pseudo-symmetry as shown in Scheme 4-2 and the result of structure determination on $P2_1/c$, there is a possibility that both two arrangements (head type, tail type) are mixed in the crystal structure. To regard the possibility of having two types of patterns of the adjacent molecules (head-to-head, head-to-tail), Z=2, space group $P2_1/c$ and 2 model molecules were injected and structure analysis were done.

The unit cell parameters and profile parameters obtained from the Le Bail fitting procedure were used in the following calculation of structure solution. The structure solution was carried out using the direct-space genetic algorithm (GA) technique incorporated in the program EAGER.

For the following structure solution, Rietveld refinement[178] was carried out using the GSAS program[179]. Standard restraints were applied to bond lengths and bond angles, planar restraints were applied to aromatic rings, and a global isotropic displacement parameter was used.

The final Rietveld refinement gave following parameters: a = 6.08291(13) Å, b = 3.96797(6) Å, c = 25.4915(11) Å, β = 91.5402(17)°, V = 615.06(4) Å^3, R_{wp} = 2.77%, R_p = 1.96%, R_F^2 = 4.13% (2θ range, 5.0 – 69.99°; 6500 profile points; 126 refined variables). The final Rietveld plot is shown in Figure 4-8 and crystal structures is shown in Figure 4-9.

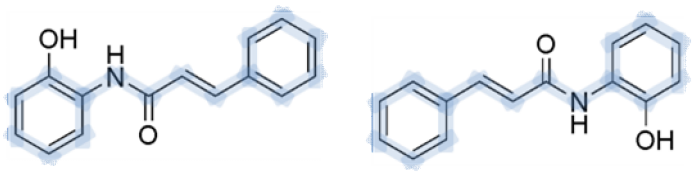

Scheme 4-2: Pseudo-symmetry of **8**.

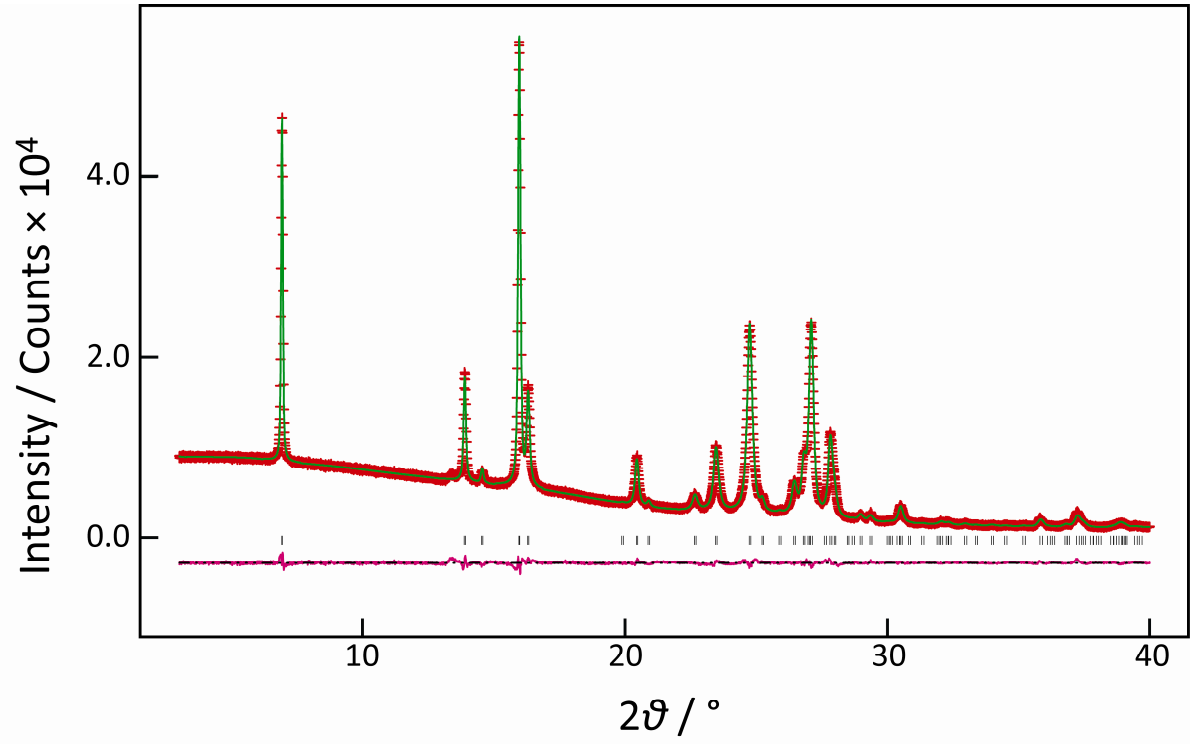

Figure 4-8: Final Rietveld refinement of **8-B**, showing the experimental powder X-ray diffraction pattern (+ marks), calculated powder X-ray diffraction pattern (solid line) and difference profile (lower line). Tick marks indicate peak positions.

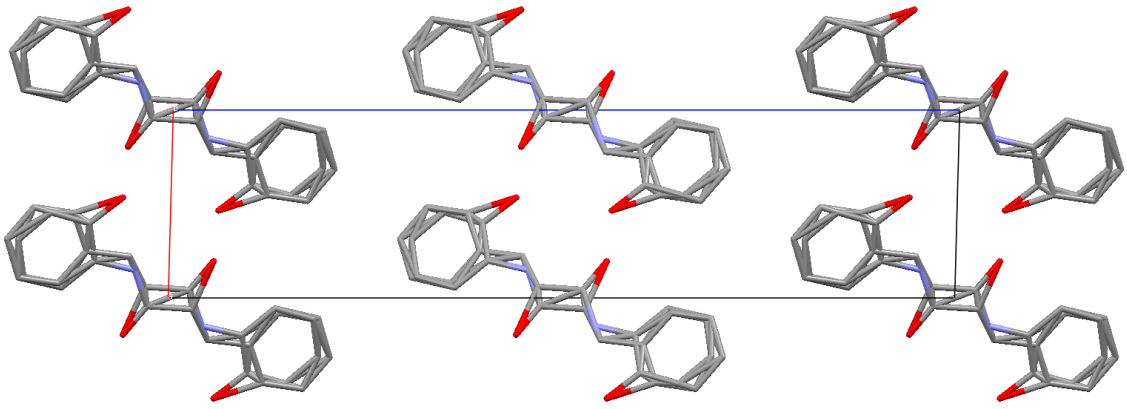

Figure 4-9: Crystal structure of **8-B** viewed along the *b*-axis. The hydrogen atoms are omitted in the figure.

The most fitted refinement included two types of arrangements (head and tail) for each molecule; the combination of the adjacent molecule should be one of four patterns. The four patterns of combination are head-to-head (H-H), head-to-tail (H-T), tail-to-head (T-H), and tail-to-tail (T-T). Since the H-T and T-H combination and H-H and T-T combination can be the reputation of same displacement in the molecule structure, the final structure must be one of the results named I and II. Result I will be the structure where the repetition of head-to-tail packing in the adjacent molecules are aligned, and result II will be the repetition of head-to-head packing in the adjacent molecules.

The double bond distance and the overlap parameter for each combination are listed in Table 4-2. The distance between the centers of double bond of the adjacent molecules are 3.97 Å, 5.72 Å, 3.91 Å, and 3.97 Å for H-H, H-T, T-H, and T-T respectively. θ_1 for all the combination are 0.0°, θ_2 is 123.39°, 147.53°, 96.80°, and 123.39°, and θ_3 is 84.97°, 75.02°, 69.25°, and 84.97°, respectively. From this result, it is apparent that H-H and T-T are equal in arrangement. And it is also obvious that H-H (and T-T) and T-H fulfills the Schmidt's topochemical postulate, and this combination has the possibility of photodimerization to proceed.

The molecular packing of Result I is illustrated in Figure 4-10, and only the T-H combination squared in blue has the possibility for dimerization to proceed. The photodimer obtained from this structure is assumed to be the α-type. From the molecular packing of Result II illustrated in Figure 4-11, since the combination of H-H and T-T are found to be equal, each pair of the adjacent molecules has the possibility for photodimerization to proceed, and resulting in the β-type.

From the *ab initio* structure analysis of **8-B**, two possible results were obtained as the crystal structure. And both structures were found to possess photodimerizable packing of molecules, resulting in α-type photodimer for Result I and β-type photodimer for Result II. Therefore, no matter which structure that **8-B** belongs to, the difference against photoirradiation between the polymorphs was indicated.

Table 4-2: Double bond distance and overlap parameter for each combination from the *ab initio* structure analysis of **8-B**.

combination	distance [Å]	θ_1 [deg]	θ_2 [deg]	θ_3 [deg]
head-to-head	3.97	0.00	123.39	84.97
head-to-tail	5.72	0.00	147.53	75.02
tail-to-head	3.91	0.00	96.80	69.25
tail-to-tail	3.97	0.00	123.39	84.97

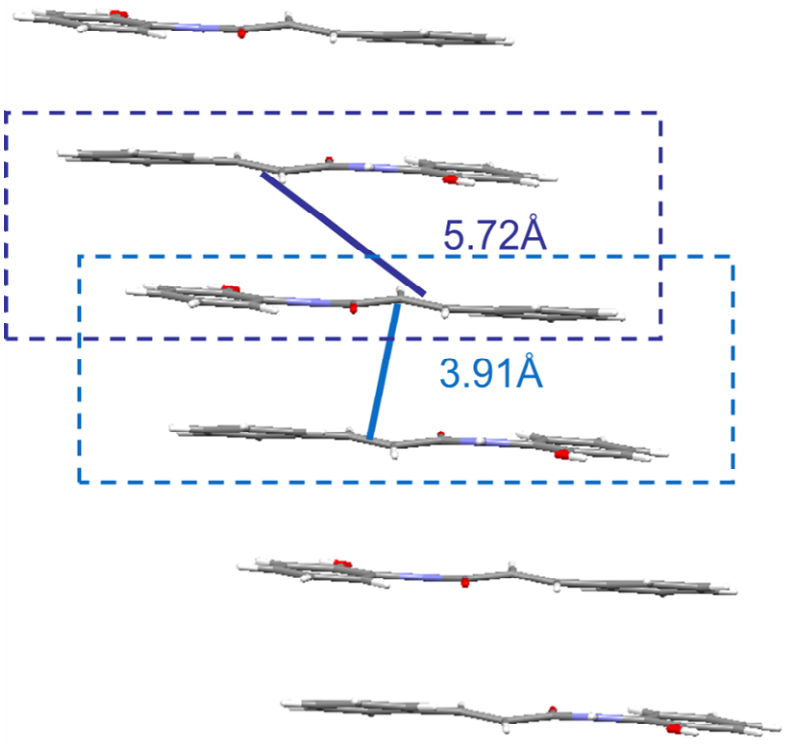

Figure 4-10: Molecular packing of adjacent molecules of result I (repetition head-to-tail).

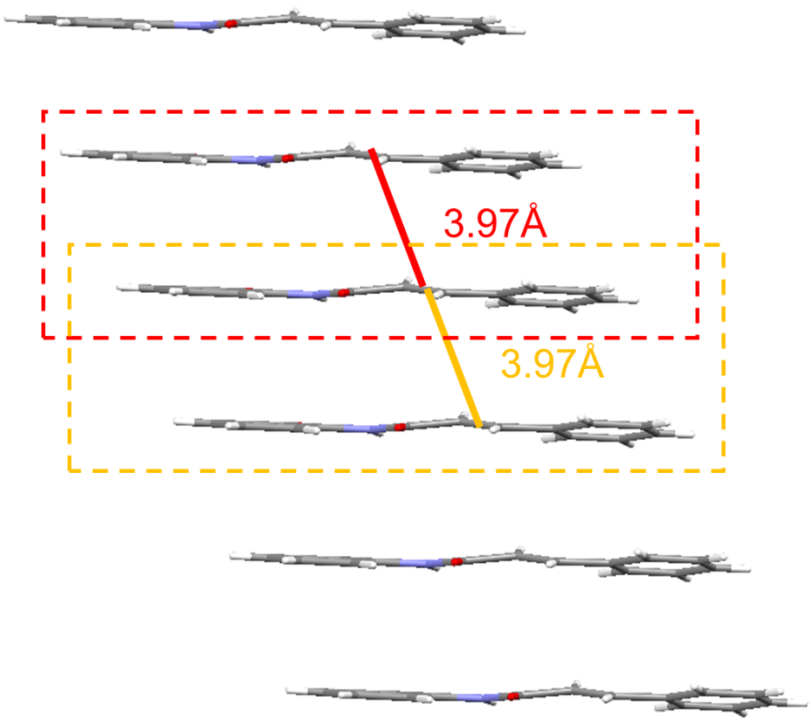

Figure 4-11: Molecular packing of adjacent molecules of result II (repetition head-to-tail).

4.4.5. Difference of Photoreactivity Between Phases of Cinnamic Amide Derivative 8

As shown in Chapter 2 and 3, cinnamic amide derivatives possess different reactivity against photoirradiation between the derivatives. As the reason described in detail in Chapter 2, the difference arises from the satisfaction of the Schmidt's topochemical postulate, and from the point of dynamic environment. From the crystal structure analyses of the different phases of derivative **8**, the difference of photoreactivity was indicated. If there is a difference against photoirradiation between polymorphs, the reason can be assumed to be also arisen from the above two reasons in the crystal structures. Therefore, photoirradiation test against two phases of **8** was taken place.

To observe the behavior during light irradiation, **8-A** and **8-B** was exposed to light in the solid state by using SUNTESTER at ambient temperature. Since the obtained amount of **8-B** was scarce through thermal transition, the reaction was monitored by HPLC measurements which can detect with lesser amount than NMR. The light irradiation was continued until no further changes were observed in the HPLC pattern.

The HPLC results for (a) 32 hours, (b) 64 hours and (c) 144 hours of photoirradation for **8-A** is shown in Figure 4-12, and for **8-B** is shown in Figure 4-13. The result of **8-A** clarifies that no change observed during photoirradiation. The result of **8-B** clarifies that the peak originated from **8** gradually decreases and peak of another single product increases.

Figure 4-14 and Figure 4-15 shows the transition in area % of cinnamic amide derivative sample against photoirradiation time throughout the test. The blue line shows the percentage of derivative **8** and the light blue line shows the total area% of other peaks observed from the test samples. From the test result, no change in residual percentage was observed for phase **A**, and the percentage maintained 100% up to 172 hours of test time. On the other hand, the area % of the peak originated from **8** gradually declines by photoirradiation, and a peak of another product appears by photoirradiation to phase **B**. The area % of **8** reaches approximately 40% after 150 hours of irradiation time. It should be noteworthy that photoirradiation against cinnamic amide derivative **1** described in Chapter 2, reached up to 0% after 4 hours of irradiation under same

condition. Therefore, this change observed for cinnamic amide derivative **8** can be said to proceed slower and without full accomplishment compared to derivative **1**. One of the reasons that can be possible for the less accomplishment might be due to the orientation of **8-B** since the orientation in one particular direction, and the irradiation was not enough in that direction.

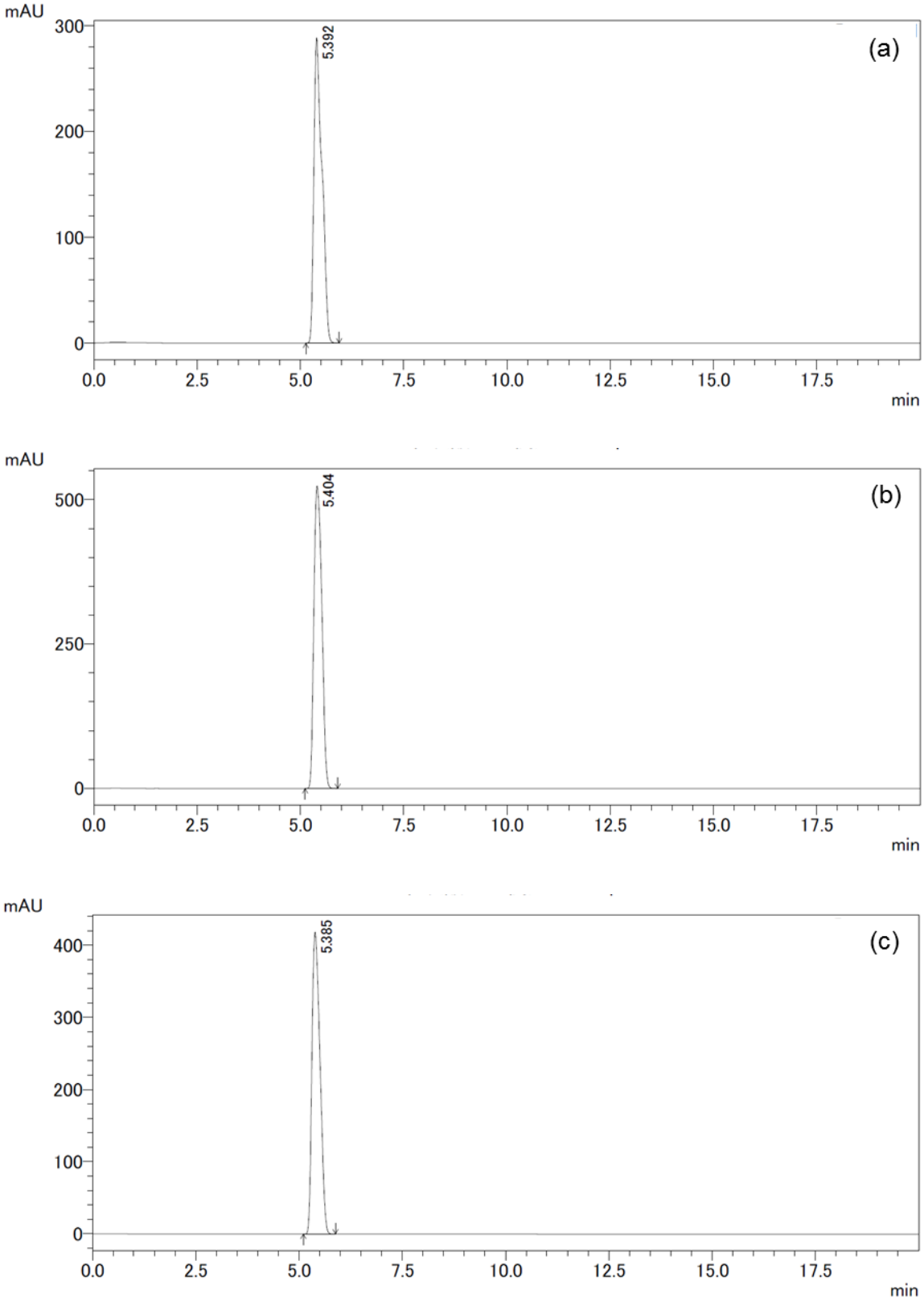

Figure 4-12: HPLC measurements of **8-A** after (a) 32 hours, (b) 64 hours and (c) 144 hours of photoirradiation in the solid state.

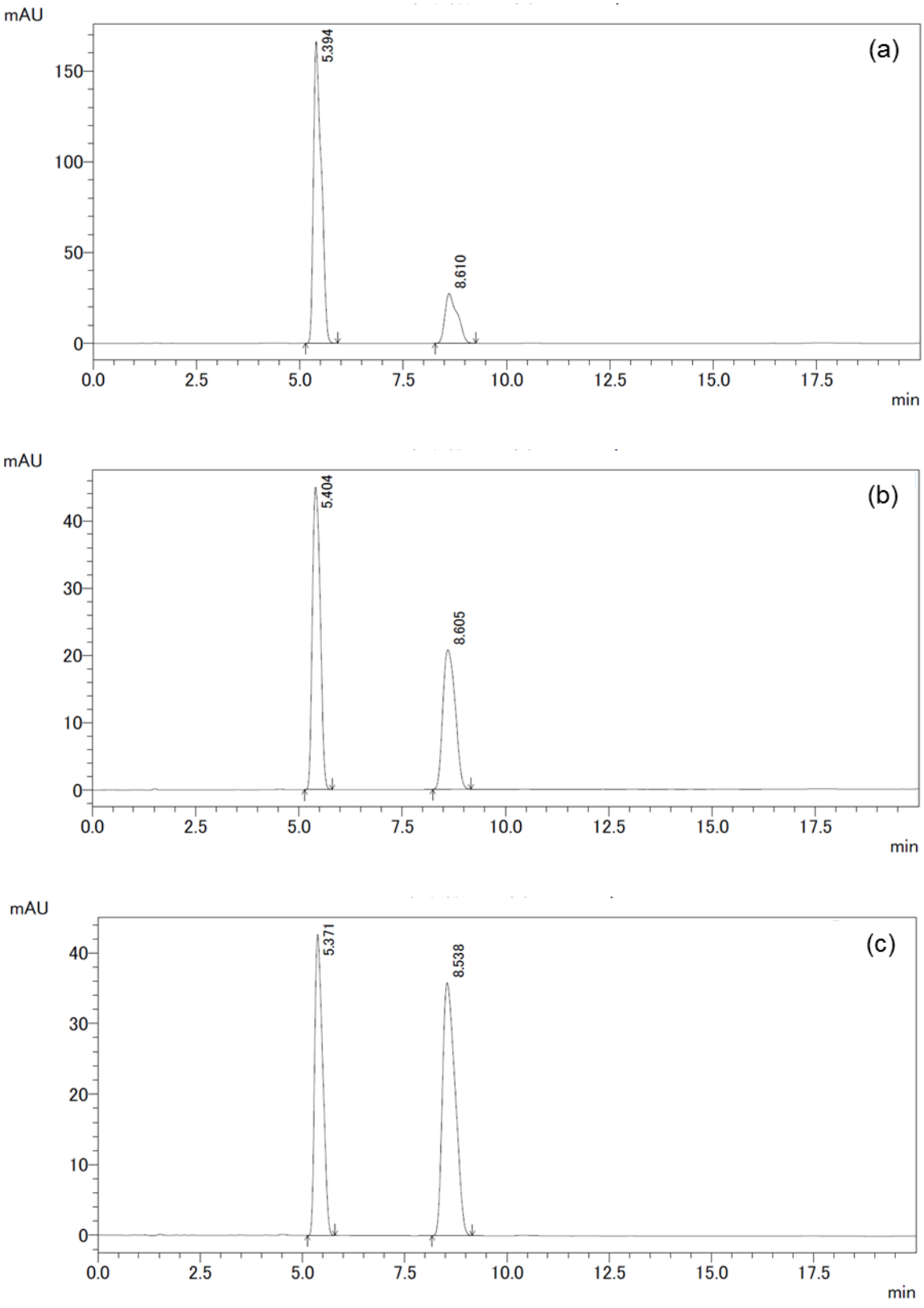

Figure 4-13: HPLC measurements of **8-B** after (a) 32 hours, (b) 64 hours and (c) 144 hours of photoirradiation in the solid state.

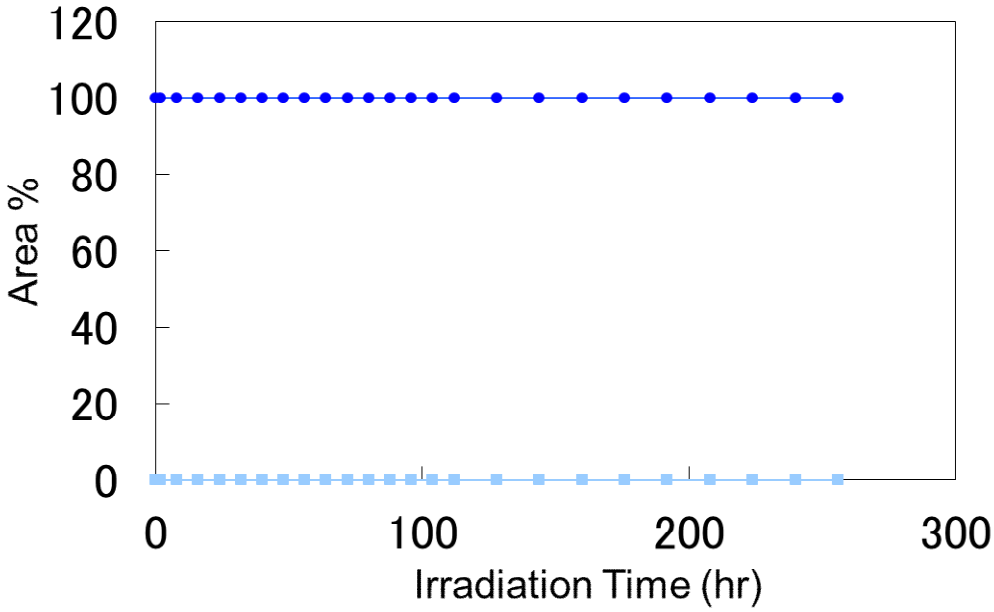

Figure 4-14: Transition of area % in HPLC measurement of **8-A** (●, blue line) and other products (■, light blue line) during photoirradiation in the solid-state.

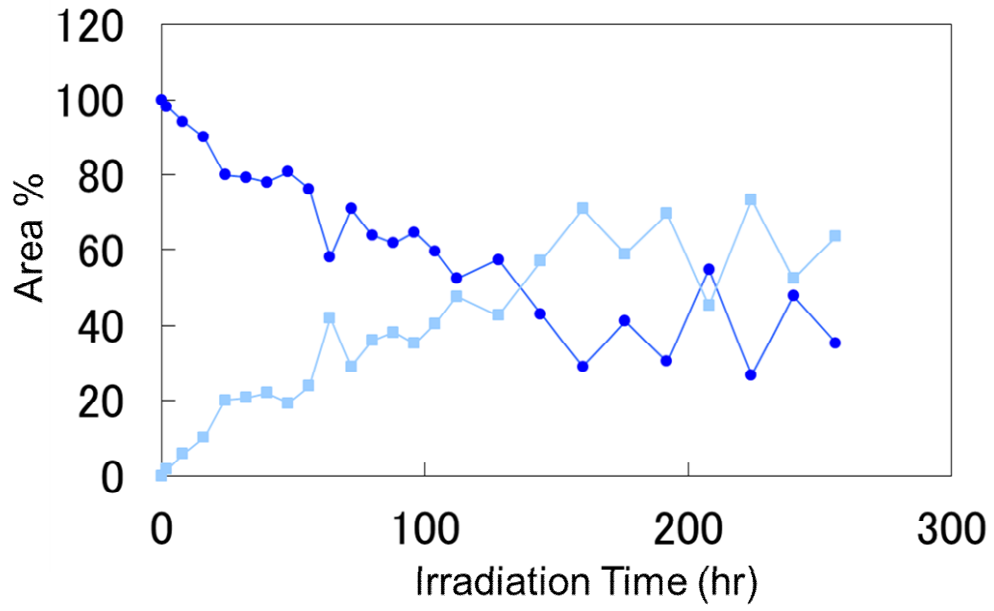

Figure 4-15: Transition of area % in HPLC measurement of **8-B** (●, blue line) and other products (■, light blue line) during photoirradiation in the solid state.

To observe the degradation of phase **B** in detail, light irradiation in the solid state followed by the NMR measurements were taken place. Powdered crystals of **8-B** were placed between two Pyrex plates and light irradiated using SUNTESTER up to 144 hours. The progress was measured by recording ^{1}H NMR (solvent : acetone-d_6) spectra at various stages of irradiation. Figure 4-16 shows the ^{1}H NMR spectra of 1 (a) before photoirradiation, for photoirradiation for (b) 16 hour, (c) 56 hours, and (d) 144 hours. The figure shows that by photoirradiation, the signal originated from **8** disappears, and signals of another product appear. This change by photoirradiation can be assumed that intermolecular double bonds in the cinnamic moiety reacted, and the corresponding cyclodimer has formed.

The formation of the photodimer was evidenced by the disappearance of the olefinic protons of **8** at 7.07 and 7.75 ppm and the emergence of two signals for the corresponding cyclobutane protons in the dimer at 4.39 and 4.65 ppm, as also shown in Chapter 2. From the results shown, the degradation of derivative **8** by light irradiation was determined as the progress of [2+2] photodimerization in the solid state. And this result clarified the difference against photoirradiation between the two polymorphs. The difference in reactivity against photoirradiation observed is correlated with the results of the crystal structure analysis observed in section 4.4.4., and photodimerization preceded only on **8-B** which fulfilled the Schmidt's topochemical postulate.

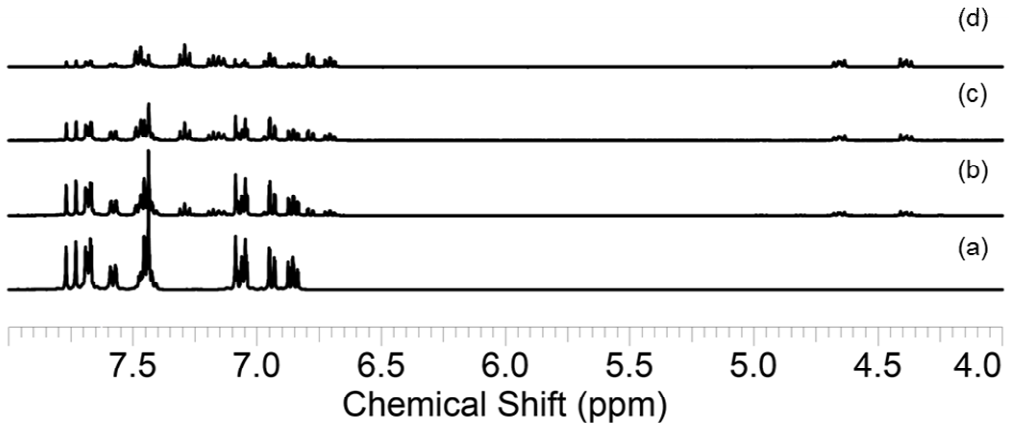

Figure 4-16: ^{1}H NMR spectra in DMSO-d_6: (a) **8-B** before irradiation, (b) **8-B** after irradiation for 16 hours, (c) **8-B** after irradiation for 56 hours, (d) **8-B** after irradiation for 144 hours.

Fortunately, the **8-B** after photoirradiation was successfully isolated from the fully irradiated materials of **8-B** by column chromatography (SiO_2, EtOAc : hexane = 3 : 1). The isolated compound was crystallized from slow evaporation of chloroform solution and confirmed the structure with single-crystal analysis. The result revealed that the obtained photoproduct is a photodimer of **8**, and determined that [2+2] photodimerization in the solid state proceeded by photo irradiation to **8-B** (Figure 4-17).

From the structure, the obtained photodimer **9** is found to be the α-type, which results from a reaction between head-to-tail conformation of the adjacent cinnamic amide molecules. The conformation that fulfills the condition of the adjacent molecules was found to be from result I among the two results of the analysis shown in section 4.4.4. Therefore, the structure of **8-B** is assumed to be result I, and the photoreaction proceeded between the double bonds of the adjacent molecules of combination T-H with the separation between the center of the double bonds being 3.91 Å.

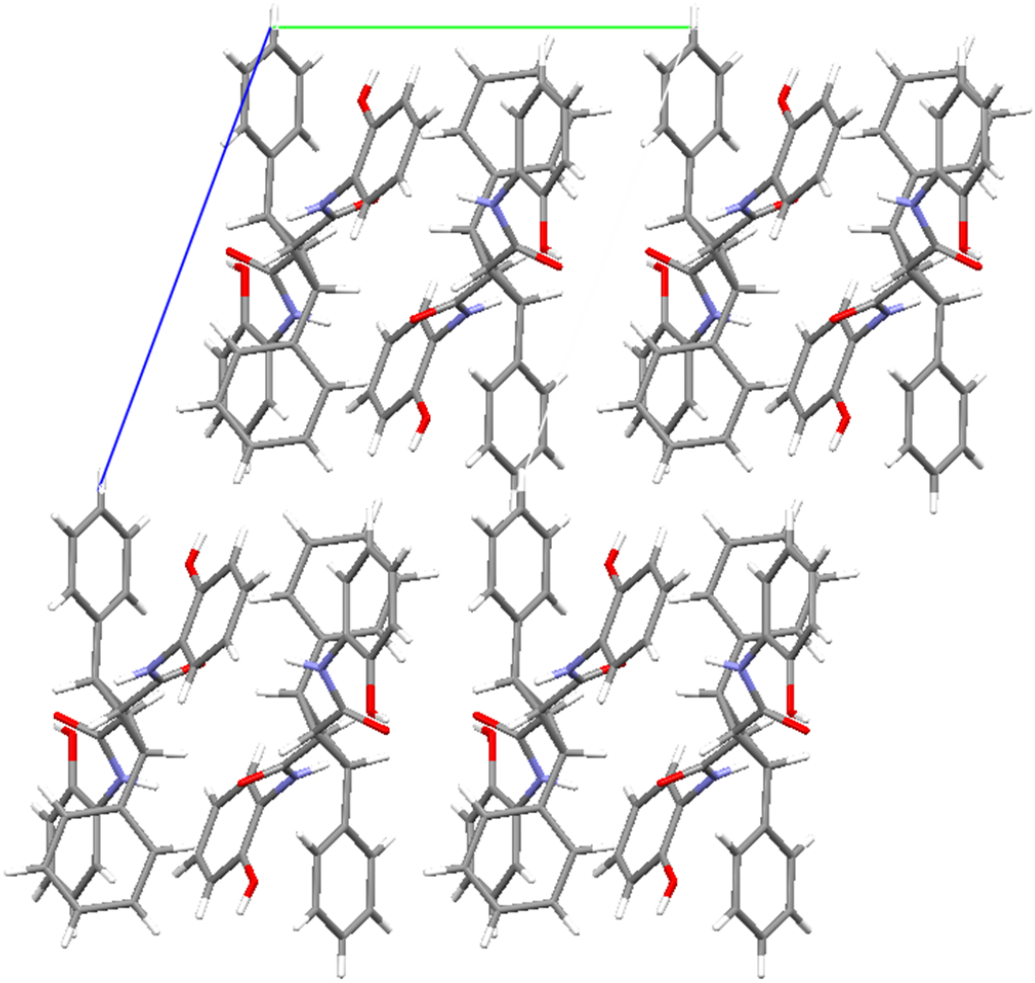

Figure 4-17: Molecular packing of photodimer **9**.

4.4.6. Determination of Difference in Photoreactivity Between the Two Results of *ab-intio* Structure Analysis

From the crystal structure analysis of the obtained photodimer, the structure of **8-B** was confirmed be result I. But as shown in section 4.4.4, both result I and II fulfills the Schmidt's topochemical postulate and had the possibility for photodimerization to proceed from the point of static environment of the crystal structure. And since there still is a possibility that result II or head-to-head structure might be mixed within the sample of **8-B**. And in that case, the reason why β–type photodimer is not obtained is not unclear. To clarify the difference between the two results and the progress of photodimerization, observation of the two results from the dynamic environment will be taken place in detail.

Since the potentially reactive molecules in both results are aligned as a reputation in a single direction, the reaction cavity used in Chapter 3 cannot be calculated. Therefore, the photodimer was drawn overlapped in the drawing with each result of **8-B**, and seek in progress of the photodimerization is acceptable or not. Figure 4-18 and Figure 4-19 shows the overlap of each result (stick) and the photodimer (ball and stick). Since the photodimerization in a head-to-head manner did not proceed, the structure of the photodimer overlapped is created by starting from the structure of photodimer **9**.

From the overlap drawing of result I, it can be said that no major problem can be observed in the structure of the photodimer in the drawing. Therefore, the formation of structure of **9** from result I can be said to be able to tolerate when the molecular movement of photodimerization proceeded.

On the other hand, the overlap drawing of result II shows that the resulting photodimer are crossed to each other, which is located in the dotted circle region. Therefore, it can be said that the formation of the photodimer from result II cannot be tolerated, and the photodimerization is assumed to have less possibility to proceed. And for this case, lack of toleration of the resulting dimer is the reason why only head-to-tail photodimer **9** resulted even though the molecules in both results also satisfied the Schmidt's topochemical postulate. Thus, observation of the dynamic environment in this case is also found to be the key factor to govern reactivity, and will be contributory to determining the outcome of the results obtained from *ab initio* crystal structure analysis.

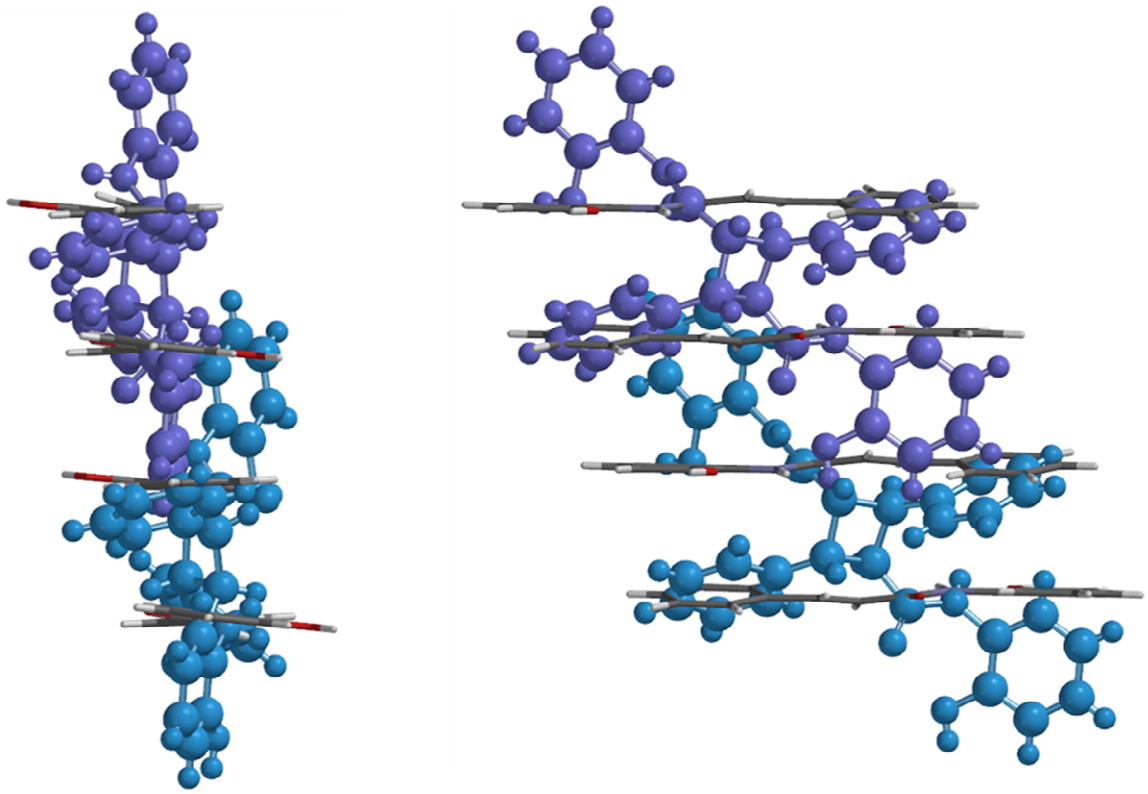

Figure 4-17: Overlap of result I (stick) and photodimer **9** (ball and stick).

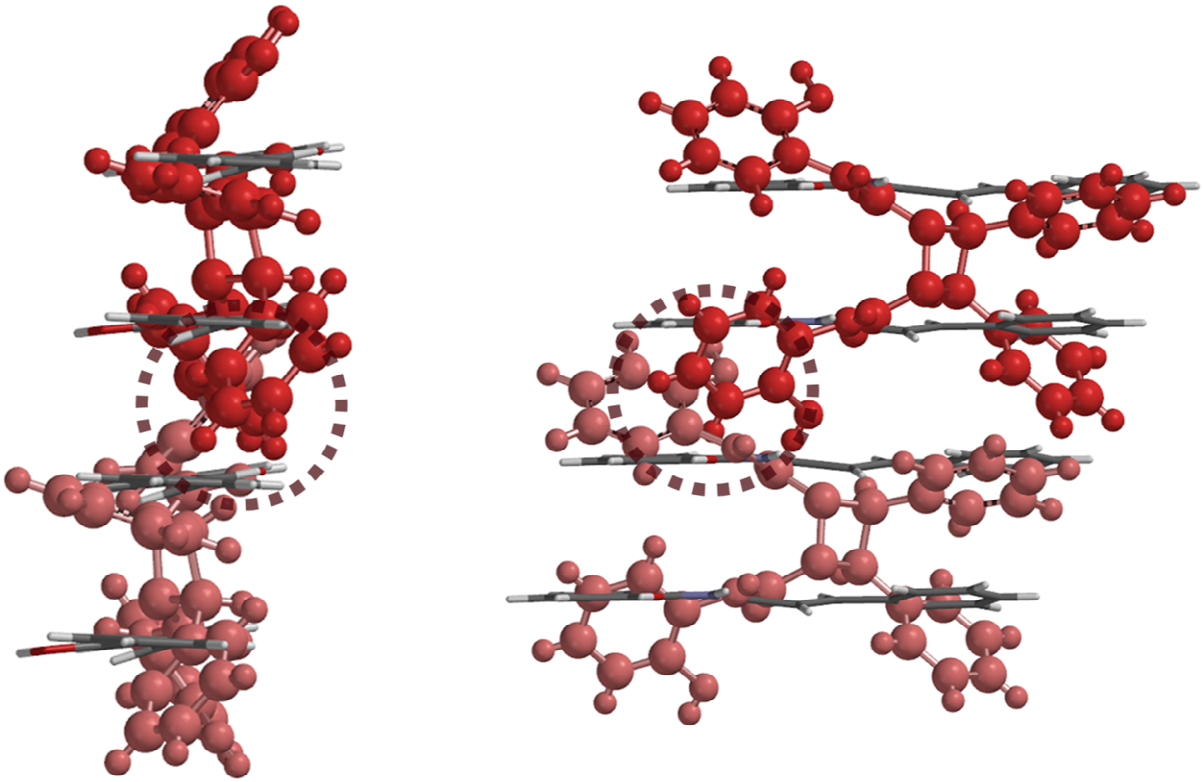

Figure 4-18: Overlap of result II (stick) and the predicted photodimer (ball and stick).

4.4.7. Difference Between the Stability of Polymorphs: Density and Lattice Energy Calculation

The difference in the molecular arrangements, i.e. crystal packing, also causes differences in the crystal densities. The densities are calculated from the crystal structure analysis to be 1.27 g cm^{-1} (at 298K) for **8-A** and 1.29 g cm^{-1} (at 298K) for **8-B**. The difference in between the two phases is small, but phase **A** has a denser crystal packing than phase **B**. According to the density rule introduced by Burger and Ramberger,[180,181] the less stable polymorph may have a lower density than the stable polymorph. The results from the density show that the phase **A** is expected to be less stable than phase **B**. The difference in stability calculated from crystal densities and the fact that only **8-A** crystallizes from various solvents does not agree. Since the difference in density was too small to reach a conclusion, the lattice energy calculations were carried out for these two crystals to evaluate the energetic relationship between **8-A** and **8-B**.

The lattice energy calculations were carried out for the crystal structures of

8-A and **8-B** using the Forcite module in Material Studio 4.0 software from Accelrys.[182] In all force fields (COMPASS[183] and pcff*d*), **8-A** has lower lattice energy than **8-B** for 3.7-7.2 kcal mol^{-1}. This result indicates that phase **A** is more stable than phase **B**. The crystallization processes cannot be determined only by the lattice energy, but this difference might be one of the reasons why only **8-A** can be crystallized from various solvents.

Table 4-3: The relative lattice energies of **8-A** and **8-B** by various force fields.

Forcefield	COMPASS		pcff	
	8-A	**8-B**	**8-A**	**8-B**
Total energy	0.00	+3.78	0.00	+7.14
Intramolecular energy	0.00	+2.60	0.00	+3.34
Intermolecuar energy	0.00	+1.17	0.00	+3.80

The energy differences of the molecular conformation (intramolecular energy) between **8-A** and **8-B** are less than 3.4 kcal mol^{-1}. Also the difference in intermolecular energy, such as van der Waals and electrostatic interactions, are less than 3.8 kcal mol^{-1}. Therefore, it is difficult to determine whether intramolecular energy or intermolecular energy has the larger contribution to the difference in total lattice energy in this case.

4.5. Concluding Remarks

From the thermal analysis, two phases of cinnamic amide derivative **8** was found and obtained through thermal transition. Among the two phases, phase **A** was stable against photoirradiation, while phase **B** showed progress of [2+2] photodimerization. Single crystal structure analysis of phase **A** determined that the conformation does not fulfill the displacement for photodimerization to proceed. From *ab initio* crystal structure analysis of phase **B**, two possibilities of crystal structure was observed, both fulfilling the Schmidt's topochemical postulate. And from the structure of the obtained photodimer, result I was determined as the structure of phase **B**. The difference between the results obtained were analyzed from the viewpoint of photoreactivity, and found that the dynamic environment in the crystal structure displayed the difference in the possibility against toleration of photodimerization.

The result in this chapter reveals that observation of dynamic environment was also found to be a helpful tool for determining and scrutinizing the result of the *ab initio* analysis. And also, it can be assumed that if "Reaction Cavity" can be calculated, it would supplement more detail in the determination.

Chapter 5

General Conclusion

In this dissertation, properties of novel cinnamic amide derivatives against photoirradiation in the solid state were investigated. In all studies, determination of the dynamic environment in the crystal structure acted as the important role, because difference in photoreactivity could not be revealed only by using the traditional method determining the static environment in the crystal structure.

In chapter 2, synthesis of novel cinnamic amide derivatives and its property used as the developer in thermosensitive paper was determined, and successfully revealed that the novel derivatives can afford lightfastness to the paper on both image and background regions just by replacing the traditional developers. And from the detailed study, we have determined that to afford lightfastness by this method, not only just the UV-absorbent ability but also durability against light is needed for the achievement.

In chapter 3, crystal structure of cinnamic amide derivatives were determined by single crystal structure analysis, and found three derivatives fulfill the Schmidt's topochemical criteria, but only one of them preceded [2+2] photodimerization in the solid state. The difference in photoreactivity was able to clarify by calculation of the "reaction cavity", and determined that fulfillment of the suited size and shape in the dynamic environment is also important for solid state reaction to proceed.

In chapter 4, thermal transformation of a derivative of cinnamic amide was observed and the phases were determined by single crystal analysis or by *ab initio* powder X-ray diffraction analysis. The difference in photoreactivity and the progress of [2+2] photodimerization among the polymorphs was in good

correlation with the results of the crystal structure analysis. In addition, the observation of dynamic environment was also found to be a helpful tool for determining and scrutinizing the result of the *ab initio* powder X-ray diffraction analysis.

Clearly, determination of the dynamic environment in the crystal structure, that is the area or the space in which atomic movements tolerate, acted as the forceful method for determining the reactivity of the solid state reaction, and fulfillment of *ab initio* structure analysis. Successful examples using this method for determining photoreactivity in the solid state were exhibited in the present dissertation. Furthermore, the results opened a new page for establishing high lightfast thermosensitive paper, and are now in development.

Reference

(1) Gregory, P. *Dyes Pigm.* **1990**, *13*, 251–268.

(2) Yoshida, Z.; Kitao, T. *Chemistry of Functional Dyes*; Mita Press, 1989; pp. 397–415.

(3) Zollinger, H. *Color Chemistry*; Wiley-VCH, 2003; pp. 537–539.

(4) Yanagita, M.; Aoki, I.; Tokita, S. *Bull. Chem. Soc. Jpn.* **1998**, *70*, 2757–2763.

(5) Takahashi, Y.; Shirai, A.; Segawa, T.; Takahashi, T.; Sakakibara, K. *Bull. Chem. Soc. Jpn.* **2002**, *75*, 2225–2231.

(6) Meiqin, S.; Yun, S.; Qiyu, T. *Dyes Pigm.* **1995**, *29*, 45–55.

(7) White, M. *J. Chem. Educ.* **1998**, *75*, 1119–1120.

(8) Inouye, M.; Tsuchiya, K.; Kitao, T. *Angew. Chem., Int. Ed.* **1992**, *31*, 204–205.

(9) Azizian, F.; Field, A. J.; Griffiths, J.; Heron, B. M. *Dyes Pigm.* **2012**, *92*, 524–530.

(10) Hinckley, D. a.; Seybold, P. G. *Spectrochim. Acta, Part A* **1988**, *44*, 1053–1059.

(11) Hinckley, D. a.; Seybold, P. G.; Borris, D. P. *Spectrochim. Acta, Part A* **1986**, *42*, 747–754.

(12) Hojo, M.; Ueda, T.; Yamasaki, M.; Inoue, A.; Tokita, S.; Yanagita, M. *Bull. Chem. Soc. Jpn.* **2002**, *75*, 1569–1576.

(13) Sekiguchi, Y.; Takayama, S.; Gotanda, T.; Sano, K. *Chem. Lett.* **2007**, *36*, 1010–1011.

(14) Mizuguchi, J. *Acta Crystallogr., Sect. E: Struct. Rep.* **2008**, *64*, o1238–o1239.

(15) Mizuguchi, J.; Sato, K. *Acta Crystallographica Section E Structure Reports Online* **2009**, *65*, o701–o702.

(16) MacLaren, D. C.; White, M. a. *J. Mater. Sci.* **2005**, *40*, 669–676.

(17) MacLaren, D. C.; White, M. A. *J. Mater. Chem.* **2003**, *13*, 1695.

(18) MacLaren, D. C.; White, M. A. *J. Mater. Chem.* **2003**, *13*, 1701.

(19) Luthern, J.; Peredes, A. *J. Mater. Sci. Lett.* **2000**, *19*, 185–188.

(20) Burkinshaw, S.; Griffiths, J.; Towns, A. D. *J. Mater. Chem.* **1998**, *8*, 2677–2683.

(21) Naito, K. *J. Mater. Chem.* **1998**, *8*, 1379–1384.

(22) Yamamoto, S.; Furuya, H.; Tsutsui, K.; Ueno, S.; Sato, K. *Cryst. Growth Des.* **2008**, *8*, 2256–2263.

(23) Tsutsui, K.; Yamaguchi, T.; Sato, K. *Jpn. J. Appl. Phys., Part 1* **1994**, *33*, 5925–5928.

(24) Horiguchi, T.; Koshiba, Y.; Ueda, Y.; Origuchi, C.; Tsutsui, K. *Thin Solid Films* **2008**, *516*, 2591–2594.

(25) Hirata, S.; Watanabe, T. *Adv. Mater. (Weinheim, Ger.)* **2006**, *18*, 2725–2729.

(26) Hirata, S.; Lee, K.-S.; Watanabe, T. *Advanced Functional Materials* **2008**, *18*, 2869–2879.

(27) Wang, B.; Ye, Z.; Ji, L.; Hu, N. *Advanced Materials Research* **2011**, *284-286*, 2442–2445.

(28) Drochioiu, G.; Sandu, I.; Olteanu, G. I.; Mangalagiu, I. *International Journal of Criminal Investigation* **2006**, *1*, 37–58.

(29) Jasuja, O. P.; Singh, G. *Forensic Sci. Int.* **2009**, *192*, e11–6.

(30) Ma, R.; Wei, Q. *J. Forensic Ident.* **2006**, *56*, 364–373.

(31) Broniek, B.; Knaap, W. *J. Forensic Ident.* **2002**, *52*, 427–432.

(32) Wakefield, M.; Armitage, S. *J. Forensic Ident.* **2005**, *55*, 202–213.

(33) Patton, E. L. T.; Brown, D. H.; Lewis, S. W. *Anal. Methods* **2010**, *2*, 631–637.

(34) Mendum, T.; Stoler, E.; VanBenschoten, H.; Warner, J. C. *Green Chemistry Letters and Reviews* **2011**, *4*, 81–86.

(35) Oda, H. *Dyes Pigm.* **2008**, *76*, 270–276.

(36) Caine, M. a; McCabe, R. W.; Wang, L.; Brown, R. G.; Hepworth, J. D. *Dyes Pigm.* **2002**, *52*, 55–65.

(37) Caine, M. a.; McCabe, R. W.; Wang, L.; Brown, R. G.; Hepworth, J. D. *Dyes Pigm.* **2001**, *49*, 135–143.

(38) Allen, N.; Hughes, N.; Mahon, P. *Journal of photochemistry* **1987**, *37*, 379–390.

(39) Allen, N.; Mohajerani, B.; Richards, J. *Dyes Pigm.* **1981**, *2*, 31–35.

(40) Oda, H. *Dyes and Pigments* **2005**, *66*, 103–108.

(41) Kelly, P. F.; King, R. S. P.; Bleay, S. M.; Daniel, T. O. *Forensic Sci. Int.* **2012**, *217*, e27–30.

(42) Yanagita, M.; Takahashi, S.; Aoki, I. *Journal of the Japan Society of Colour Material* **1996**, *69*, 649–657.

(43) Kawasaki, K.; Sakakibara, K. *Bull. Chem. Soc. Jpn.* **2007**, *80*, 358–364.

(44) Matsumoto, S.; Takeshima, S.; Satoh, S.; Kabashima, K. *Dyes and Pigments* **2010**, *85*, 139–142.

(45) Stabile, R. G.; Dicks, A. P. *J. c* **2004**, *81*, 1488–1491.

(46) Oda, H. **2001**, *48*, 151–157.

(47) Crawford, J. C. *Prog. Polym. Sci.* **1999**, *24*, 7–43.

(48) Yang, Y. Y.; Li, H. Q.; He, X. D.; Mu, B. N.; Chen, Y. J.; Nan, Y.; Zou, Y. *Advanced Materials Research* **2011**, *233-235*, 219–224.

(49) Kehayoglou, A. H.; Tsatsaroni, E. G. *Dyes and pigments* **1993**, *23*, 53–63.

(50) Tsatsaroni, E. G.; Kehayoglou, A. H. *Dyes and Pigments* **1995**, *28*, 123–130.

(51) Waiblinger, F.; Keck, J.; Fluegge, A. P.; Kramer, H. E. A.; Leppard, D.; Rytz, G. *Journal of Photochemistry and Photobiology A: Chemistry* **1999**, *126*, 43–49.

(52) Kocher, C.; Weder, C.; Smith, P. *J. Mater. Chem.* **2003**, *13*, 9–15.

(53) Giokas, D. L.; Salvador, A.; Chisvert, A. *Trends in Analytical Chemistry* **2007**, *26*, 360–374.

(54) Salvador, A.; Chisvert, A. *Anal. Chim. Acta* **2005**, *537*, 1–14.

(55) Gasparro, F. P.; Mitchnick, M.; Nash, J. F. *Photochem. Photobiol.* **1998**, *68*, 243–256.

(56) Kikuchi, A.; Yukimaru, S.; Oguchi, N.; Miyazawa, K.; Yagi, M. *Chem. Lett.* **2010**, *39*, 633–635.

(57) Jiménez, M. M.; Pelletier, J.; Bobin, M. F.; Martini, M. C. *Int. J. Pharm.* **2004**, *272*, 45–55.

(58) Perugini, P.; Simeoni, S.; Scalia, S.; Genta, I.; Modena, T.; Conti, B.; Pavanetto, F. *Int. J. Pharm.* **2002**, *246*, 37–45.

(59) MacManus-Spencer, L. A.; Tse, M. L.; Klein, J. L.; Kracunas, A. E. *Environ. Sci. Technol* **2011**, *45*, 3931–3937.

(60) Davis, M. R.; Quigley, M. N. *J. Chem. Educ.* **1995**, *72*, 279–281.

(61) Venditti, E.; Spadoni, T.; Tiano, L.; Astolfi, P.; Greci, L.; Littarru, G. P.; Damiani, E. *Free Radical Biol. Med.* **2008**, *45*, 345–54.

(62) Nourary, C.; Castellan, A.; Davidson, R. S. *J. Photochem. Photobiol., A* **1994**, *84*, 317–326.

(63) Kikuchi, A.; Saito, H.; Mori, M.; Yagi, M. *Photochem. Photobiol. Sci.* **2011**, *10*, 1902–9.

(64) Chawla, H. M.; Pant, N.; Kumar, S.; Mrig, S.; Srivastava, B.; Kumar, N.; Black, D. S. *Journal of photochemistry and photobiology. B, Biology* **2011**, *105*, 25–33.

(65) Wiesner, J.; Mitsch, A.; Wissner, P.; Jomaa, H.; Schlitzer, M. *Bioorg. Med. Chem. Lett.* **2001**, *11*, 423–424.

(66) Luadthong, C.; Tachaprutinun, A.; Wanichwecharungruang, S. P. *European Polymer Journal* **2008**, *44*, 1285–1295.

(67) Franck, G.; Brödner, K.; Helmchen, G. *Org. Lett.* **2010**, *12*, 3886–9.

(68) De, P.; Koumba Yoya, G.; Constant, P.; Bedos-Belval, F.; Duran, H.; Saffon, N.; Daffé, M.; Baltas, M. *J. Med. Chem.* **2011**, *54*, 1449–61.

(69) Vishnoi, S.; Agrawal, V.; Kasana, V. K. *J. Agric. Food. Chem.* **2009**, *57*, 3261–3265.

(70) Lapeyre, C.; Delomenede, M.; Bedos-Belval, F.; Duran, H.; Negre-Salvayre, A.; Baltas, M. *J. Med. Chem.* **2005**, *48*, 8115–8124.

(71) Kihara, H.; Norikane, Y.; Yoshida, M. *Tetrahedron* **2012**, *68*, 5513–5521.

(72) Okada, K. *Journal of Molecular Structure* **1996**, *380*, 223–233.

(73) Sato, K.; Shima, H.; Mizuguchi, J. *Acta Crystallogr., Sect. E: Struct. Rep.* **2009**, *65*, o391.

(74) Toda, F. *Acc. Chem. Res.* **1995**, *28*, 480–486.

(75) Hoffmann, N. *Chem. Rev.* **2008**, *108*, 1052–103.

(76) Kuzmanich, G.; Vogelsberg, C. S.; Maverick, E. F.; Netto-Ferreira, J. C.; Scaiano, J. C.; Garcia-Garibay, M. A. *J. Am. Chem. Soc.* **2012**, *134*, 1115–23.

(77) Wagner, P. J.; Giri, B. P.; Scaiano, J. C.; Ward, D. L.; Gabe, E.; Lee, F. L. *J. Am. Chem. Soc.* **1985**, *107*, 5483–5490.

(78) Badger, G.; Buttery, R. *J. Chem. Soc.* **1954**, *4*, 2243–2245.

(79) Berson, J. A.; Brown, E. *J. Am. Chem. Soc.* **1955**, *77*, 447–450.

(80) *Tetrahedron Letters* **1971**, 2757–2760.

(81) Masu, H.; Ohmori, K.; Kishikawa, K.; Yamamoto, M.; Yamaguchi, K.; Kohmoto, S. *Bull. Chem. Soc. Jpn.* **2005**, *78*, 1127–1131.

(82) Ng, D.; Yang, Z.; Garcia-Garibay, M. a *Organic letters* **2004**, *6*, 645–7.

(83) Fonseca, I.; Baias, M.; Hayes, S. E.; Pickard, C. J.; Bertmer, M. *J. Phys. Chem. C* **2012**, *116*, 12212–12218.

(84) Santra, R.; Biradha, K. *CrystEngComm* **2011**, *13*, 3246–3257.

(85) Bhogala, B. R.; Captain, B.; Parthasarathy, A.; Ramamurthy, V. *J. Am. Chem. Soc.* **2010**, *132*, 13434–42.

(86) Mori, Y.; Matsumoto, A. *Chem. Lett.* **2007**, *36*, 510–511.

(87) Bertmer, M.; Nieuwendaal, R. C.; Barnes, A. B.; Hayes, S. E. *J. Phys. Chem. B* **2006**, *110*, 6270–6273.

(88) Cohen, M. D.; Schmidt, G. M. J. *J. Chem. Soc.* **1964**, 1996–2000.

(89) Cohen, M.; Schmidt, G. *J. Chem. Soc.* **1964**, 2000–2013.

(90) Schmidt, G. *J. Chem. Soc.* **1964**, 2014–2021.

(91) Ramamurthy, V.; Venkatesan, K. *Chem. Rev.* **1987**, *87*, 433–481.

(92) Schmidt, G. M. J. *Pure Appl. Chem.* **1971**, *27*, 647–678.

(93) Cohen, M. D. *Angew. Chem. Int. Ed.* **1975**, *307*, 386–393.

(94) Sharma, C. V. K.; Panneerselvam, K.; Shimoni, L.; Katz, H.; Carrell, Q. H. L.; Desiraju, G. R. *Chem. Mater.* **1994**, *6*, 1282–1292.

(95) Murthy, G. S.; Arjunan, P.; Venkatesan, K.; Ramamurthy, V. *Tetrahedron* **1987**, *43*, 1225–1240.

(96) Sasada, Y.; Shimanouchi, H.; Nakanishi, H.; Hasegawa, M. *Bull. Chem. Soc. Jpn.* **1971**, *44*, 1262–1270.

(97) Nakanishi, H.; Ueno, K. *Acta Crystallogr., Sect. B:* **1976**, *96*, 3352–3354.

(98) Nakanishi, H.; Ueno, K.; Sasada, Y. *Acta crystallographica. Section B, Structural science* **1976**, *32*, 1616–1618.

(99) Nakanishi, H.; Ueno, K.; Hasegawa, M.; Sasada, Y. *Chem. Lett.* **1972**, 301–304.

(100) Ariel, S.; Trotter, J. *Acta Crystallogr., Sect. C: Cryst. Struct. Commun.* **1984**, *40*, 2084–2086.

(101) Ariel, S.; Askari, S.; Scheffer, J.; Trotter, J.; Walsh, L. *J. Am. Chem. Soc.* **1984**, *1*, 5726–5728.

(102) Trotter, J. *Acta Crystallographica Section B: Structural Science* **1983**, *39*, 373–381.

(103) Appel, W.; Jiang, Z.; Scheffer, J.; Walsh, L. *J. Am. Chem. Soc.* **1983**, *105*, 5354–5363.

(104) Hanson, A. *Section B: Structural Crystallography and Crystal* **1975**, *31*, 1963–1965.

(105) Kanagapushpam, B. Y. D.; Ramamurthy, V.; Venkatesan, K. *Acta Crystallogr., Sect. C: Cryst. Struct. Commun.* **1987**, *43*, 1128–1131.

(106) Kumar, V. A.; Venkatesan, K. *J. Chem. Soc., Perkin Trans. 2* **1993**, *40*, 2429–2433.

(107) Venugopalan, P.; Venkatesan, K. *Acta Crystallographica Section B Structural Science* **1992**, *48*, 532–537.

(108) Theocharis, C.; Jones, W.; Thomas, J.; Motevalli, M.; Hursthouse, M. B. *J. Chem. Soc., Perkin Trans. 2* **1984**, *42*, 71–76.

(109) Jones, W.; Ramdas, S.; Theocharis, C. R.; Thomas, J. M.; Thomas, N. W. *J. Phys. Chem.* **1981**, *85*, 2594–2597.

(110) Jones, W.; Nakanishi, H.; Theocharis, C. R.; Thomas, J. M. *J. Chem. Soc., Chem. Commun.* **1980**, *93*, 610–611.

(111) Theocharis, C. R.; Nakanishi, H.; Jones, W. *Acta Crystallographica Section B Structural Science* **1981**, *37*, 756–758.

(112) Gnanaguru, K.; Ramasubbu, N.; Venkatesan, K.; Ramamurthy, V. *J. Org. Chem.* **1985**, *50*, 2337–2346.

(113) Busing, W. R. WMIN, a Computer Program to Model Molecules and Crystals in Terms of Potential Energy Function **1981**, Report ORNL–5747.

(114) Ohashi, Y.; Yanagi, K.; Kurihara, T.; Sasada, Y.; Ohgo, Y. *J. Am. Chem. Soc.* **1981**, *103*, 5805–5812.

(115) Brittain, H. *Journal of pharmaceutical sciences* **2012**, *101*, 464–484.

(116) Brittain, H. G. *Journal of pharmaceutical sciences* **2011**, *100*, 1260–1279.

(117) Stahly, G. P. *Cryst. Growth Des.* **2007**, *7*, 1007–1026.

(118) Seddon, K. R. *Cryst. Growth Des.* **2004**, *4*, 1087–1087.

(119) Bernstein, J. *Cryst. Growth Des.* **2005**, *5*, 5–6.

(120) Bernstein, J. *Cryst. Growth Des.* **2011**, *11*, 632–650.

(121) Desiraju, G. R. *Cryst. Growth Des.* **2004**, *4*, 1089–1090.

(122) Nangia, A. *Cryst. Growth Des.* **2006**, *6*, 2–4.

(123) Gao, Y.; Zhou, W.; Li, L.; Wu, J. *Cryst. Growth Des.* **2008**, *9*, 253–257.

(124) Fan, Y.; Song, W.; Yu, D.; Ye, K.; Zhang, J.; Wang, Y. *CrystEngComm* **2009**, *11*, 1716.

(125) Kinuta, T.; Sato, T.; Tajima, N.; Matsubara, Y.; Miyazawa, M.; Imai, Y. *CrystEngComm* **2012**, *14*, 1016–1020.

(126) Mei, J.; Wang, J.; Qin, A.; Zhao, H.; Yuan, W.; Zhao, Z. *J. Mater. Chem.* **2012**, *22*, 4290–4298.

(127) Fujii, K.; Sakon, A.; Sekine, A. *Cryst. Growth Des.* **2011**, *11*, 4305–4308.

(128) Bashkirava, A.; Andrews, P. C.; Junk, P. C.; Robertson, E. G.; Spiccia, L.; Vanderhoek, N. *Chemistry, an Asian journal* **2007**, *2*, 530–538.

(129) Yamamura, S.; Sugawara, Y.; Terao, H.; Matsushita, M. M.; Sugawara, T. *Chemical Physics* **2006**, *322*, 392–398.

(130) Hisaki, I.; Kometani, E.; Shigemitsu, H.; Saeki, A.; Seki, S.; Tohnai, N.; Miyata, M. *Cryst. Growth Des.* **2011**, *11*, 5488–5497.

(131) Hall, S.; Kolinsky, P.; Jones, R.; Allen, S.; Gordon, P.; Bothwell, B.; Bloor, D.; Norman, P. A.; Hursthouse, M.; Karaulov, A.; Baldwin, J.; Goodyear, M.; Bishop, D. *Journal of Crystal Growth* **1986**, *79*, 745–751.

(132) Pan, F.; Bosshard, C.; Wong, M. S.; Serbutoviez, C.; Schenk, K.; Gfamlich, V.; Günter, P. *Chem. Mater.* **1997**, 1328–1334.

(133) Kwon, O.; Jazbinsek, M.; Yun, H.; Seo, J.-I.; Kim, E.-M.; Lee, Y.-S.; Günter, P. *Cryst. Growth Des.* **2008**, *8*, 4021–4025.

(134) Urbanczyk-Lipkowska, Z.; Kalicki, P.; Gawinkowski, S.; Waluk, J.; Yokoyama, M.; Tanaka, K. *CrystEngComm* **2011**, *13*, 3170.

(135) Johmoto, K.; Sekine, A.; Uekusa, H.; Ohashi, Y. *Bull. Chem. Soc. Jpn.* **2009**, *82*, 50–57.

(136) Abdelmoty, I.; Buchholz, V.; Di, L.; Guo, C.; Kowitz, K.; Enkelmann, V.; Wegner, G.; Foxman, B. M. *Crystal Growth & Design* **2005**, *5*, 2210–2217.

(137) Moorthy, J. N.; Venkatakrishnan, P. *Cryst. Growth Des.* **2007**, *7*, 2–7.

(138) Wu, H.; Reeves-McLaren, N.; Jones, S.; Ristic, R. I.; Fairclough, J. P. a.; West, A. R. *Cryst. Growth Des.* **2010**, *10*, 988–994.

(139) Wu, H.; Reeves-McLaren, N.; Pokorny, J.; Yarwood, J.; West, A. R. *Crystal Growth & Design* **2010**, *10*, 3141–3148.

(140) Potrzebowski, M. J.; Bujacz, G. D.; Bujacz, A.; Olejniczak, S.; Napora, P.; Heliński, J.; Ciesielski, W.; Gajda, J. *J. Phys. Chem. B* **2006**, *110*, 761–71.

(141) Gunn, E.; Guzei, I.; Cai, T.; Yu, L. *Cryst. Growth Des.* **2012**, *12*, 2037–2043.

(142) Zimmermann, A.; Frøstrup, B.; Bond, A. D. *Cryst. Growth Des.* **2012**, *12*, 2961–2968.

(143) Chopra, D. *Cryst. Growth Des.* **2008**, *8*, 848–853.

(144) van Eupen, J. T. H.; Elffrink, W. W. J.; Keltjens, R.; Bennema, P.; de Gelder, R.; Smits, J. M. M.; van Eck, E. R. H.; Kentgens, A. P. M.; Deij, M. A.; Meekes, H.; Vlieg, E. *Cryst. Growth Des.* **2008**, *8*, 71–79.

(145) Bernstein, J.; Henck, J.-O. *Crystal engineering* **1998**, *1*, 119–128.

(146) Chu, Q.; Swenson, D. C.; MacGillivray, L. R. *Angew. Chem., Int. Ed.* **2005**, *44*, 3569–72.

(147) Santra, R.; Biradha, K. *CrystEngComm* **2008**, *10*, 1524–1526.

(148) Atkinson, M. B. J.; Halasz, I.; Bučar, D.-K.; Dinnebier, R. E.; Mariappan, S. V. S.; Sokolov, A. N.; MacGillivray, L. R. *Chem. Commun. (Cambridge, U.K.)* **2011**, *47*, 236–238.

(149) Chung, C.; Kunita, A.; Hayashi, K.; Nakamura, F.; Saigo, K.; Hasegawa, M. *J. Am. Chem. Soc.* **1991**, *113*, 7316–7322.

(150) Hasegawa, M.; Arioka, H.; Harashina, H.; Nohara, M.; Kubo, M.; Nishikubo, T. *Israel Journal of Chemistry* **1985**, *25*, 302–305.

(151) Gavezzotti, A.; Simonetta, M. *Chem. Rev.* **1982**, *82*, 1–13.

(152) Grove, R. C.; Malehorn, S. H.; Breen, M. E.; Wheeler, K. A. *Chem. Commun.* **2010**, *46*, 7322–7324.

(153) Wheeler, K. A.; Malehorn, S. H.; Egan, A. E. *Chem. Commun.* **2012**, *48*, 519–521.

(154) Kole, G. K.; Tan, G. K.; Vittal, J. J. *CrystEngComm* **2011**, *13*, 3138–3145.

(155) Yamada, S.; Kawamura, C. *Org. Lett.* **2012**, *14*, 1572–5.

(156) Yamada, S.; Tokugawa, Y. *J. a* **2009**, *131*, 2098–2099.

(157) Yamada, S.; Tokugawa, Y.; Nojiri, Y.; Takamori, E. *Chem. Commun.* **2012**, *48*, 1763–1765.

(158) Iliopoulos, K.; Krupka, O.; Gindre, D.; Sallé, M. *J. Am. Chem. Soc.* **2010**, *132*, 14343–14345.

(159) Sokolov, A. N.; Bucar, D.-K.; Baltrusaitis, J.; Gu, S. X.; MacGillivray, L. R. *Angew. Chem. Int. Ed.* **2010**, *49*, 4273–4277.

(160) Bučar, D.-K.; Sen, A.; Mariappan, S. V. S.; MacGillivray, L. R. *Chem. Commun.* **2012**, *48*, 1790–2.

(161) Yamada, S.; Nojiri, Y. *Chem. Commun.* **2011**, *47*, 9143–9145.

(162) Liu, D.; Ren, Z.-G.; Li, H.-X.; Lang, J.-P.; Li, N.-Y.; Abrahams, B. F. *Angew. Chem. Int. Ed.* **2010**, *49*, 4767–4770.

(163) Santra, R.; Biradha, K. *Cryst. Growth Des.* **2010**, *10*, 3315–3320.

(164) Sakamoto, M.; Yagishita, F.; Kanehiro, M.; Kasashima, Y.; Mino, T.; Fujita, T. *Org. Lett.* **2010**, *12*, 4435–4437.

(165) Sheldrick, G. M. *Acta crystallographica. Section A, Foundations of crystallography* **2008**, *64*, 112–122.

(166) Mori, Y.; Matsumoto, A. *Cryst. Growth Des.* **2007**, *7*, 377–385.

(167) Davaasambuu, J.; Busse, G.; Techert, S. *J. Phys. Chem. A* **2006**, *110*, 3261–3265.

(168) Gavezzotti, A. *J. Am. Chem. Soc.* **1983**, *105*, 5220–5225.

(169) Ohashi, Y.; Tomotake, Y.; Uchida, A.; Sasada, Y. *J. Am. Chem. Soc.* **1986**, *108*, 1196–1202.

(170) Weiss, R.; Ramamurthy, V.; Hammond, G. S. *Acc. Chem. Res.* **1993**, *26*, 530–536.

(171) Zimmerman, H. E.; Nesterov, E. E. *Acc. Chem. Res.* **2002**, *35*, 77–85.

(172) Takayama, T.; Mitsumori, T.; Kawano, M.; Sekine, A.; Uekusa, H.; Ohashi, Y.; Sugawara, T. *Acta crystallographica. Section B, Structural science* **2010**, *66*, 639–46.

(173) Arii, T.; Kishi, A. *Thermochimica Acta* **2003**, *400*, 175–185.

(174) Arii, T.; Kishi, A. *J. Therm. Anal. Cal.* **2006**, *83*, 253–260.

(175) Neumann, M. a. *J. Appl. Cryst.* **2003**, *36*, 356–365.

(176) de Wolff, P. M. *J. Appl. Cryst.* **1972**, *5*, 243–243.

(177) Pawley, G. S. *J. Appl. Cryst.* **1981**, *14*, 357–361.

(178) Rietveld, H. M. *J. Ap* **1969**, *2*, 65–71.

(179) Larson, A. C.; Dreele, R. B. V. *"General Structure Analysis System(GSAS)", Los Alamos National Laboratory Report* **2004**, LAUR 86–748.

(180) Burger, A.; Ramberger, R. *Microchimica Acta* **1979**, *2*, 259–271.

(181) Burger, A.; Ramberger, R. *Microchimica Acta* **1979**, *2*, 273–31.

(182) Material Studio, Packages: Discover and Forcite **2006**, Version 4.0, Accelrys Inc, San Diego.

(183) Sun, H. *J. Phys. Chem. B* **1998**, *102*, 7338–7364.

Appendix : Crystallographic Data

N-(4-hydroxyphenyl)-4-methylcinnamoyl amide (1)

Table A-1. Crystal data and structure refinement for **1**.

Identification code	**1**	
Empirical formula	C16 H15 N O2	
Formula weight	253.29	
Temperature	293(2) K	
Wavelength	0.71075 Å	
Crystal system	monoclinic	
Space group	$P2_1/n$	
Unit cell dimensions	a = 6.6796(4) Å	α= 90°.
	b = 21.6754(14) Å	β= 94.919(2)°.
	c = 9.7556(7) Å	γ = 90°.
Volume	1407.24(16) $Å^3$	
Z	4	
Density (calculated)	1.196 Mg/m^3	
Absorption coefficient	0.079 mm^{-1}	
F(000)	536	
Crystal size	0.15 x 0.14 x 0.04 mm^3	
Theta range for data collection	3.20 to 27.40°.	
Index ranges	-8<=h<=8, -28<=k<=28, -12<=l<=12	
Reflections collected	23644	
Independent reflections	3196 [R(int) = 0.0555]	
Completeness to theta = 27.40°	99.7 %	
Max. and min. transmission	0.9968 and 0.9882	
Refinement method	Full-matrix least-squares on F^2	
Data / restraints / parameters	3196 / 0 / 172	
Goodness-of-fit on F^2	1.030	
Final R indices [I>2sigma(I)]	R1 = 0.0438, wR2 = 0.1189	
R indices (all data)	R1 = 0.1032, wR2 = 0.1495	
Largest diff. peak and hole	0.150 and -0.162 $e.Å^{-3}$	

Table A-2. Atomic coordinates (x 10^4) and equivalent isotropic displacement parameters ($Å^2$x 10^3) for **1**. U(eq) is defined as one third of the trace of the orthogonalized U^{ij} tensor.

	x	y	z	U(eq)
N(1)	1236(2)	1516(1)	4215(2)	53(1)
O(1)	4210(2)	992(1)	4509(1)	61(1)
O(2)	2430(2)	3383(1)	433(2)	71(1)
C(1)	1640(3)	-199(1)	7443(2)	57(1)
C(11)	3423(2)	2049(1)	2650(2)	56(1)
C(7)	2432(3)	207(1)	6423(2)	58(1)
C(8)	1466(3)	664(1)	5739(2)	53(1)
C(12)	3648(3)	2516(1)	1717(2)	59(1)
C(10)	1637(2)	1983(1)	3265(2)	50(1)
C(9)	2431(2)	1061(1)	4771(2)	50(1)
C(14)	335(3)	2871(1)	1992(2)	64(1)
C(13)	2112(3)	2930(1)	1372(2)	54(1)
C(15)	104(3)	2403(1)	2921(2)	62(1)
C(2)	-313(3)	-160(1)	7826(2)	62(1)
C(6)	2881(4)	-649(1)	8096(2)	79(1)
C(3)	-969(3)	-547(1)	8823(2)	71(1)
C(4)	277(4)	-988(1)	9483(2)	77(1)
C(5)	2196(4)	-1028(1)	9090(3)	90(1)
C(16)	-473(5)	-1400(1)	10571(3)	109(1)

Table A-3. Bond lengths [Å] and angles [°] for **1**.

N(1)-C(9)	1.353(2)
N(1)-C(10)	1.415(2)
N(1)-H(1)	0.8600
O(1)-C(9)	1.2453(19)
O(2)-C(13)	1.372(2)
O(2)-H(13)	0.8200
C(1)-C(2)	1.390(3)
C(1)-C(6)	1.397(3)
C(1)-C(7)	1.461(3)
C(11)-C(12)	1.378(2)
C(11)-C(10)	1.388(2)
C(11)-H(11)	0.9300
C(7)-C(8)	1.330(2)
C(7)-H(7)	0.9300
C(8)-C(9)	1.467(2)
C(8)-H(8)	0.9300
C(12)-C(13)	1.383(2)
C(12)-H(12)	0.9300
C(10)-C(15)	1.389(2)
C(14)-C(15)	1.377(2)
C(14)-C(13)	1.383(2)
C(14)-H(14)	0.9300
C(15)-H(15)	0.9300
C(2)-C(3)	1.384(3)
C(2)-H(2)	0.9300
C(6)-C(5)	1.379(3)
C(6)-H(6)	0.9300
C(3)-C(4)	1.389(3)
C(3)-H(3)	0.9300
C(4)-C(5)	1.372(3)
C(4)-C(16)	1.504(3)
C(5)-H(5)	0.9300

C(16)-H(16A)	0.9600
C(16)-H(16B)	0.9600
C(16)-H(16C)	0.9600

C(9)-N(1)-C(10)	130.25(14)
C(9)-N(1)-H(1)	114.9
C(10)-N(1)-H(1)	114.9
C(13)-O(2)-H(13)	109.5
C(2)-C(1)-C(6)	117.00(19)
C(2)-C(1)-C(7)	123.30(17)
C(6)-C(1)-C(7)	119.70(18)
C(12)-C(11)-C(10)	120.43(16)
C(12)-C(11)-H(11)	119.8
C(10)-C(11)-H(11)	119.8
C(8)-C(7)-C(1)	127.01(17)
C(8)-C(7)-H(7)	116.5
C(1)-C(7)-H(7)	116.5
C(7)-C(8)-C(9)	122.59(17)
C(7)-C(8)-H(8)	118.7
C(9)-C(8)-H(8)	118.7
C(11)-C(12)-C(13)	121.13(16)
C(11)-C(12)-H(12)	119.4
C(13)-C(12)-H(12)	119.4
C(11)-C(10)-C(15)	118.19(16)
C(11)-C(10)-N(1)	125.06(15)
C(15)-C(10)-N(1)	116.75(15)
O(1)-C(9)-N(1)	123.15(16)
O(1)-C(9)-C(8)	122.74(16)
N(1)-C(9)-C(8)	114.09(15)
C(15)-C(14)-C(13)	120.29(17)
C(15)-C(14)-H(14)	119.9
C(13)-C(14)-H(14)	119.9
O(2)-C(13)-C(12)	118.21(15)
O(2)-C(13)-C(14)	123.09(16)
C(12)-C(13)-C(14)	118.70(16)

C(14)-C(15)-C(10)	121.26(16)
C(14)-C(15)-H(15)	119.4
C(10)-C(15)-H(15)	119.4
C(3)-C(2)-C(1)	120.84(19)
C(3)-C(2)-H(2)	119.6
C(1)-C(2)-H(2)	119.6
C(5)-C(6)-C(1)	121.1(2)
C(5)-C(6)-H(6)	119.5
C(1)-C(6)-H(6)	119.5
C(2)-C(3)-C(4)	122.0(2)
C(2)-C(3)-H(3)	119.0
C(4)-C(3)-H(3)	119.0
C(5)-C(4)-C(3)	116.7(2)
C(5)-C(4)-C(16)	122.4(2)
C(3)-C(4)-C(16)	120.8(3)
C(4)-C(5)-C(6)	122.3(2)
C(4)-C(5)-H(5)	118.8
C(6)-C(5)-H(5)	118.8
C(4)-C(16)-H(16A)	109.5
C(4)-C(16)-H(16B)	109.5
H(16A)-C(16)-H(16B)	109.5
C(4)-C(16)-H(16C)	109.5
H(16A)-C(16)-H(16C)	109.5
H(16B)-C(16)-H(16C)	109.5

Symmetry transformations used to generate equivalent atoms:

Table A-4. Torsion angles [°] for **1**.

C(2)-C(1)-C(7)-C(8)	0.9(3)
C(6)-C(1)-C(7)-C(8)	-178.28(18)
C(1)-C(7)-C(8)-C(9)	177.60(16)
C(10)-C(11)-C(12)-C(13)	0.1(3)
C(12)-C(11)-C(10)-C(15)	-0.5(3)
C(12)-C(11)-C(10)-N(1)	178.91(16)
C(9)-N(1)-C(10)-C(11)	2.8(3)
C(9)-N(1)-C(10)-C(15)	-177.76(17)
C(10)-N(1)-C(9)-O(1)	1.1(3)
C(10)-N(1)-C(9)-C(8)	179.49(15)
C(7)-C(8)-C(9)-O(1)	0.9(3)
C(7)-C(8)-C(9)-N(1)	-177.51(16)
C(11)-C(12)-C(13)-O(2)	-179.79(17)
C(11)-C(12)-C(13)-C(14)	0.6(3)
C(15)-C(14)-C(13)-O(2)	179.59(18)
C(15)-C(14)-C(13)-C(12)	-0.8(3)
C(13)-C(14)-C(15)-C(10)	0.4(3)
C(11)-C(10)-C(15)-C(14)	0.3(3)
N(1)-C(10)-C(15)-C(14)	-179.19(17)
C(6)-C(1)-C(2)-C(3)	0.8(3)
C(7)-C(1)-C(2)-C(3)	-178.45(18)
C(2)-C(1)-C(6)-C(5)	-1.0(3)
C(7)-C(1)-C(6)-C(5)	178.2(2)
C(1)-C(2)-C(3)-C(4)	0.1(3)
C(2)-C(3)-C(4)-C(5)	-0.7(3)
C(2)-C(3)-C(4)-C(16)	179.52(19)
C(3)-C(4)-C(5)-C(6)	0.4(3)
C(16)-C(4)-C(5)-C(6)	-179.8(2)
C(1)-C(6)-C(5)-C(4)	0.5(4)

Symmetry transformations used to generate equivalent atoms:

N-(4-hydroxyphenyl)-3-methylcinnamoyl amide (2)

Table A-5. Crystal data and structure refinement for **2**.

Identification code	**2**	
Empirical formula	C16 H15 N O2	
Formula weight	253.29	
Temperature	293(2) K	
Wavelength	0.71075 Å	
Crystal system	Monoclinic	
Space group	$P2_1/n$	
Unit cell dimensions	a = 7.1644(15) Å	α= 90°.
	b = 17.790(4) Å	β= 96.590(5)°.
	c = 10.796(2) Å	γ = 90°.
Volume	1366.9(5) $Å^3$	
Z	4	
Density (calculated)	1.231 Mg/m^3	
Absorption coefficient	0.081 mm^{-1}	
F(000)	536	
Crystal size	0.40 x 0.20 x 0.20 mm^3	
Theta range for data collection	3.08 to 27.48°.	
Index ranges	-9<=h<=9, -22<=k<=23, -14<=l<=13	
Reflections collected	13037	
Independent reflections	3109 [R(int) = 0.0944]	
Completeness to theta = 27.48°	99.6 %	
Max. and min. transmission	0.9839 and 0.9682	
Refinement method	Full-matrix least-squares on F^2	
Data / restraints / parameters	3109 / 0 / 172	
Goodness-of-fit on F^2	1.026	
Final R indices [I>2sigma(I)]	R1 = 0.0627, wR2 = 0.1451	
R indices (all data)	R1 = 0.1512, wR2 = 0.1886	
Largest diff. peak and hole	0.207 and -0.167 $e.Å^{-3}$	

Table A-6. Atomic coordinates (x 10^4) and equivalent isotropic displacement parameters ($Å^2$x 10^3) for **2**. U(eq) is defined as one third of the trace of the orthogonalized U^{ij} tensor.

	x	y	z	U(eq)
N(1)	4101(3)	1441(1)	9477(2)	60(1)
O(2)	1148(2)	1046(1)	9697(2)	71(1)
O(1)	3039(2)	3641(1)	5793(2)	79(1)
C(10)	3762(3)	2005(1)	8547(2)	55(1)
C(13)	3336(3)	3107(1)	6714(2)	61(1)
C(15)	2006(3)	2208(2)	8009(2)	68(1)
C(9)	2860(4)	1013(1)	10017(2)	59(1)
C(8)	3722(4)	523(1)	11018(2)	63(1)
C(11)	5295(3)	2365(2)	8175(2)	68(1)
C(1)	3346(4)	-427(2)	12680(2)	68(1)
C(12)	5091(3)	2917(2)	7265(2)	71(1)
C(6)	5180(4)	-429(2)	13235(2)	71(1)
C(14)	1804(4)	2751(2)	7098(3)	74(1)
C(7)	2684(4)	58(2)	11623(2)	68(1)
C(2)	2050(5)	-886(2)	13176(3)	90(1)
C(5)	5766(4)	-869(2)	14273(3)	77(1)
C(4)	4430(6)	-1316(2)	14729(3)	96(1)
C(3)	2613(6)	-1332(2)	14205(4)	109(1)
C(16)	7753(5)	-864(2)	14856(3)	103(1)

Table A-7. Bond lengths [Å] and angles [°] for **2**.

N(1)-C(9)	1.351(3)
N(1)-C(10)	1.421(3)
N(1)-H(1)	0.8600
O(2)-C(9)	1.237(3)
O(1)-C(13)	1.374(3)
O(1)-H(1)	0.8200
C(10)-C(11)	1.371(3)
C(10)-C(15)	1.372(3)
C(13)-C(12)	1.370(3)
C(13)-C(14)	1.372(3)
C(15)-C(14)	1.373(3)
C(15)-H(15)	0.9300
C(9)-C(8)	1.470(4)
C(8)-C(7)	1.332(3)
C(8)-H(8)	0.9300
C(11)-C(12)	1.384(3)
C(11)-H(11)	0.9300
C(1)-C(6)	1.380(4)
C(1)-C(2)	1.389(4)
C(1)-C(7)	1.465(4)
C(12)-H(12)	0.9300
C(6)-C(5)	1.391(4)
C(6)-H(6)	0.9300
C(14)-H(14)	0.9300
C(7)-H(7)	0.9300
C(2)-C(3)	1.388(4)
C(2)-H(2)	0.9300
C(5)-C(4)	1.378(4)
C(5)-C(16)	1.489(4)
C(4)-C(3)	1.358(5)
C(4)-H(4)	0.9300
C(3)-H(3)	0.9300

C(16)-H(16A)	0.9600
C(16)-H(16B)	0.9600
C(16)-H(16C)	0.9600

C(9)-N(1)-C(10)	129.4(2)
C(9)-N(1)-H(1)	115.3
C(10)-N(1)-H(1)	115.3
C(13)-O(1)-H(1)	109.5
C(11)-C(10)-C(15)	118.6(2)
C(11)-C(10)-N(1)	117.3(2)
C(15)-C(10)-N(1)	124.0(2)
C(12)-C(13)-C(14)	118.7(2)
C(12)-C(13)-O(1)	122.9(2)
C(14)-C(13)-O(1)	118.4(2)
C(10)-C(15)-C(14)	120.3(2)
C(10)-C(15)-H(15)	119.9
C(14)-C(15)-H(15)	119.9
O(2)-C(9)-N(1)	122.3(2)
O(2)-C(9)-C(8)	123.6(2)
N(1)-C(9)-C(8)	114.2(2)
C(7)-C(8)-C(9)	121.2(2)
C(7)-C(8)-H(8)	119.4
C(9)-C(8)-H(8)	119.4
C(10)-C(11)-C(12)	121.1(2)
C(10)-C(11)-H(11)	119.5
C(12)-C(11)-H(11)	119.5
C(6)-C(1)-C(2)	118.4(3)
C(6)-C(1)-C(7)	123.1(2)
C(2)-C(1)-C(7)	118.4(3)
C(13)-C(12)-C(11)	120.0(2)
C(13)-C(12)-H(12)	120.0
C(11)-C(12)-H(12)	120.0
C(1)-C(6)-C(5)	122.4(3)
C(1)-C(6)-H(6)	118.8
C(5)-C(6)-H(6)	118.8

C(13)-C(14)-C(15)	121.2(2)
C(13)-C(14)-H(14)	119.4
C(15)-C(14)-H(14)	119.4
C(8)-C(7)-C(1)	126.8(3)
C(8)-C(7)-H(7)	116.6
C(1)-C(7)-H(7)	116.6
C(3)-C(2)-C(1)	120.0(3)
C(3)-C(2)-H(2)	120.0
C(1)-C(2)-H(2)	120.0
C(4)-C(5)-C(6)	117.0(3)
C(4)-C(5)-C(16)	121.5(3)
C(6)-C(5)-C(16)	121.5(3)
C(3)-C(4)-C(5)	122.4(3)
C(3)-C(4)-H(4)	118.8
C(5)-C(4)-H(4)	118.8
C(4)-C(3)-C(2)	119.8(3)
C(4)-C(3)-H(3)	120.1
C(2)-C(3)-H(3)	120.1
C(5)-C(16)-H(16A)	109.5
C(5)-C(16)-H(16B)	109.5
H(16A)-C(16)-H(16B)	109.5
C(5)-C(16)-H(16C)	109.5
H(16A)-C(16)-H(16C)	109.5
H(16B)-C(16)-H(16C)	109.5

Symmetry transformations used to generate equivalent atoms:

Table A-8. Torsion angles [°] for **2**.

C(9)-N(1)-C(10)-C(11)	179.0(2)
C(9)-N(1)-C(10)-C(15)	-1.0(4)
C(11)-C(10)-C(15)-C(14)	1.2(4)
N(1)-C(10)-C(15)-C(14)	-178.8(2)
C(10)-N(1)-C(9)-O(2)	3.5(4)
C(10)-N(1)-C(9)-C(8)	-175.6(2)
O(2)-C(9)-C(8)-C(7)	2.1(4)
N(1)-C(9)-C(8)-C(7)	-178.8(2)
C(15)-C(10)-C(11)-C(12)	-0.7(4)
N(1)-C(10)-C(11)-C(12)	179.3(2)
C(14)-C(13)-C(12)-C(11)	1.1(4)
O(1)-C(13)-C(12)-C(11)	-179.0(2)
C(10)-C(11)-C(12)-C(13)	-0.5(4)
C(2)-C(1)-C(6)-C(5)	-0.4(4)
C(7)-C(1)-C(6)-C(5)	177.0(2)
C(12)-C(13)-C(14)-C(15)	-0.5(4)
O(1)-C(13)-C(14)-C(15)	179.5(2)
C(10)-C(15)-C(14)-C(13)	-0.7(4)
C(9)-C(8)-C(7)-C(1)	-176.3(2)
C(6)-C(1)-C(7)-C(8)	3.8(4)
C(2)-C(1)-C(7)-C(8)	-178.8(3)
C(6)-C(1)-C(2)-C(3)	-0.1(4)
C(7)-C(1)-C(2)-C(3)	-177.6(3)
C(1)-C(6)-C(5)-C(4)	0.6(4)
C(1)-C(6)-C(5)-C(16)	179.9(3)
C(6)-C(5)-C(4)-C(3)	-0.3(5)
C(16)-C(5)-C(4)-C(3)	-179.6(3)
C(5)-C(4)-C(3)-C(2)	-0.2(6)
C(1)-C(2)-C(3)-C(4)	0.4(5)

Symmetry transformations used to generate equivalent atoms:

(E)-N-(4-hydroxyphenyl)-3-*p*-tolylacrylamide (3)

Table A-9. Crystal data and structure refinement for **3**.

Identification code	**3**	
Empirical formula	C15 H13 N O2	
Formula weight	239.26	
Temperature	297(2) K	
Wavelength	0.71075 Å	
Crystal system	monoclinic	
Space group	$P2_1/n$	
Unit cell dimensions	a = 6.8140(3) Å	α = 90°.
	b = 18.4539(9) Å	β = 95.1700(10)°.
	c = 10.2513(5) Å	γ = 90°.
Volume	1283.80(11) $Å^3$	
Z	4	
Density (calculated)	1.238 Mg/m3	
Absorption coefficient	0.083 mm-1	
F(000)	504	
Crystal size	0.47 x 0.17 x 0.17 mm3	
Theta range for data collection	3.20 to 27.47°.	
Index ranges	-8<=h<=8, -23<=k<=22, -13<=l<=13	
Reflections collected	12450	
Independent reflections	2925 [R(int) = 0.0225]	
Completeness to theta = 27.47°	99.4 %	
Max. and min. transmission	0.9861 and 0.9622	
Refinement method	Full-matrix least-squares on F^2	
Data / restraints / parameters	2925 / 0 / 171	
Goodness-of-fit on F2	1.084	
Final R indices [I>2sigma(I)]	R1 = 0.0402, wR2 = 0.1131	
R indices (all data)	R1 = 0.0506, wR2 = 0.1212	
Largest diff. peak and hole	0.143 and -0.220 e.$Å^{-3}$	

Table A-10. Atomic coordinates (x 10^4) and equivalent isotropic displacement parameters ($Å^2$x 10^3) for **3**. U(eq) is defined as one third of the trace of the orthogonalized U^{ij} tensor.

	x	y	z	U(eq)
N(1)	5700(1)	1385(1)	475(1)	48(1)
O(2)	6814(1)	3642(1)	4083(1)	67(1)
C(10)	6052(1)	1943(1)	1410(1)	45(1)
O(1)	8786(1)	951(1)	304(1)	60(1)
C(9)	7000(1)	953(1)	-65(1)	46(1)
C(8)	6137(2)	496(1)	-1145(1)	50(1)
C(13)	6496(2)	3082(1)	3211(1)	52(1)
C(15)	7898(2)	2112(1)	2025(1)	54(1)
C(11)	4437(2)	2351(1)	1717(1)	56(1)
C(14)	8103(2)	2675(1)	2912(1)	58(1)
C(12)	4653(2)	2913(1)	2603(1)	59(1)
C(7)	7228(2)	51(1)	-1804(1)	54(1)
C(4)	6556(2)	-410(1)	-2914(1)	57(1)
C(3)	4575(2)	-471(1)	-3387(1)	64(1)
C(1)	5373(3)	-1307(1)	-5033(2)	91(1)
C(5)	7923(2)	-812(1)	-3536(2)	77(1)
C(2)	4002(3)	-915(1)	-4434(2)	79(1)
C(6)	7328(3)	-1257(1)	-4595(2)	98(1)

Table A-11. Bond lengths [Å] and angles [°] for **3**.

N(1)-C(9)	1.3482(14)
N(1)-C(10)	1.4113(14)
N(1)-H(13)	0.892(14)
O(2)-C(13)	1.3702(14)
O(2)-H(17)	0.878(17)
C(10)-C(15)	1.3908(15)
C(10)-C(11)	1.3924(15)
O(1)-C(9)	1.2420(12)
C(9)-C(8)	1.4715(16)
C(8)-C(7)	1.3309(16)
C(8)-H(8)	0.9300
C(13)-C(14)	1.3850(16)
C(13)-C(12)	1.3864(15)
C(15)-C(14)	1.3789(17)
C(15)-H(15)	0.9300
C(11)-C(12)	1.3777(17)
C(11)-H(11)	0.9300
C(14)-H(14)	0.9300
C(12)-H(12)	0.9300
C(7)-C(4)	1.4611(18)
C(7)-H(7)	0.9300
C(4)-C(5)	1.3903(19)
C(4)-C(3)	1.3975(19)
C(3)-C(2)	1.378(2)
C(3)-H(3)	0.9300
C(1)-C(2)	1.369(2)
C(1)-C(6)	1.370(3)
C(1)-H(1)	0.9300
C(5)-C(6)	1.391(2)
C(5)-H(5)	0.9300
C(2)-H(2)	0.9300

C(6)-H(6)	0.9300
C(9)-N(1)-C(10)	129.28(9)
C(9)-N(1)-H(13)	115.1(8)
C(10)-N(1)-H(13)	115.4(8)
C(13)-O(2)-H(17)	111.1(11)
C(15)-C(10)-C(11)	118.46(11)
C(15)-C(10)-N(1)	124.25(10)
C(11)-C(10)-N(1)	117.29(9)
O(1)-C(9)-N(1)	122.59(10)
O(1)-C(9)-C(8)	122.81(10)
N(1)-C(9)-C(8)	114.59(9)
C(7)-C(8)-C(9)	122.10(11)
C(7)-C(8)-H(8)	119.0
C(9)-C(8)-H(8)	119.0
O(2)-C(13)-C(14)	118.15(10)
O(2)-C(13)-C(12)	123.10(10)
C(14)-C(13)-C(12)	118.74(11)
C(14)-C(15)-C(10)	120.14(10)
C(14)-C(15)-H(15)	119.9
C(10)-C(15)-H(15)	119.9
C(12)-C(11)-C(10)	121.12(10)
C(12)-C(11)-H(11)	119.4
C(10)-C(11)-H(11)	119.4
C(15)-C(14)-C(13)	121.27(10)
C(15)-C(14)-H(14)	119.4
C(13)-C(14)-H(14)	119.4
C(11)-C(12)-C(13)	120.27(10)
C(11)-C(12)-H(12)	119.9
C(13)-C(12)-H(12)	119.9
C(8)-C(7)-C(4)	127.14(11)
C(8)-C(7)-H(7)	116.4
C(4)-C(7)-H(7)	116.4
C(5)-C(4)-C(3)	117.60(13)
C(5)-C(4)-C(7)	119.53(12)

C(3)-C(4)-C(7)	122.87(11)
C(2)-C(3)-C(4)	121.04(13)
C(2)-C(3)-H(3)	119.5
C(4)-C(3)-H(3)	119.5
C(2)-C(1)-C(6)	119.99(16)
C(2)-C(1)-H(1)	120.0
C(6)-C(1)-H(1)	120.0
C(4)-C(5)-C(6)	120.85(15)
C(4)-C(5)-H(5)	119.6
C(6)-C(5)-H(5)	119.6
C(1)-C(2)-C(3)	120.37(16)
C(1)-C(2)-H(2)	119.8
C(3)-C(2)-H(2)	119.8
C(1)-C(6)-C(5)	120.13(16)
C(1)-C(6)-H(6)	119.9
C(5)-C(6)-H(6)	119.9

Symmetry transformations used to generate equivalent atoms:

Table A-12. Torsion angles [°] for **3**.

C(9)-N(1)-C(10)-C(15)	-4.80(18)
C(9)-N(1)-C(10)-C(11)	174.44(11)
C(10)-N(1)-C(9)-O(1)	6.82(17)
C(10)-N(1)-C(9)-C(8)	-171.98(10)
O(1)-C(9)-C(8)-C(7)	-0.49(17)
N(1)-C(9)-C(8)-C(7)	178.30(10)
C(11)-C(10)-C(15)-C(14)	-0.34(18)
N(1)-C(10)-C(15)-C(14)	178.90(11)
C(15)-C(10)-C(11)-C(12)	0.42(18)
N(1)-C(10)-C(11)-C(12)	-178.87(11)
C(10)-C(15)-C(14)-C(13)	0.07(19)
O(2)-C(13)-C(14)-C(15)	-178.82(11)
C(12)-C(13)-C(14)-C(15)	0.12(19)
C(10)-C(11)-C(12)-C(13)	-0.2(2)
O(2)-C(13)-C(12)-C(11)	178.85(12)
C(14)-C(13)-C(12)-C(11)	0.0(2)
C(9)-C(8)-C(7)-C(4)	-177.94(10)
C(8)-C(7)-C(4)-C(5)	176.40(12)
C(8)-C(7)-C(4)-C(3)	-3.92(19)
C(5)-C(4)-C(3)-C(2)	-0.1(2)
C(7)-C(4)-C(3)-C(2)	-179.74(12)
C(3)-C(4)-C(5)-C(6)	0.3(2)
C(7)-C(4)-C(5)-C(6)	179.97(14)
C(6)-C(1)-C(2)-C(3)	-0.3(3)
C(4)-C(3)-C(2)-C(1)	0.1(2)
C(2)-C(1)-C(6)-C(5)	0.5(3)
C(4)-C(5)-C(6)-C(1)	-0.5(3)

Symmetry transformations used to generate equivalent atoms:

N-(4-hydroxyphenyl)-2-methylcinnamoyl amide (4)

Table A-13. Crystal data and structure refinement for **4**.

Identification code	**4**	
Empirical formula	C16 H15 N O2	
Formula weight	253.29	
Temperature	293(2) K	
Wavelength	1.54178 Å	
Crystal system	monoclinic	
Space group	$P2_1/n$	
Unit cell dimensions	a = 20.0583(4) Å	α= 90°.
	b = 7.16980(10) Å	β= 113.1500(10)°.
	c = 20.3740(4) Å	γ = 90°.
Volume	2694.13(8) $Å^3$	
Z	8	
Density (calculated)	1.249 Mg/m^3	
Absorption coefficient	0.662 mm^{-1}	
F(000)	1072	
Crystal size	0.26 x 0.04 x 0.04 mm	
Theta range for data collection	3.97 to 68.18°.	
Index ranges	-23<=h<=24, -8<=k<=8, -24<=l<=24	
Reflections collected	29894	
Independent reflections	4893 [R(int) = 0.0394]	
Completeness to theta = 68.18°	99.1 %	
Refinement method	Full-matrix least-squares on F^2	
Data / restraints / parameters	4893 / 0 / 338	
Goodness-of-fit on F^2	1.122	
Final R indices [I>2sigma(I)]	R1 = 0.0594, wR2 = 0.1728	
R indices (all data)	R1 = 0.0948, wR2 = 0.2300	
Largest diff. peak and hole	0.448 and -0.420 $e.Å^{-3}$	

Table A-14. Atomic coordinates (x 10^4) and equivalent isotropic displacement parameters ($Å^2$x 10^3) for **4** U(eq) is defined as one third of the trace of the orthogonalized U^{ij} tensor.

	x	y	z	U(eq)
O(17)	13000(1)	9443(3)	6697(1)	65(1)
O(2)	8633(1)	2259(3)	2191(1)	67(1)
O(18)	12302(1)	5729(3)	3580(1)	63(1)
N(1)	11630(1)	2077(3)	2969(1)	55(1)
N(17)	12969(1)	6329(3)	6501(1)	54(1)
C(26)	12802(1)	6282(4)	5756(1)	50(1)
O(1)	11852(1)	-1005(3)	2888(1)	60(1)
C(10)	10866(2)	2056(4)	2774(1)	50(1)
C(11)	10518(2)	3765(4)	2670(1)	54(1)
C(12)	9775(2)	3869(4)	2479(1)	54(1)
C(23)	13415(2)	8749(4)	8174(2)	57(1)
C(13)	9375(2)	2262(4)	2387(1)	53(1)
C(29)	12459(2)	5956(4)	4295(1)	53(1)
C(7)	13357(2)	-215(4)	3478(1)	55(1)
C(31)	12513(2)	7782(4)	5305(1)	56(1)
C(24)	13263(2)	7410(4)	7688(1)	56(1)
C(25)	13064(1)	7808(4)	6931(1)	53(1)
C(14)	9721(2)	565(4)	2502(2)	73(1)
C(9)	12079(2)	619(4)	3030(1)	50(1)
C(30)	12343(2)	7609(4)	4580(1)	55(1)
C(2)	14594(2)	-1532(4)	4084(2)	60(1)
C(17)	13643(2)	8576(4)	8945(2)	56(1)
C(8)	12855(2)	1095(4)	3285(1)	53(1)
C(27)	12916(2)	4622(4)	5467(2)	61(1)
C(22)	13585(2)	6886(5)	9255(2)	71(1)
C(28)	12747(2)	4466(4)	4745(2)	64(1)
C(1)	14145(2)	-9(4)	3755(1)	55(1)
C(3)	15339(2)	-1278(5)	4345(2)	77(1)
C(18)	13927(2)	10123(4)	9386(2)	61(1)

C(6)	14461(2)	1678(5)	3701(2)	67(1)
C(15)	10464(2)	454(4)	2690(2)	70(1)
C(32)	14004(2)	12001(4)	9096(2)	79(1)
C(21)	13810(2)	6705(5)	9983(2)	83(1)
C(19)	14145(2)	9897(5)	10123(2)	73(1)
C(5)	15203(2)	1879(5)	3960(2)	81(1)
C(4)	15641(2)	398(6)	4290(2)	85(1)
C(16)	14287(2)	-3410(5)	4152(2)	79(1)
C(20)	14089(2)	8212(6)	10415(2)	81(1)

Table A-15. Bond lengths [Å] and angles [°] for **4**

O(17)-C(25)	1.253(3)
O(2)-C(13)	1.381(3)
O(2)-H(2)	0.8200
O(18)-C(29)	1.375(3)
O(18)-H(18)	0.8200
N(1)-C(9)	1.353(3)
N(1)-C(10)	1.424(3)
N(1)-H(1)	0.8600
N(17)-C(25)	1.341(3)
N(17)-C(26)	1.421(3)
N(17)-H(17)	0.8600
C(26)-C(31)	1.384(4)
C(26)-C(27)	1.386(4)
O(1)-C(9)	1.242(3)
C(10)-C(15)	1.374(4)
C(10)-C(11)	1.385(3)
C(11)-C(12)	1.385(4)
C(11)-H(11)	0.9300
C(12)-C(13)	1.374(4)
C(12)-H(12)	0.9300
C(23)-C(24)	1.325(4)
C(23)-C(17)	1.459(4)
C(23)-H(23)	0.9300
C(13)-C(14)	1.374(4)
C(29)-C(28)	1.378(4)
C(29)-C(30)	1.379(4)
C(7)-C(8)	1.319(4)
C(7)-C(1)	1.461(4)
C(7)-H(7)	0.9300
C(31)-C(30)	1.386(4)
C(31)-H(31)	0.9300
C(24)-C(25)	1.461(4)

C(24)-H(24)	0.9300
C(14)-C(15)	1.388(4)
C(14)-H(14)	0.9300
C(9)-C(8)	1.475(4)
C(30)-H(30)	0.9300
C(2)-C(3)	1.388(4)
C(2)-C(1)	1.407(4)
C(2)-C(16)	1.509(4)
C(17)-C(22)	1.391(4)
C(17)-C(18)	1.400(4)
C(8)-H(8)	0.9300
C(27)-C(28)	1.379(4)
C(27)-H(27)	0.9300
C(22)-C(21)	1.376(4)
C(22)-H(22)	0.9300
C(28)-H(28)	0.9300
C(1)-C(6)	1.391(4)
C(3)-C(4)	1.370(5)
C(3)-H(3)	0.9300
C(18)-C(19)	1.398(4)
C(18)-C(32)	1.502(4)
C(6)-C(5)	1.376(4)
C(6)-H(6)	0.9300
C(15)-H(15)	0.9300
C(32)-H(32A)	0.9600
C(32)-H(32B)	0.9600
C(32)-H(32C)	0.9600
C(21)-C(20)	1.367(5)
C(21)-H(21)	0.9300
C(19)-C(20)	1.370(5)
C(19)-H(19)	0.9300
C(5)-C(4)	1.373(5)
C(5)-H(5)	0.9300
C(4)-H(4)	0.9300
C(16)-H(16A)	0.9600

C(16)-H(16B)	0.9600
C(16)-H(16C)	0.9600
C(20)-H(20)	0.9300

C(13)-O(2)-H(2)	109.5
C(29)-O(18)-H(18)	109.5
C(9)-N(1)-C(10)	128.5(2)
C(9)-N(1)-H(1)	115.8
C(10)-N(1)-H(1)	115.8
C(25)-N(17)-C(26)	129.1(2)
C(25)-N(17)-H(17)	115.5
C(26)-N(17)-H(17)	115.5
C(31)-C(26)-C(27)	118.8(3)
C(31)-C(26)-N(17)	123.5(2)
C(27)-C(26)-N(17)	117.6(2)
C(15)-C(10)-C(11)	119.0(3)
C(15)-C(10)-N(1)	123.8(2)
C(11)-C(10)-N(1)	117.1(2)
C(10)-C(11)-C(12)	120.8(3)
C(10)-C(11)-H(11)	119.6
C(12)-C(11)-H(11)	119.6
C(13)-C(12)-C(11)	119.9(3)
C(13)-C(12)-H(12)	120.0
C(11)-C(12)-H(12)	120.0
C(24)-C(23)-C(17)	128.7(3)
C(24)-C(23)-H(23)	115.6
C(17)-C(23)-H(23)	115.6
C(14)-C(13)-C(12)	119.4(3)
C(14)-C(13)-O(2)	117.5(3)
C(12)-C(13)-O(2)	123.1(2)
O(18)-C(29)-C(28)	118.3(2)
O(18)-C(29)-C(30)	122.8(3)
C(28)-C(29)-C(30)	118.9(3)
C(8)-C(7)-C(1)	128.8(3)
C(8)-C(7)-H(7)	115.6

C(1)-C(7)-H(7)	115.6
C(26)-C(31)-C(30)	120.0(3)
C(26)-C(31)-H(31)	120.0
C(30)-C(31)-H(31)	120.0
C(23)-C(24)-C(25)	122.3(3)
C(23)-C(24)-H(24)	118.9
C(25)-C(24)-H(24)	118.9
O(17)-C(25)-N(17)	121.7(3)
O(17)-C(25)-C(24)	121.9(3)
N(17)-C(25)-C(24)	116.4(2)
C(13)-C(14)-C(15)	120.9(3)
C(13)-C(14)-H(14)	119.6
C(15)-C(14)-H(14)	119.6
O(1)-C(9)-N(1)	122.2(3)
O(1)-C(9)-C(8)	122.5(2)
N(1)-C(9)-C(8)	115.2(2)
C(29)-C(30)-C(31)	121.0(3)
C(29)-C(30)-H(30)	119.5
C(31)-C(30)-H(30)	119.5
C(3)-C(2)-C(1)	118.2(3)
C(3)-C(2)-C(16)	119.9(3)
C(1)-C(2)-C(16)	121.9(3)
C(22)-C(17)-C(18)	119.0(3)
C(22)-C(17)-C(23)	121.0(3)
C(18)-C(17)-C(23)	120.0(3)
C(7)-C(8)-C(9)	121.2(3)
C(7)-C(8)-H(8)	119.4
C(9)-C(8)-H(8)	119.4
C(28)-C(27)-C(26)	120.7(3)
C(28)-C(27)-H(27)	119.7
C(26)-C(27)-H(27)	119.7
C(21)-C(22)-C(17)	121.4(3)
C(21)-C(22)-H(22)	119.3
C(17)-C(22)-H(22)	119.3
C(29)-C(28)-C(27)	120.6(3)

C(29)-C(28)-H(28)	119.7
C(27)-C(28)-H(28)	119.7
C(6)-C(1)-C(2)	119.1(3)
C(6)-C(1)-C(7)	121.0(3)
C(2)-C(1)-C(7)	119.9(3)
C(4)-C(3)-C(2)	121.9(3)
C(4)-C(3)-H(3)	119.1
C(2)-C(3)-H(3)	119.1
C(19)-C(18)-C(17)	118.3(3)
C(19)-C(18)-C(32)	119.3(3)
C(17)-C(18)-C(32)	122.4(3)
C(5)-C(6)-C(1)	121.2(3)
C(5)-C(6)-H(6)	119.4
C(1)-C(6)-H(6)	119.4
C(10)-C(15)-C(14)	120.0(3)
C(10)-C(15)-H(15)	120.0
C(14)-C(15)-H(15)	120.0
C(18)-C(32)-H(32A)	109.5
C(18)-C(32)-H(32B)	109.5
H(32A)-C(32)-H(32B)	109.5
C(18)-C(32)-H(32C)	109.5
H(32A)-C(32)-H(32C)	109.5
H(32B)-C(32)-H(32C)	109.5
C(20)-C(21)-C(22)	119.8(3)
C(20)-C(21)-H(21)	120.1
C(22)-C(21)-H(21)	120.1
C(20)-C(19)-C(18)	121.6(3)
C(20)-C(19)-H(19)	119.2
C(18)-C(19)-H(19)	119.2
C(4)-C(5)-C(6)	119.6(3)
C(4)-C(5)-H(5)	120.2
C(6)-C(5)-H(5)	120.2
C(3)-C(4)-C(5)	120.0(3)
C(3)-C(4)-H(4)	120.0
C(5)-C(4)-H(4)	120.0

C(2)-C(16)-H(16A)	109.5
C(2)-C(16)-H(16B)	109.5
H(16A)-C(16)-H(16B)	109.5
C(2)-C(16)-H(16C)	109.5
H(16A)-C(16)-H(16C)	109.5
H(16B)-C(16)-H(16C)	109.5
C(21)-C(20)-C(19)	120.0(3)
C(21)-C(20)-H(20)	120.0
C(19)-C(20)-H(20)	120.0

Symmetry transformations used to generate equivalent atoms:

Table A-16. Torsion angles [°] for **4**.

C(25)-N(17)-C(26)-C(31)	-18.5(4)
C(25)-N(17)-C(26)-C(27)	163.5(3)
C(9)-N(1)-C(10)-C(15)	7.6(4)
C(9)-N(1)-C(10)-C(11)	-172.8(2)
C(15)-C(10)-C(11)-C(12)	-0.5(4)
N(1)-C(10)-C(11)-C(12)	180.0(2)
C(10)-C(11)-C(12)-C(13)	-0.4(4)
C(11)-C(12)-C(13)-C(14)	1.5(4)
C(11)-C(12)-C(13)-O(2)	-179.5(2)
C(27)-C(26)-C(31)-C(30)	0.0(4)
N(17)-C(26)-C(31)-C(30)	-178.1(2)
C(17)-C(23)-C(24)-C(25)	-177.8(2)
C(26)-N(17)-C(25)-O(17)	1.0(4)
C(26)-N(17)-C(25)-C(24)	-177.6(2)
C(23)-C(24)-C(25)-O(17)	-2.8(4)
C(23)-C(24)-C(25)-N(17)	175.8(3)
C(12)-C(13)-C(14)-C(15)	-1.9(5)
O(2)-C(13)-C(14)-C(15)	179.1(3)
C(10)-N(1)-C(9)-O(1)	2.9(4)
C(10)-N(1)-C(9)-C(8)	-176.5(2)
O(18)-C(29)-C(30)-C(31)	-179.7(2)
C(28)-C(29)-C(30)-C(31)	0.0(4)
C(26)-C(31)-C(30)-C(29)	0.0(4)
C(24)-C(23)-C(17)-C(22)	-13.5(5)
C(24)-C(23)-C(17)-C(18)	166.3(3)
C(1)-C(7)-C(8)-C(9)	-178.6(2)
O(1)-C(9)-C(8)-C(7)	-10.6(4)
N(1)-C(9)-C(8)-C(7)	168.9(2)
C(31)-C(26)-C(27)-C(28)	0.1(4)
N(17)-C(26)-C(27)-C(28)	178.3(3)
C(18)-C(17)-C(22)-C(21)	-0.9(5)
C(23)-C(17)-C(22)-C(21)	179.0(3)

O(18)-C(29)-C(28)-C(27)	179.8(3)
C(30)-C(29)-C(28)-C(27)	0.1(4)
C(26)-C(27)-C(28)-C(29)	-0.2(5)
C(3)-C(2)-C(1)-C(6)	0.2(4)
C(16)-C(2)-C(1)-C(6)	-179.1(3)
C(3)-C(2)-C(1)-C(7)	-179.5(3)
C(16)-C(2)-C(1)-C(7)	1.1(4)
C(8)-C(7)-C(1)-C(6)	-14.5(5)
C(8)-C(7)-C(1)-C(2)	165.3(3)
C(1)-C(2)-C(3)-C(4)	0.1(5)
C(16)-C(2)-C(3)-C(4)	179.5(3)
C(22)-C(17)-C(18)-C(19)	0.4(4)
C(23)-C(17)-C(18)-C(19)	-179.4(3)
C(22)-C(17)-C(18)-C(32)	-179.7(3)
C(23)-C(17)-C(18)-C(32)	0.5(4)
C(2)-C(1)-C(6)-C(5)	0.2(4)
C(7)-C(1)-C(6)-C(5)	-180.0(3)
C(11)-C(10)-C(15)-C(14)	0.2(5)
N(1)-C(10)-C(15)-C(14)	179.7(3)
C(13)-C(14)-C(15)-C(10)	1.0(5)
C(17)-C(22)-C(21)-C(20)	0.7(5)
C(17)-C(18)-C(19)-C(20)	0.3(5)
C(32)-C(18)-C(19)-C(20)	-179.7(3)
C(1)-C(6)-C(5)-C(4)	-1.1(5)
C(2)-C(3)-C(4)-C(5)	-0.9(5)
C(6)-C(5)-C(4)-C(3)	1.4(5)
C(22)-C(21)-C(20)-C(19)	0.0(5)
C(18)-C(19)-C(20)-C(21)	-0.5(5)

Symmetry transformations used to generate equivalent atoms:

Photodimer of Cinnamic Amide Derivative 1 (7)

Table A-18. Crystal data and structure refinement for **7**.

Identification code	**7**	
Empirical formula	C32 H30 N2 O4	
Formula weight	506.58	
Temperature	293(2) K	
Wavelength	0.71075 Å	
Crystal system	monoclinic	
Space group	$P2_1/n$	
Unit cell dimensions	a = 6.8016(6) Å	α= 90°.
	b = 12.5421(10) Å	β= 93.012(2)°.
	c = 16.2644(14) Å	γ = 90°.
Volume	1385.5(2) $Å^3$	
Z	2	
Density (calculated)	1.214 Mg/m^3	
Absorption coefficient	0.080 mm^{-1}	
F(000)	536	
Crystal size	0.35 x 0.29 x 0.13 mm^3	
Theta range for data collection	2.99 to 27.42°.	
Index ranges	-8<=h<=8, -16<=k<=16, -20<=l<=18	
Reflections collected	13035	
Independent reflections	3147 [R(int) = 0.0495]	
Completeness to theta = 27.42°	99.5 %	
Refinement method	Full-matrix least-squares on F^2	
Data / restraints / parameters	3147 / 0 / 232	
Goodness-of-fit on F^2	1.049	
Final R indices [I>2sigma(I)]	R1 = 0.0454, wR2 = 0.1075	
R indices (all data)	R1 = 0.1159, wR2 = 0.1460	
Largest diff. peak and hole	0.188 and -0.170 e.$Å^{-3}$	

Table A-19. Atomic coordinates (x 10^4) and equivalent isotropic displacement parameters ($Å^2$x 10^3) for **7**. U(eq) is defined as one third of the trace of the orthogonalized U^{ij} tensor.

	x	y	z	U(eq)
N(1)	777(3)	3323(1)	1556(1)	64(1)
O(2)	-2379(2)	3645(1)	1118(1)	72(1)
O(1)	490(2)	-595(1)	3165(1)	93(1)
C(16)	152(3)	4813(2)	661(1)	59(1)
C(10)	-1087(3)	1073(2)	2794(1)	67(1)
C(8)	1372(3)	4554(2)	-114(1)	60(1)
C(11)	-1029(3)	2049(2)	2393(1)	68(1)
C(5)	1737(3)	3406(2)	-318(1)	63(1)
C(9)	467(3)	377(2)	2773(1)	67(1)
C(15)	-619(3)	3883(2)	1132(1)	58(1)
C(12)	590(3)	2327(2)	1969(1)	59(1)
C(14)	2085(3)	656(2)	2346(2)	84(1)
C(13)	2145(3)	1624(2)	1945(2)	78(1)
C(4)	3620(4)	2987(2)	-200(2)	77(1)
C(6)	257(4)	2736(2)	-629(2)	81(1)
C(3)	3997(5)	1936(2)	-387(2)	99(1)
C(7)	672(5)	1680(2)	-812(2)	101(1)
C(2)	2552(5)	1268(2)	-696(2)	106(1)
C(1)	2978(12)	116(4)	-911(5)	189(3)

Table A-20. Bond lengths [Å] and angles [°] for **7**.

N(1)-C(15)	1.343(2)
N(1)-C(12)	1.427(3)
N(1)-H(10)	0.94(2)
O(2)-C(15)	1.232(2)
O(1)-C(9)	1.375(2)
O(1)-H(15)	0.96(3)
C(16)-C(15)	1.504(3)
C(16)-C(8)#1	1.550(3)
C(16)-C(8)	1.578(3)
C(16)-H(9)	0.946(19)
C(10)-C(9)	1.372(3)
C(10)-C(11)	1.388(3)
C(10)-H(14)	0.97(2)
C(8)-C(5)	1.501(3)
C(8)-C(16)#1	1.550(3)
C(8)-H(8)	1.026(18)
C(11)-C(12)	1.375(3)
C(11)-H(13)	0.95(2)
C(5)-C(6)	1.387(3)
C(5)-C(4)	1.388(3)
C(9)-C(14)	1.377(3)
C(12)-C(13)	1.379(3)
C(14)-C(13)	1.379(3)
C(14)-H(11)	0.97(2)
C(13)-H(12)	0.96(2)
C(4)-C(3)	1.380(3)
C(4)-H(5)	1.04(3)
C(6)-C(7)	1.390(3)
C(6)-H(6)	1.01(2)
C(3)-C(2)	1.367(4)
C(3)-H(4)	0.99(3)
C(7)-C(2)	1.382(4)

C(7)-H(7)	0.97(3)
C(2)-C(1)	1.518(4)
C(1)-H(3)	1.10(3)
C(1)-H(2)	0.87(3)
C(1)-H(1)	0.88(5)

C(15)-N(1)-C(12)	128.46(18)
C(15)-N(1)-H(10)	116.9(14)
C(12)-N(1)-H(10)	114.1(14)
C(9)-O(1)-H(15)	110.4(18)
C(15)-C(16)-C(8)#1	116.70(17)
C(15)-C(16)-C(8)	117.31(16)
C(8)#1-C(16)-C(8)	90.66(15)
C(15)-C(16)-H(9)	108.5(11)
C(8)#1-C(16)-H(9)	113.2(11)
C(8)-C(16)-H(9)	109.6(11)
C(9)-C(10)-C(11)	120.5(2)
C(9)-C(10)-H(14)	118.8(13)
C(11)-C(10)-H(14)	120.7(13)
C(5)-C(8)-C(16)#1	118.54(18)
C(5)-C(8)-C(16)	118.34(17)
C(16)#1-C(8)-C(16)	89.34(15)
C(5)-C(8)-H(8)	109.9(10)
C(16)#1-C(8)-H(8)	109.5(10)
C(16)-C(8)-H(8)	109.5(10)
C(12)-C(11)-C(10)	120.2(2)
C(12)-C(11)-H(13)	119.5(14)
C(10)-C(11)-H(13)	120.3(14)
C(6)-C(5)-C(4)	117.9(2)
C(6)-C(5)-C(8)	122.47(19)
C(4)-C(5)-C(8)	119.6(2)
C(10)-C(9)-O(1)	122.83(19)
C(10)-C(9)-C(14)	119.2(2)
O(1)-C(9)-C(14)	117.97(19)
O(2)-C(15)-N(1)	122.83(19)

O(2)-C(15)-C(16)	122.87(18)
N(1)-C(15)-C(16)	114.29(17)
C(11)-C(12)-C(13)	119.2(2)
C(11)-C(12)-N(1)	123.49(19)
C(13)-C(12)-N(1)	117.35(18)
C(9)-C(14)-C(13)	120.4(2)
C(9)-C(14)-H(11)	118.0(14)
C(13)-C(14)-H(11)	121.5(14)
C(14)-C(13)-C(12)	120.5(2)
C(14)-C(13)-H(12)	119.6(13)
C(12)-C(13)-H(12)	119.9(13)
C(3)-C(4)-C(5)	120.8(3)
C(3)-C(4)-H(5)	121.0(14)
C(5)-C(4)-H(5)	118.2(14)
C(5)-C(6)-C(7)	120.3(3)
C(5)-C(6)-H(6)	121.2(13)
C(7)-C(6)-H(6)	118.5(13)
C(2)-C(3)-C(4)	121.9(3)
C(2)-C(3)-H(4)	118.7(16)
C(4)-C(3)-H(4)	119.4(17)
C(2)-C(7)-C(6)	121.6(3)
C(2)-C(7)-H(7)	121.5(16)
C(6)-C(7)-H(7)	116.9(16)
C(3)-C(2)-C(7)	117.6(2)
C(3)-C(2)-C(1)	121.7(4)
C(7)-C(2)-C(1)	120.7(4)
C(2)-C(1)-H(3)	101(2)
C(2)-C(1)-H(2)	109(3)
H(3)-C(1)-H(2)	129(4)
C(2)-C(1)-H(1)	117(3)
H(3)-C(1)-H(1)	87(3)
H(2)-C(1)-H(1)	112(4)

Symmetry transformations used to generate equivalent atoms:

#1 -x,-y+1,-z

Table A-21. Torsion angles [°] for **7**.

C(15)-C(16)-C(8)-C(5)	-1.7(3)
C(8)#1-C(16)-C(8)-C(5)	-122.5(2)
C(15)-C(16)-C(8)-C(16)#1	120.8(2)
C(8)#1-C(16)-C(8)-C(16)#1	0.0
C(9)-C(10)-C(11)-C(12)	0.2(3)
C(16)#1-C(8)-C(5)-C(6)	-35.2(3)
C(16)-C(8)-C(5)-C(6)	71.0(3)
C(16)#1-C(8)-C(5)-C(4)	144.6(2)
C(16)-C(8)-C(5)-C(4)	-109.3(2)
C(11)-C(10)-C(9)-O(1)	179.5(2)
C(11)-C(10)-C(9)-C(14)	-0.3(4)
C(12)-N(1)-C(15)-O(2)	8.2(3)
C(12)-N(1)-C(15)-C(16)	-170.60(18)
C(8)#1-C(16)-C(15)-O(2)	-2.6(3)
C(8)-C(16)-C(15)-O(2)	-108.5(2)
C(8)#1-C(16)-C(15)-N(1)	176.16(16)
C(8)-C(16)-C(15)-N(1)	70.3(2)
C(10)-C(11)-C(12)-C(13)	0.2(3)
C(10)-C(11)-C(12)-N(1)	-178.7(2)
C(15)-N(1)-C(12)-C(11)	-37.9(3)
C(15)-N(1)-C(12)-C(13)	143.2(2)
C(10)-C(9)-C(14)-C(13)	0.2(4)
O(1)-C(9)-C(14)-C(13)	-179.6(2)
C(9)-C(14)-C(13)-C(12)	0.1(4)
C(11)-C(12)-C(13)-C(14)	-0.3(4)
N(1)-C(12)-C(13)-C(14)	178.6(2)
C(6)-C(5)-C(4)-C(3)	0.1(3)
C(8)-C(5)-C(4)-C(3)	-179.7(2)
C(4)-C(5)-C(6)-C(7)	0.1(4)
C(8)-C(5)-C(6)-C(7)	179.8(2)
C(5)-C(4)-C(3)-C(2)	0.1(4)
C(5)-C(6)-C(7)-C(2)	-0.4(4)
C(4)-C(3)-C(2)-C(7)	-0.4(5)

C(4)-C(3)-C(2)-C(1)	179.3(5)
C(6)-C(7)-C(2)-C(3)	0.6(5)
C(6)-C(7)-C(2)-C(1)	-179.2(5)

Symmetry transformations used to generate equivalent atoms:

#1 -x,-y+1,-z

N-(4-hydroxyphenyl)-2-methylcinnamoyl amide (8)

Table A-22. Crystal data and structure refinement for **8**.

Identification code	**8**	
Empirical formula	C15 H13 N O2	
Formula weight	239.26	
Temperature	293(2) K	
Wavelength	0.71075 Å	
Crystal system	monoclinic	
Space group	$P2_1/c$	
Unit cell dimensions	a = 8.6306(18) Å	α= 90°.
	b = 12.489(3) Å	β= 92.306(4)°.
	c = 23.180(5) Å	γ = 90°.
Volume	2496.4(9) $Å^3$	
Z	8	
Density (calculated)	1.273 Mg/m^3	
Absorption coefficient	0.085 mm^{-1}	
F(000)	1008	
Crystal size	0.62 x 0.36 x 0.18 mm^3	
Theta range for data collection	3.00 to 27.48°.	
Index ranges	-10<=h<=11, -16<=k<=16, -30<=l<=29	
Reflections collected	22443	
Independent reflections	5687 [R(int) = 0.1303]	
Completeness to theta = 27.48°	99.2 %	
Refinement method	Full-matrix least-squares on F^2	
Data / restraints / parameters	5687 / 0 / 325	
Goodness-of-fit on F^2	1.035	
Final R indices [I>2sigma(I)]	R1 = 0.1156, wR2 = 0.2986	
R indices (all data)	R1 = 0.1742, wR2 = 0.3296	
Largest diff. peak and hole	0.304 and -0.396 e.$Å^{-3}$	

Table A-23. Atomic coordinates (x 10^4) and equivalent isotropic displacement parameters ($Å^2$x 10^3) for **8**. U(eq) is defined as one third of the trace of the orthogonalized U^{ij} tensor.

	x	y	z	U(eq)
O(2)	652(4)	5868(2)	2802(1)	65(1)
N(1)	1916(4)	3905(3)	2758(2)	57(1)
O(1)	1434(4)	2123(3)	2684(2)	67(1)
C(8)	3091(5)	2936(4)	2007(2)	58(1)
C(11)	363(5)	5182(4)	3248(2)	55(1)
C(9)	2074(5)	2939(4)	2508(2)	56(1)
C(1)	4706(5)	1926(4)	1321(2)	59(1)
C(10)	998(5)	4161(4)	3234(2)	55(1)
C(12)	-521(6)	5479(4)	3706(2)	68(1)
C(15)	757(6)	3452(4)	3683(2)	67(1)
C(7)	3655(5)	2031(4)	1803(2)	57(1)
C(6)	5037(6)	2778(5)	962(2)	72(1)
C(13)	-761(6)	4784(5)	4152(2)	77(2)
C(3)	6441(7)	826(6)	784(3)	90(2)
C(14)	-125(6)	3765(5)	4139(2)	79(2)
C(4)	6753(7)	1682(6)	436(3)	93(2)
C(2)	5409(6)	948(5)	1224(2)	74(2)
C(5)	6060(8)	2653(6)	521(3)	90(2)
O(3)	3387(4)	9261(3)	2395(2)	72(1)
N(2)	2983(4)	7460(3)	2331(2)	57(1)
O(4)	4270(4)	5512(3)	2278(2)	69(1)
C(24)	2780(5)	8430(4)	2573(2)	56(1)
C(23)	1748(5)	8434(4)	3071(2)	58(1)
C(26)	4595(5)	6215(4)	1840(2)	56(1)
C(16)	108(5)	9479(4)	3740(2)	58(1)
C(27)	5533(6)	5934(4)	1389(2)	68(1)
C(30)	4178(6)	7955(4)	1421(2)	68(1)
C(25)	3937(5)	7222(4)	1860(2)	56(1)
C(22)	1156(5)	9341(4)	3262(2)	59(1)

C(18)	-1675(6)	10608(5)	4242(2)	78(2)
C(19)	-1939(7)	9798(5)	4617(3)	84(2)
C(17)	-641(6)	10452(4)	3804(2)	66(1)
C(20)	-1208(7)	8811(5)	4566(2)	82(2)
C(28)	5805(7)	6678(5)	964(2)	80(2)
C(21)	-179(6)	8660(4)	4132(2)	71(1)
C(29)	5125(7)	7677(5)	977(2)	79(2)

Table A-24. Bond lengths [Å] and angles [°] for **8**.

O(2)-C(11)	1.374(5)
O(2)-H(11)	0.8200
N(1)-C(9)	1.347(6)
N(1)-C(10)	1.421(5)
N(1)-H(1)	0.8600
O(1)-C(9)	1.238(5)
C(8)-C(7)	1.326(6)
C(8)-C(9)	1.483(6)
C(8)-H(8)	0.9300
C(11)-C(12)	1.383(6)
C(11)-C(10)	1.388(6)
C(1)-C(2)	1.385(7)
C(1)-C(6)	1.389(7)
C(1)-C(7)	1.472(6)
C(10)-C(15)	1.388(6)
C(12)-C(13)	1.372(7)
C(12)-H(12)	0.9300
C(15)-C(14)	1.384(7)
C(15)-H(15)	0.9300
C(7)-H(7)	0.9300
C(6)-C(5)	1.387(7)
C(6)-H(6)	0.9300
C(13)-C(14)	1.386(8)
C(13)-H(13)	0.9300
C(3)-C(4)	1.373(9)
C(3)-C(2)	1.389(7)
C(3)-H(3)	0.9300
C(14)-H(14)	0.9300
C(4)-C(5)	1.370(9)
C(4)-H(4)	0.9300
C(2)-H(2)	0.9300
C(5)-H(5)	0.9300

O(3)-C(24)	1.240(5)
N(2)-C(24)	1.349(5)
N(2)-C(25)	1.426(6)
N(2)-H(24)	0.8600
O(4)-C(26)	1.379(5)
O(4)-H(26)	0.8200
C(24)-C(23)	1.487(6)
C(23)-C(22)	1.325(6)
C(23)-H(23)	0.9300
C(26)-C(25)	1.382(6)
C(26)-C(27)	1.393(6)
C(16)-C(17)	1.387(6)
C(16)-C(21)	1.397(7)
C(16)-C(22)	1.469(6)
C(27)-C(28)	1.382(7)
C(27)-H(27)	0.9300
C(30)-C(29)	1.384(7)
C(30)-C(25)	1.390(6)
C(30)-H(30)	0.9300
C(22)-H(22)	0.9300
C(18)-C(19)	1.360(8)
C(18)-C(17)	1.393(7)
C(18)-H(18)	0.9300
C(19)-C(20)	1.391(8)
C(19)-H(19)	0.9300
C(17)-H(17)	0.9300
C(20)-C(21)	1.382(7)
C(20)-H(20)	0.9300
C(28)-C(29)	1.380(8)
C(28)-H(28)	0.9300
C(21)-H(21)	0.9300
C(29)-H(29)	0.9300

C(11)-O(2)-H(11)	109.5
C(9)-N(1)-C(10)	127.2(4)

C(9)-N(1)-H(1)	116.4
C(10)-N(1)-H(1)	116.4
C(7)-C(8)-C(9)	121.3(4)
C(7)-C(8)-H(8)	119.4
C(9)-C(8)-H(8)	119.4
O(2)-C(11)-C(12)	122.2(4)
O(2)-C(11)-C(10)	118.1(4)
C(12)-C(11)-C(10)	119.7(4)
O(1)-C(9)-N(1)	122.7(4)
O(1)-C(9)-C(8)	122.9(4)
N(1)-C(9)-C(8)	114.4(4)
C(2)-C(1)-C(6)	118.4(5)
C(2)-C(1)-C(7)	119.3(4)
C(6)-C(1)-C(7)	122.3(5)
C(15)-C(10)-C(11)	119.7(4)
C(15)-C(10)-N(1)	122.9(4)
C(11)-C(10)-N(1)	117.3(4)
C(13)-C(12)-C(11)	120.8(5)
C(13)-C(12)-H(12)	119.6
C(11)-C(12)-H(12)	119.6
C(14)-C(15)-C(10)	119.8(5)
C(14)-C(15)-H(15)	120.1
C(10)-C(15)-H(15)	120.1
C(8)-C(7)-C(1)	126.4(4)
C(8)-C(7)-H(7)	116.8
C(1)-C(7)-H(7)	116.8
C(5)-C(6)-C(1)	120.5(5)
C(5)-C(6)-H(6)	119.7
C(1)-C(6)-H(6)	119.7
C(12)-C(13)-C(14)	119.5(5)
C(12)-C(13)-H(13)	120.2
C(14)-C(13)-H(13)	120.2
C(4)-C(3)-C(2)	119.6(6)
C(4)-C(3)-H(3)	120.2
C(2)-C(3)-H(3)	120.2

C(15)-C(14)-C(13)	120.4(5)
C(15)-C(14)-H(14)	119.8
C(13)-C(14)-H(14)	119.8
C(5)-C(4)-C(3)	120.5(6)
C(5)-C(4)-H(4)	119.8
C(3)-C(4)-H(4)	119.8
C(1)-C(2)-C(3)	120.9(5)
C(1)-C(2)-H(2)	119.5
C(3)-C(2)-H(2)	119.5
C(4)-C(5)-C(6)	120.0(6)
C(4)-C(5)-H(5)	120.0
C(6)-C(5)-H(5)	120.0
C(24)-N(2)-C(25)	126.5(4)
C(24)-N(2)-H(24)	116.8
C(25)-N(2)-H(24)	116.8
C(26)-O(4)-H(26)	109.5
O(3)-C(24)-N(2)	123.3(4)
O(3)-C(24)-C(23)	122.1(4)
N(2)-C(24)-C(23)	114.7(4)
C(22)-C(23)-C(24)	120.8(4)
C(22)-C(23)-H(23)	119.6
C(24)-C(23)-H(23)	119.6
O(4)-C(26)-C(25)	117.4(4)
O(4)-C(26)-C(27)	122.2(4)
C(25)-C(26)-C(27)	120.4(4)
C(17)-C(16)-C(21)	118.4(5)
C(17)-C(16)-C(22)	119.2(5)
C(21)-C(16)-C(22)	122.4(4)
C(28)-C(27)-C(26)	119.1(5)
C(28)-C(27)-H(27)	120.4
C(26)-C(27)-H(27)	120.4
C(29)-C(30)-C(25)	119.3(5)
C(29)-C(30)-H(30)	120.3
C(25)-C(30)-H(30)	120.3
C(26)-C(25)-C(30)	120.1(4)

C(26)-C(25)-N(2)	117.7(4)
C(30)-C(25)-N(2)	122.1(4)
C(23)-C(22)-C(16)	127.5(5)
C(23)-C(22)-H(22)	116.2
C(16)-C(22)-H(22)	116.2
C(19)-C(18)-C(17)	119.4(5)
C(19)-C(18)-H(18)	120.3
C(17)-C(18)-H(18)	120.3
C(18)-C(19)-C(20)	121.1(5)
C(18)-C(19)-H(19)	119.5
C(20)-C(19)-H(19)	119.5
C(16)-C(17)-C(18)	121.1(5)
C(16)-C(17)-H(17)	119.5
C(18)-C(17)-H(17)	119.5
C(21)-C(20)-C(19)	119.3(6)
C(21)-C(20)-H(20)	120.3
C(19)-C(20)-H(20)	120.3
C(29)-C(28)-C(27)	120.5(5)
C(29)-C(28)-H(28)	119.8
C(27)-C(28)-H(28)	119.8
C(20)-C(21)-C(16)	120.7(5)
C(20)-C(21)-H(21)	119.7
C(16)-C(21)-H(21)	119.7
C(28)-C(29)-C(30)	120.5(5)
C(28)-C(29)-H(29)	119.7
C(30)-C(29)-H(29)	119.7

Symmetry transformations used to generate equivalent atoms:

Table A-25. Torsion angles [°] for **8**.

C(10)-N(1)-C(9)-O(1)	-2.0(7)
C(10)-N(1)-C(9)-C(8)	178.6(4)
C(7)-C(8)-C(9)-O(1)	-15.6(7)
C(7)-C(8)-C(9)-N(1)	163.8(4)
O(2)-C(11)-C(10)-C(15)	178.7(4)
C(12)-C(11)-C(10)-C(15)	-0.9(7)
O(2)-C(11)-C(10)-N(1)	0.6(6)
C(12)-C(11)-C(10)-N(1)	-179.0(4)
C(9)-N(1)-C(10)-C(15)	33.6(7)
C(9)-N(1)-C(10)-C(11)	-148.3(5)
O(2)-C(11)-C(12)-C(13)	-178.5(5)
C(10)-C(11)-C(12)-C(13)	1.0(7)
C(11)-C(10)-C(15)-C(14)	0.6(7)
N(1)-C(10)-C(15)-C(14)	178.6(4)
C(9)-C(8)-C(7)-C(1)	-178.2(4)
C(2)-C(1)-C(7)-C(8)	168.6(5)
C(6)-C(1)-C(7)-C(8)	-10.5(8)
C(2)-C(1)-C(6)-C(5)	-0.6(8)
C(7)-C(1)-C(6)-C(5)	178.6(5)
C(11)-C(12)-C(13)-C(14)	-0.9(8)
C(10)-C(15)-C(14)-C(13)	-0.4(8)
C(12)-C(13)-C(14)-C(15)	0.6(9)
C(2)-C(3)-C(4)-C(5)	0.2(10)
C(6)-C(1)-C(2)-C(3)	1.0(8)
C(7)-C(1)-C(2)-C(3)	-178.2(5)
C(4)-C(3)-C(2)-C(1)	-0.8(9)
C(3)-C(4)-C(5)-C(6)	0.1(10)
C(1)-C(6)-C(5)-C(4)	0.1(9)
C(25)-N(2)-C(24)-O(3)	2.4(8)
C(25)-N(2)-C(24)-C(23)	-178.3(4)
O(3)-C(24)-C(23)-C(22)	15.4(7)
N(2)-C(24)-C(23)-C(22)	-163.9(4)

O(4)-C(26)-C(27)-C(28)	179.8(5)
C(25)-C(26)-C(27)-C(28)	0.4(7)
O(4)-C(26)-C(25)-C(30)	-177.8(4)
C(27)-C(26)-C(25)-C(30)	1.6(7)
O(4)-C(26)-C(25)-N(2)	0.3(6)
C(27)-C(26)-C(25)-N(2)	179.7(4)
C(29)-C(30)-C(25)-C(26)	-2.3(7)
C(29)-C(30)-C(25)-N(2)	179.6(4)
C(24)-N(2)-C(25)-C(26)	149.7(5)
C(24)-N(2)-C(25)-C(30)	-32.2(7)
C(24)-C(23)-C(22)-C(16)	179.0(4)
C(17)-C(16)-C(22)-C(23)	-167.1(5)
C(21)-C(16)-C(22)-C(23)	12.3(8)
C(17)-C(18)-C(19)-C(20)	-0.8(9)
C(21)-C(16)-C(17)-C(18)	-1.1(8)
C(22)-C(16)-C(17)-C(18)	178.4(5)
C(19)-C(18)-C(17)-C(16)	0.9(8)
C(18)-C(19)-C(20)-C(21)	1.0(9)
C(26)-C(27)-C(28)-C(29)	-1.6(8)
C(19)-C(20)-C(21)-C(16)	-1.3(9)
C(17)-C(16)-C(21)-C(20)	1.3(8)
C(22)-C(16)-C(21)-C(20)	-178.1(5)
C(27)-C(28)-C(29)-C(30)	0.9(9)
C(25)-C(30)-C(29)-C(28)	1.1(8)

Symmetry transformations used to generate equivalent atoms:

Photodimer of Cinnamic Amide Derivative 8 (9)

Table A-26. Crystal data and structure refinement for **9**.

Identification code	**9**	
Empirical formula	C30 H26 N2 O4	
Formula weight	478.53	
Temperature	293(2) K	
Wavelength	0.71075 Å	
Crystal system	triclinic	
Space group	*P*	
Unit cell dimensions	a = 9.9569(11) Å	α= 107.589(3)°.
	b = 10.4775(11) Å	β= 104.422(3)°.
	c = 12.8043(12) Å	γ = 96.820(3)°.
Volume	1205.7(2) $Å^3$	
Z	2	
Density (calculated)	1.318 Mg/m^3	
Absorption coefficient	0.088 mm^{-1}	
F(000)	504	
Crystal size	0.12 x 0.03 x 0.04 mm^3	
Theta range for data collection	3.03 to 27.44°.	
Index ranges	-12<=h<=12, -12<=k<=13, -16<=l<=15	
Reflections collected	11881	
Independent reflections	5444 [R(int) = 0.0662]	
Completeness to theta = 27.44°	98.8 %	
Refinement method	Full-matrix least-squares on F^2	
Data / restraints / parameters	5444 / 0 / 325	
Goodness-of-fit on F^2	0.949	
Final R indices [I>2sigma(I)]	R1 = 0.0590, wR2 = 0.1472	
R indices (all data)	R1 = 0.1799, wR2 = 0.2214	
Largest diff. peak and hole	0.266 and -0.396 e.$Å^{-3}$	

Table A-27. Atomic coordinates (x 10^4) and equivalent isotropic displacement parameters ($Å^2$x 10^3) for **9**. U(eq) is defined as one third of the trace of the orthogonalized U^{ij} tensor.

	x	y	z	U(eq)
O(3)	2832(3)	4003(3)	3702(2)	59(1)
N(2)	7764(3)	3120(3)	6185(2)	50(1)
O(4)	6868(3)	1015(3)	4838(2)	62(1)
O(2)	9593(3)	1540(3)	5230(2)	61(1)
C(26)	4618(3)	3414(3)	5630(3)	43(1)
N(1)	906(3)	2784(3)	3855(2)	51(1)
O(1)	685(3)	2817(4)	1578(2)	87(1)
C(19)	9848(4)	2022(4)	6395(3)	52(1)
C	-132(4)	3343(4)	3249(3)	49(1)
C(29)	6748(4)	2207(4)	5279(3)	46(1)
C(20)	8949(4)	2793(4)	6877(3)	51(1)
C(28)	3216(3)	2454(3)	4744(3)	45(1)
C(30)	5451(3)	2705(3)	4803(3)	44(1)
C(25)	4118(3)	1596(3)	4065(3)	45(1)
C(12)	5543(4)	4535(4)	7765(3)	54(1)
C(27)	2320(3)	3158(4)	4070(3)	45(1)
C(8)	4785(4)	2102(4)	7006(3)	53(1)
C(14)	-1302(4)	3845(5)	1588(3)	69(1)
C(16)	-2147(4)	4383(4)	3217(3)	60(1)
C(4)	3675(4)	1149(3)	2779(3)	49(1)
C(13)	-227(4)	3338(4)	2153(3)	58(1)
C(17)	-1114(4)	3854(4)	3772(3)	54(1)
C(7)	4972(3)	3344(4)	6818(3)	46(1)
C(3)	2372(4)	244(4)	2131(3)	61(1)
C(24)	11003(4)	1788(5)	7108(4)	67(1)
C(9)	5126(4)	2068(4)	8110(3)	61(1)
C(5)	4526(5)	1563(4)	2188(3)	68(1)
C(21)	9220(4)	3276(5)	8058(3)	69(1)
C(15)	-2245(4)	4381(4)	2128(3)	64(1)

C(10)	5667(4)	3251(5)	9032(3)	67(1)
C(11)	5883(4)	4488(5)	8868(3)	66(1)
C(22)	10372(5)	3022(5)	8759(4)	79(1)
C(2)	1943(5)	-199(5)	959(4)	78(1)
C(23)	11268(5)	2285(5)	8286(4)	82(1)
C(1)	2776(6)	227(5)	383(4)	85(1)
C(6)	4067(6)	1107(5)	987(4)	86(2)

Table A-28. Bond lengths [Å] and angles [°] for shelxl.

O(3)-C(27)	1.237(4)
N(2)-C(29)	1.341(4)
N(2)-C(20)	1.433(5)
N(2)-H(2)	0.8600
O(4)-C(29)	1.239(4)
O(2)-C(19)	1.367(4)
O(2)-H(2A)	0.8200
C(26)-C(7)	1.500(4)
C(26)-C(28)	1.560(5)
C(26)-C(30)	1.572(4)
C(26)-H(26)	0.9800
N(1)-C(27)	1.350(4)
N(1)-C	1.427(4)
N(1)-H(1)	0.8600
O(1)-C(13)	1.368(4)
O(1)-H(1A)	0.8200
C(19)-C(24)	1.377(5)
C(19)-C(20)	1.406(5)
C-C(13)	1.380(5)
C-C(17)	1.388(5)
C(29)-C(30)	1.507(5)
C(20)-C(21)	1.385(5)
C(28)-C(27)	1.498(5)
C(28)-C(25)	1.575(5)
C(28)-H(28)	0.9800
C(30)-C(25)	1.533(5)
C(30)-H(30)	0.9800
C(25)-C(4)	1.499(5)
C(25)-H(25)	0.9800
C(12)-C(11)	1.385(5)
C(12)-C(7)	1.387(5)
C(12)-H(12)	0.9300

C(8)-C(9)	1.381(5)
C(8)-C(7)	1.392(5)
C(8)-H(8)	0.9300
C(14)-C(15)	1.374(6)
C(14)-C(13)	1.390(5)
C(14)-H(14)	0.9300
C(16)-C(17)	1.372(5)
C(16)-C(15)	1.373(5)
C(16)-H(16)	0.9300
C(4)-C(5)	1.382(5)
C(4)-C(3)	1.402(5)
C(17)-H(17)	0.9300
C(3)-C(2)	1.366(6)
C(3)-H(3)	0.9300
C(24)-C(23)	1.381(6)
C(24)-H(24)	0.9300
C(9)-C(10)	1.364(6)
C(9)-H(9)	0.9300
C(5)-C(6)	1.399(6)
C(5)-H(5)	0.9300
C(21)-C(22)	1.377(6)
C(21)-H(21)	0.9300
C(15)-H(15)	0.9300
C(10)-C(11)	1.375(6)
C(10)-H(10)	0.9300
C(11)-H(11)	0.9300
C(22)-C(23)	1.382(7)
C(22)-H(22)	0.9300
C(2)-C(1)	1.359(7)
C(2)-H(2)	0.9300
C(23)-H(23)	0.9300
C(1)-C(6)	1.376(7)
C(1)-H(1)	0.9300
C(6)-H(6)	0.9300

C(29)-N(2)-C(20)	125.0(3)
C(29)-N(2)-H(2)	117.5
C(20)-N(2)-H(2)	117.5
C(19)-O(2)-H(2A)	109.5
C(7)-C(26)-C(28)	116.6(3)
C(7)-C(26)-C(30)	118.6(3)
C(28)-C(26)-C(30)	88.7(2)
C(7)-C(26)-H(26)	110.4
C(28)-C(26)-H(26)	110.4
C(30)-C(26)-H(26)	110.4
C(27)-N(1)-C	124.9(3)
C(27)-N(1)-H(1)	117.6
C-N(1)-H(1)	117.6
C(13)-O(1)-H(1A)	109.5
O(2)-C(19)-C(24)	120.4(3)
O(2)-C(19)-C(20)	120.2(3)
C(24)-C(19)-C(20)	119.4(4)
C(13)-C-C(17)	119.5(3)
C(13)-C-N(1)	122.5(3)
C(17)-C-N(1)	117.9(3)
O(4)-C(29)-N(2)	122.1(3)
O(4)-C(29)-C(30)	121.1(3)
N(2)-C(29)-C(30)	116.8(3)
C(21)-C(20)-C(19)	119.6(4)
C(21)-C(20)-N(2)	118.3(3)
C(19)-C(20)-N(2)	122.1(3)
C(27)-C(28)-C(26)	113.6(3)
C(27)-C(28)-C(25)	113.2(3)
C(26)-C(28)-C(25)	89.4(2)
C(27)-C(28)-H(28)	112.9
C(26)-C(28)-H(28)	112.9
C(25)-C(28)-H(28)	112.9
C(29)-C(30)-C(25)	116.1(3)
C(29)-C(30)-C(26)	119.4(3)
C(25)-C(30)-C(26)	90.5(2)

C(29)-C(30)-H(30)	109.8
C(25)-C(30)-H(30)	109.8
C(26)-C(30)-H(30)	109.8
C(4)-C(25)-C(30)	121.2(3)
C(4)-C(25)-C(28)	119.5(3)
C(30)-C(25)-C(28)	89.6(2)
C(4)-C(25)-H(25)	108.3
C(30)-C(25)-H(25)	108.3
C(28)-C(25)-H(25)	108.3
C(11)-C(12)-C(7)	120.6(4)
C(11)-C(12)-H(12)	119.7
C(7)-C(12)-H(12)	119.7
O(3)-C(27)-N(1)	121.7(3)
O(3)-C(27)-C(28)	122.5(3)
N(1)-C(27)-C(28)	115.8(3)
C(9)-C(8)-C(7)	120.6(4)
C(9)-C(8)-H(8)	119.7
C(7)-C(8)-H(8)	119.7
C(15)-C(14)-C(13)	120.2(4)
C(15)-C(14)-H(14)	119.9
C(13)-C(14)-H(14)	119.9
C(17)-C(16)-C(15)	120.5(4)
C(17)-C(16)-H(16)	119.8
C(15)-C(16)-H(16)	119.8
C(5)-C(4)-C(3)	117.6(3)
C(5)-C(4)-C(25)	122.4(3)
C(3)-C(4)-C(25)	119.9(3)
O(1)-C(13)-C	122.4(3)
O(1)-C(13)-C(14)	117.9(3)
C-C(13)-C(14)	119.7(3)
C(16)-C(17)-C	120.2(3)
C(16)-C(17)-H(17)	119.9
C-C(17)-H(17)	119.9
C(12)-C(7)-C(8)	118.3(3)
C(12)-C(7)-C(26)	119.9(3)

C(8)-C(7)-C(26)	121.8(3)
C(2)-C(3)-C(4)	121.5(4)
C(2)-C(3)-H(3)	119.2
C(4)-C(3)-H(3)	119.2
C(19)-C(24)-C(23)	120.5(4)
C(19)-C(24)-H(24)	119.7
C(23)-C(24)-H(24)	119.7
C(10)-C(9)-C(8)	120.4(4)
C(10)-C(9)-H(9)	119.8
C(8)-C(9)-H(9)	119.8
C(4)-C(5)-C(6)	120.2(4)
C(4)-C(5)-H(5)	119.9
C(6)-C(5)-H(5)	119.9
C(22)-C(21)-C(20)	120.4(4)
C(22)-C(21)-H(21)	119.8
C(20)-C(21)-H(21)	119.8
C(16)-C(15)-C(14)	119.9(4)
C(16)-C(15)-H(15)	120.0
C(14)-C(15)-H(15)	120.0
C(9)-C(10)-C(11)	120.1(4)
C(9)-C(10)-H(10)	119.9
C(11)-C(10)-H(10)	119.9
C(10)-C(11)-C(12)	120.0(4)
C(10)-C(11)-H(11)	120.0
C(12)-C(11)-H(11)	120.0
C(21)-C(22)-C(23)	120.0(4)
C(21)-C(22)-H(22)	120.0
C(23)-C(22)-H(22)	120.0
C(1)-C(2)-C(3)	120.6(5)
C(1)-C(2)-H(2)	119.7
C(3)-C(2)-H(2)	119.7
C(24)-C(23)-C(22)	120.2(4)
C(24)-C(23)-H(23)	119.9
C(22)-C(23)-H(23)	119.9
C(2)-C(1)-C(6)	119.8(4)

C(2)-C(1)-H(1)	120.1
C(6)-C(1)-H(1)	120.1
C(1)-C(6)-C(5)	120.3(4)
C(1)-C(6)-H(6)	119.8
C(5)-C(6)-H(6)	119.8

Symmetry transformations used to generate equivalent atoms:

Table A-29. Torsion angles [°] for **9**.

C(27)-N(1)-C-C(13)	55.9(5)
C(27)-N(1)-C-C(17)	-127.0(4)
C(20)-N(2)-C(29)-O(4)	-12.3(5)
C(20)-N(2)-C(29)-C(30)	168.7(3)
O(2)-C(19)-C(20)-C(21)	-180.0(3)
C(24)-C(19)-C(20)-C(21)	-1.5(6)
O(2)-C(19)-C(20)-N(2)	-1.0(5)
C(24)-C(19)-C(20)-N(2)	177.4(3)
C(29)-N(2)-C(20)-C(21)	-128.9(4)
C(29)-N(2)-C(20)-C(19)	52.1(5)
C(7)-C(26)-C(28)-C(27)	133.3(3)
C(30)-C(26)-C(28)-C(27)	-105.1(3)
C(7)-C(26)-C(28)-C(25)	-111.6(3)
C(30)-C(26)-C(28)-C(25)	10.1(2)
O(4)-C(29)-C(30)-C(25)	20.9(4)
N(2)-C(29)-C(30)-C(25)	-160.1(3)
O(4)-C(29)-C(30)-C(26)	127.6(3)
N(2)-C(29)-C(30)-C(26)	-53.4(4)
C(7)-C(26)-C(30)-C(29)	-11.2(4)
C(28)-C(26)-C(30)-C(29)	-131.0(3)
C(7)-C(26)-C(30)-C(25)	109.6(3)
C(28)-C(26)-C(30)-C(25)	-10.3(2)
C(29)-C(30)-C(25)-C(4)	-101.5(4)
C(26)-C(30)-C(25)-C(4)	135.1(3)
C(29)-C(30)-C(25)-C(28)	133.7(3)
C(26)-C(30)-C(25)-C(28)	10.2(2)
C(27)-C(28)-C(25)-C(4)	-21.0(4)
C(26)-C(28)-C(25)-C(4)	-136.6(3)
C(27)-C(28)-C(25)-C(30)	105.3(3)
C(26)-C(28)-C(25)-C(30)	-10.3(2)
C-N(1)-C(27)-O(3)	-3.2(5)
C-N(1)-C(27)-C(28)	178.8(3)

C(26)-C(28)-C(27)-O(3)	40.5(4)
C(25)-C(28)-C(27)-O(3)	-59.6(4)
C(26)-C(28)-C(27)-N(1)	-141.5(3)
C(25)-C(28)-C(27)-N(1)	118.5(3)
C(30)-C(25)-C(4)-C(5)	9.0(5)
C(28)-C(25)-C(4)-C(5)	118.5(4)
C(30)-C(25)-C(4)-C(3)	-173.0(3)
C(28)-C(25)-C(4)-C(3)	-63.6(5)
C(17)-C-C(13)-O(1)	-178.3(4)
N(1)-C-C(13)-O(1)	-1.2(6)
C(17)-C-C(13)-C(14)	0.1(6)
N(1)-C-C(13)-C(14)	177.2(4)
C(15)-C(14)-C(13)-O(1)	-179.9(4)
C(15)-C(14)-C(13)-C	1.6(6)
C(15)-C(16)-C(17)-C	1.8(6)
C(13)-C-C(17)-C(16)	-1.8(6)
N(1)-C-C(17)-C(16)	-179.0(3)
C(11)-C(12)-C(7)-C(8)	-1.6(5)
C(11)-C(12)-C(7)-C(26)	-179.7(3)
C(9)-C(8)-C(7)-C(12)	1.7(5)
C(9)-C(8)-C(7)-C(26)	179.7(3)
C(28)-C(26)-C(7)-C(12)	-140.1(3)
C(30)-C(26)-C(7)-C(12)	115.7(4)
C(28)-C(26)-C(7)-C(8)	41.9(4)
C(30)-C(26)-C(7)-C(8)	-62.3(4)
C(5)-C(4)-C(3)-C(2)	-1.0(6)
C(25)-C(4)-C(3)-C(2)	-179.1(4)
O(2)-C(19)-C(24)-C(23)	179.5(4)
C(20)-C(19)-C(24)-C(23)	1.0(6)
C(7)-C(8)-C(9)-C(10)	-0.7(6)
C(3)-C(4)-C(5)-C(6)	1.5(6)
C(25)-C(4)-C(5)-C(6)	179.5(4)
C(19)-C(20)-C(21)-C(22)	0.9(6)
N(2)-C(20)-C(21)-C(22)	-178.1(4)
C(17)-C(16)-C(15)-C(14)	0.0(6)

C(13)-C(14)-C(15)-C(16)	-1.7(7)
C(8)-C(9)-C(10)-C(11)	-0.3(6)
C(9)-C(10)-C(11)-C(12)	0.4(6)
C(7)-C(12)-C(11)-C(10)	0.6(6)
C(20)-C(21)-C(22)-C(23)	0.2(7)
C(4)-C(3)-C(2)-C(1)	0.1(7)
C(19)-C(24)-C(23)-C(22)	0.1(7)
C(21)-C(22)-C(23)-C(24)	-0.7(7)
C(3)-C(2)-C(1)-C(6)	0.4(7)
C(2)-C(1)-C(6)-C(5)	0.1(8)
C(4)-C(5)-C(6)-C(1)	-1.0(7)

Symmetry transformations used to generate equivalent atoms: